CHEMICAL REVIEWS

Review

Square-Planar Pd(II), Pt(II), and Au(III) Terpyridine Complexes: Their Syntheses, Physical Properties, Supramolecular Constructs, and Biomedical Activities

Ibrahim Eryazici, Charles N. Moorefield, and George R. Newkome

Chem. Rev., **2008**, 108 (6), 1834-1895 • DOI: 10.1021/cr0781059 • Publication Date (Web): 11 June 2008

Square-Planar Pd(II), Pt(II), and Au(III) Terpyridine Complexes: Their Syntheses, Physical Properties, Supramolecular Constructs, and Biomedical Activities

Ibrahim Eryazici,[†] Charles N. Moorefield,[‡] and George R. Newkome*[,†,‡,§]

Departments of Polymer Science and Chemistry and the Maurice Morton Institute of Polymer Science, The University of Akron, Akron, Ohio 44325-4717

Received October 2, 2007

Contents

1. Introduction 1834
2. Chemistry and Properties 1834
   2.1. Syntheses 1834
   2.2. Characterization 1837
   2.3. Single X-ray Crystal Structures and Their Molecular Packing 1838
   2.4. Dimerization and Its Constant (K_D) 1841
   2.5. Photophysical Properties 1841
   2.6. Electrochemical Properties 1844
   2.7. Fluxionality 1844
3. Applications of Mononuclear Terpyridine Complexes 1846
   3.1. Luminescent Pt−Terpyridine Complexes 1846
   3.2. Molecular Stacking and Induced Self-Assembly 1847
   3.3. Molecular Sensors and Switches 1850
   3.4. Photocatalytic Activities 1854
   3.5. Miscellaneous Applications 1857
4. Metallo-Supramolecular Terpyridine Architectures 1860
   4.1. Dyads and Triads 1860
   4.2. Supramolecular Self-Assemblies 1867
   4.3. Molecular Recognition by Host−Guest Interaction 1868
   4.4. Multimetallic Peptide Scaffolds 1872
5. Biological Activities 1872
   5.1. DNA Intercalation 1872
      5.1.1. UV−Vis Spectroscopic Analysis and Binding Modes 1872
      5.1.2. Viscosity and Thermal Denaturation 1874
      5.1.3. Induced Circular Dichroism 1875
      5.1.4. Competitive Fluorescence Spectroscopy 1875
      5.1.5. Closed Circular DNA 1876
      5.1.6. Stereochemical Changes in DNA 1876
      5.1.7. Site-Specific Intercalation 1877
      5.1.8. Other Mononuclear Intercalators 1877
      5.1.9. Multinuclear Intercalators 1878
   5.2. Covalent Binding to Biomolecules 1881
   5.3. Labeling Biomolecules 1882
   5.4. Cytotoxicity 1885
      5.4.1. Chemotherapeutic Agents 1886
      5.4.2. Radiotherapeutic Agents 1892
6. Conclusion 1892
7. Acknowledgments 1892
8. References 1893

* To whom correspondence should be addressed. E-mail: newkome@uakron.edu.
[†] Department of Polymer Science, The University of Akron.
[‡] Maurice Morton Institute of Polymer Science, The University of Akron.
[§] Department of Chemistry, The University of Akron.

1. Introduction

Metal−ligand interactions are inherent in a succession of important self-assembly strategies used in supramolecular chemistry. To this extent, the development of chelating ligands and their transition metal complexes has been of increasing interest. Since the 1980s, terpyridine ligands have been intensely studied specifically for their octahedral complexes with various transition metals, for example, Fe(II), Ru(II), Zn(II), and so forth, in order to capitalize their unique photophysical, electrochemical, magnetic, and optical properties.[1] In the 1970s, terpyridines were also found to form stable square-planar complexes with d^8 late transition metal ions, such as Pt(II), Pd(II), and Au(III). Later in the 1990s, the Pt(II), as opposed to Pd(II) and Au(III), terpyridine complexes were extensively investigated due to their unique luminescent properties[2–4] offering potential applications in chemosensing for solvents[5–7] and metal ions,[8] photocatalysis[9,10] and biological activities, such as DNA intercalation[11–13] and covalent binding to biomolecules[14–19] with potential applications, as antitumor,[20–22] radiotherapy,[23–25] antiprotozoal agents[26,27] and protein probes.[16–18] In turn, Pd(II) terpyridine complexes have been utilized as supramolecular recognition centers[28] and the Au(III) complexes have been demonstrated to possess antitumor[29] activity. Whereas octahedral terpyridine complexes have been surveyed,[1,30] this review is directed at syntheses, physical and structural properties, supramolecular chemistry, and biomedical applications of the interesting square-planar terpyridine complexes.

2. Chemistry and Properties

2.1. Syntheses

In 1934, Morgan and Burstall[31] initially isolated [Pt(tpy)(Cl)]-[Cl]·$3H_2O$, as a minor product, from a red aqueous filtrate derived from the reaction of terpyridine with 1 equiv of K_2PtCl_4 in H_2O after refluxing for 6 h. Unfortunately, the major product of this reaction was the orange-brown precipitate $[Pt(tpy)(Cl)]_2[Pt(Cl)_4]$. Notably, 4 decades later, when the reaction mixture was refluxed until a clear red solution was realized (20−100 h), [Pt(tpy)(Cl)][Cl]·$3H_2O$

10.1021/cr0781059 CCC: $71.00
Published on Web 06/11/2008

Ibrahim Eryazici was born in Erzurum, Turkey, in 1979. He studied chemistry at Bogazici University, Istanbul, Turkey. Then, he joined the Ph.D. program at Polymer Science Department of The University of Akron, in Akron, Ohio. He recently completed his dissertation in supramolecular chemistry of functionalized terpyridines, under the supervision of Professor G. R. Newkome at the Center of Molecular Design and Recognition. His research interest is in the supramolecular self-assemblies and their potential applications in molecular electronics.

Charles N. Moorefield received both his B.S. in Chemistry and his M.S. in Industrial Chemistry from the University of Central Florida. Upon completion of two years of graduate study at Louisiana State University, he transferred to the University of South Florida to continue working with Professor George R. Newkome, where he received his Ph.D. in 1991. During his graduate career, he earned several academic honors, a graduate fellowship, and the Outstanding Doctoral Student Award presented by the USF Sigma Xi Research Society. After completing a postdoctoral appointment, he accepted a research faculty position at the Center for Molecular Design and Recognition (*CMDR*) at the University of South Florida. In 2001, he moved along with Prof. Newkome to The University of Akron to continue working as the Assistant Director of *CMDR* within the Maurice Morton Institute for Polymer Science. His interests include molecular architecture and physical properties and their function within the supramolecular regime.

George R. Newkome received his B.S. and Ph.D. in chemistry from Kent State University. He joined Louisiana State University in 1968 becoming a full professor in 1978 and Distinguished Research Master in 1982. In 1986, he moved to the University of South Florida as Vice President for Research and Professor of Chemistry, becoming a Distinguished Research Professor in 1992. In 2001, he was appointed as Oelschlager Professor of Science and Technology at the University of Akron, where he is also Professor of Polymer Science and Chemistry, Vice President for Research, Dean of the Graduate School, and President of the University's Research Foundation. He has 20 edited and authored books, over 400 journal publications, and numerous patents resulting from research in supra-(macro)molecular chemistry, molecular dendritic and fractal assemblies, nanochemistry, inorganic−organic interfaces, molecular inclusion chemistry, molecular electronics, and photonics.

was isolated in 65% yield and recrystallized from hot H_2O/EtOH (1:1) affording orange-red needle-like crystals, as the trihydrate, which was subsequently transformed to the dihydrate upon drying *in vacuo* (Route A, Scheme 1).[32,33] Counterion exchange of the Cl^- ion of [Pt(tpy)(Cl)][Cl]·$2H_2O$ was achieved by its dissolution in water and reprecipitation by the addition of an excess of an appropriate salt (e.g., $NaClO_4$, NH_4PF_6, CF_3SO_3Na, or CF_3SO_3Ag).[34,35] Similarly, treatment of *t*-Bu_3-tpy with K_2PtCl_4 in MeCN/H_2O generated a clear yellow solution of [Pt(*t*-Bu_3-tpy)(Cl)][Cl], which was filtered into aqueous $NaClO_4$ to generate [Pt(*t*-Bu_3-tpy)(Cl)][ClO_4] as a yellow precipitate upon cooling. Its recrystallization by vapor diffusion of Et_2O into an MeCN solution of the complex afforded yellow crystals in 65% overall yield (Route B).[36]

The treatment of terpyridine ligands (4′-R^1-tpy; R^1 = H, phenyl, *p*-toluoyl) with *cis*-[$Pt(DMSO)_2(Cl)_2$][37–39] or *trans*-[$Pt(DMSO)_2(R^2)(Cl)$][37,40] (R^2 = Me, phenyl) in MeOH[37,40] for up to 2 h at 25 °C or in $CHCl_3$[38,39] for 24 h at 25 °C afforded the desired [Pt(4′-R^1-tpy)(Cl)][Cl] or [Pt(4′-R^1-tpy)(R^2)][Cl], respectively, (Scheme 2) in high (64−93%) overall yield. The external Cl^- counterion in [Pt(4′-R^1-tpy)(R^2)][Cl] was easily exchanged by addition of $AgNO_3$, KPF_6, $LiClO_4$ or $NaB(Ph)_4$ (Route C, Scheme 2).[40] However, a terpyridine ligand treated with *cis*-[$Pt(DMSO)_2(Cl)_2$] in acetone for 12 h in the dark at 20 °C exclusively formed [Pt(tpy)(Cl)][$Pt(DMSO)(Cl)_3$], as a red microcrystalline precipitate, which was recrystallized from DMSO (Route A, Scheme 2).[41] When this reaction was conducted in refluxing MeOH over 1 h, [Pt(tpy)(Cl)][X] possessing a mixture of counterions, where X = Cl^- and [$Pt(DMSO)(Cl)_3$]$^-$, was generated.[42] It was suggested that [$Pt(DMSO)(Cl)_3$]$^-$ was formed by addition of the Cl^- ion to *cis*-[$Pt(DMSO)_2(Cl)_2$] to give the product + DMSO.

Another synthetic approach was developed to afford [Pt(4′-R-tpy)(Cl)][X] (X = SbF_6^-, BF_4^-, $CF_3SO_3^-$; Scheme 3),[43–47] in which an equimolar amount of AgX was added to a suspension of [$Pt(PhCN)_2(Cl)_2$] in MeCN, then refluxed for 15 h to give the [$Pt(PhCN)_2$(Cl)(MeCN)][X]; after filtration, 1 equiv of the terpyridine ligand was then added and refluxed for 16−24 h affording [Pt(4′-R-tpy)(Cl)][X], as orange-red crystals, in a 70−91% overall yield.

Annibale et al.[42] reported a new synthetic method that gave [Pt(tpy)(Cl)][Cl] in quantitative yield, in which a suspension of [$Pt(COD)(Cl)_2$][48] (COD = 1,5-cyclooctadiene) with an equivalent amount of terpyridine in MeOH or H_2O afforded the desired complex after 15 min at 50 °C. It was proposed that the cis-orientation of the coordinated diolefin and its lability when monocoordinated to Pt(II) was the rationale for this high yield conversion. A similar method was utilized

Scheme 1. Synthesis of [Pt(tpy)(Cl)][X]·2H$_2$O[32–35] and [Pt(*t*-Bu$_3$-tpy)(Cl)][ClO$_4$][36]

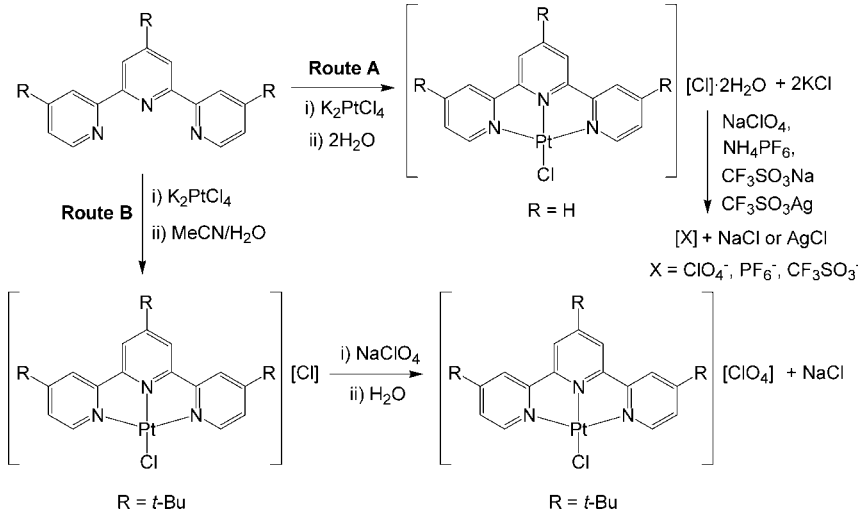

Scheme 2. Synthesis of [Pt(4′-R^1-tpy)(Cl)][Cl][37–39] and [Pt(4′-R^1-tpy)(R^2)][X][37,40]

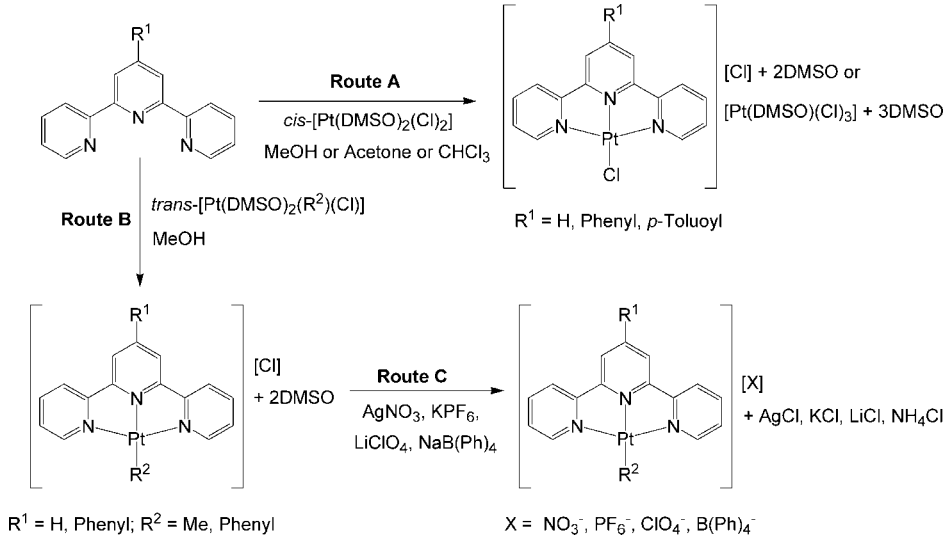

Scheme 3. Synthesis of [Pt(4′-R-tpy)(Cl)][X][43–47]

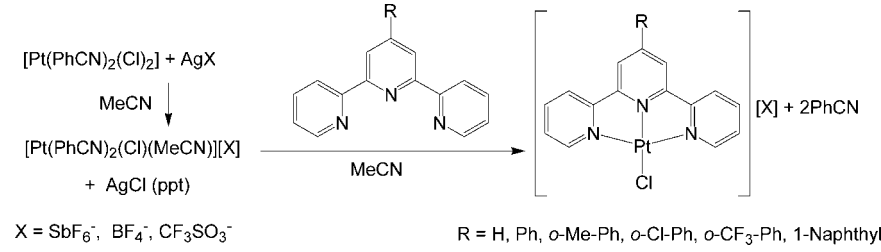

for the synthesis of Pt(II) complexes with a variety of other terpyridine ligands.[49–52]

When a vapor-extraction apparatus is used, the co-ligand (Cl) of [Pt(tpy)(Cl)][X] (X = Cl$^-$, SbF$_6^-$) can be substituted by H$_2$O or MeCN. In this process, the continuous extraction of solid [Pt(tpy)(Cl)][X] into refluxing H$_2$O or MeCN with an excess of AgX generated the soluble [Pt(tpy)(R^1)][(X)$_2$] (R^1 = H$_2$O, MeCN) (Route A, Scheme 4).[43,53] Moreover, diverse co-ligand functionality, that is, OH, Br, I, SCN, N$_3$, NH$_3$, has also been introduced into these Pt(II) complexes (Route B, Scheme 4).[35,54] Such [Pt(tpy)(R^1)][(X)$_n$] [R^1 (*n*) = Cl (1), H$_2$O (2), MeCN (2); X = Cl$^-$, SbF$_6^-$] complexes have been easily converted to other Pt(II)-based terpyridine complexes *via* simple substitution of labile co-ligands, that is, R = Cl, H$_2$O, MeCN, with ROH, RSH, and pyridine (Route C, Scheme 4).[33,53–55] Biomolecules containing thiol, imidazole, and guanidine were also substituted with the Cl co-ligand in these Pt(II) complexes, which will be considered later in the text.

A series of Pt(II) terpyridine complexes **1**, containing alkynyl groups, was prepared by a reaction of [Pt(tpy)(Cl)]$^+$ with H-C≡C-R in DMF in the presence of a catalyst (e.g., CuI and NEt$_3$) at 25 °C (Scheme 5) in reasonable yields of ca. 75%.[56]

An equimolar amount of HAuCl$_4$ and terpyridine, which was refluxed in H$_2$O at pH 3−5 for 24 h, gave the desired [Au(tpy)(Cl)][(Cl)$_2$] in 80% yield along with traces of {[Au(tpy)(Cl)]$_2$[AuCl$_2$]$_3$[AuCl$_4$]} (Route A, Scheme 6), whereas at pH 1.9−3, the protonated terpyridines ([Htpy][H$_2$tpy][AuCl$_4$]$_3$) were isolated after 24 h in 52% yield

Scheme 4. Introduction of Different Co-Ligands to the Pt(II)−tpy Complex[33,35,43,53–55]

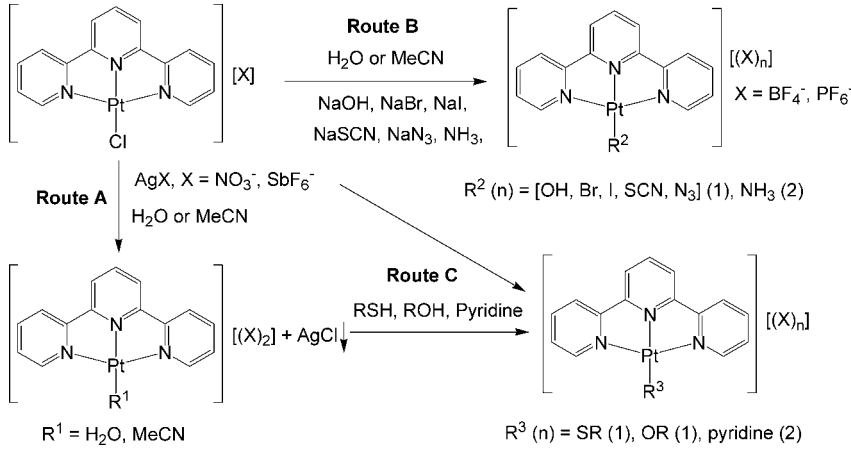

Scheme 5. Synthesis of a Pt−Alkyne Linkage[56]

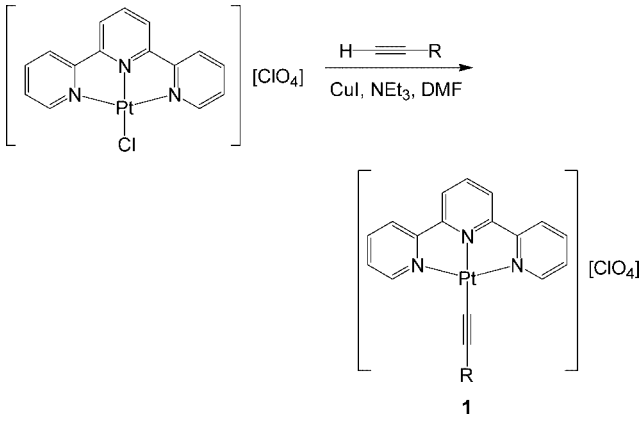

along with similar amounts of {[Au(tpy)(Cl)]$_2$-[AuCl$_2$]$_3$[AuCl$_4$]} (Route B, Scheme 6).[57] Further, the [AuCl$_4$]$^-$ salts of the protonated terpyridines at pH 6 afforded the desired {[Au(tpy)(Cl)][(Cl)$_2$]} under reflux conditions in 62% yield. To avoid side products, the functionalized terpyridines were subsequently treated with KAuCl$_4$ and LiPF$_6$, LiClO$_4$, or AgCF$_3$SO$_3$ to generate the desired {[Au(tpy)(Cl)][(X)$_2$]} (X = PF$_6^-$, ClO$_4^-$, or CF$_3$SO$_3^-$, respectively) in 63−80% yield (Route C, Scheme 6).[36,58] The {[Au(tpy)(OH)][(ClO$_4$)$_2$]} was formed by treating {[Au(tpy)(Cl)][(ClO$_4$)$_2$]} with AgClO$_4$ in a hot aqueous media.[59] It was suggested that the initially formed {[Au(tpy)(H$_2$O)][(ClO$_4$)$_3$]} disassociated to give the corresponding hydroxo species, since the Au(III) metal center can act as a strong acid.

The {[Pd(4′-R-tpy)(Cl)][Cl]}, R = H, CH$_3$(CH$_2$)$_2$O, Ph(CH$_2$)$_3$O, complexes were prepared in 90−93% yield by treatment of terpyridine with diverse Pd(II) sources, such as PdCl$_2$ either in MeNO$_2$[60] or concentrated HCl,[61] *cis*-[Pd(DMSO)$_2$Cl$_2$] in MeOH,[61] and [Pd(MeCN)$_2$Cl$_2$] in THF.[62] The labile Cl co-ligand of the {[Pd(tpy)(Cl)][Cl]} complex was subsequently exchanged with various functional groups, such as H$_2$O,[63] OH,[64] pyridine,[65,66] 3,4-dimethylphenol,[67] phenylcyanamides,[68] and biomolecules, such as L-cysteine,[61,63] glutathione,[63] DL-penicillamine,[63] and 1-Me-cytosine.[69] Furthermore, treatment of terpyridine ligand with {[Pd(MeCN)$_4$]-[(X)$_2$]} (X = PF$_6^-$, BF$_4^-$) in MeCN afforded the corresponding {[Pd(tpy)(MeCN)][X]} complexes, which were later converted to {[Pd(tpy)(Cl)][X]} by the addition of NH$_4$Cl or were directly utilized in the construction of metallosupramolecular architectures.[70,71]

2.2. Characterization

The Pt-based terpyridine complexes were mainly characterized by NMR spectroscopy, in which [Pt(tpy)(Cl)]$^+$ showed downfield shifts for the 4,4″-tpy*H*s ($\Delta\delta$ = 0.51 ppm), 5,5″-tpy*H*s ($\Delta\delta$ = 0.46 ppm), and 6,6″-tpy*H*s ($\Delta\delta$ = 0.20 ppm) (Figure 1) relative to the ligand due to the influence of the metal−ligand bond.[41] Similar shifts upon complexation were observed for the Au(III) and Pd(II) terpyridine com-

Scheme 6. Synthesis of {[Au(tpy)(Cl)][(X)$_2$]}[36,57–59]

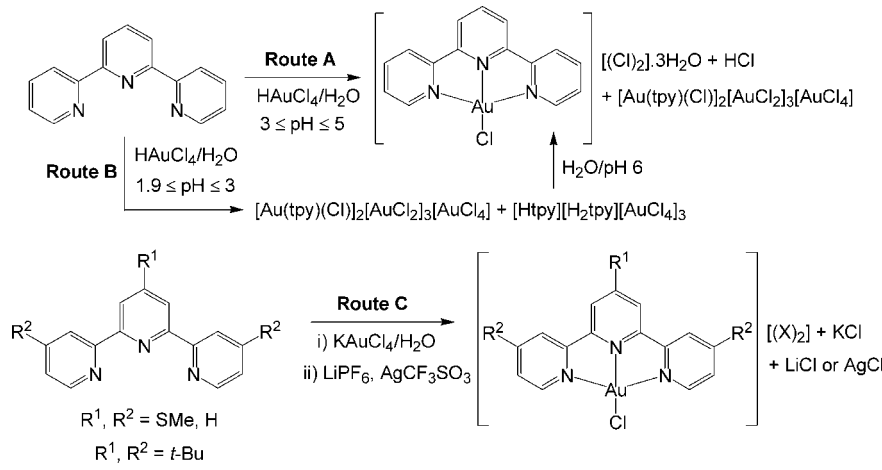

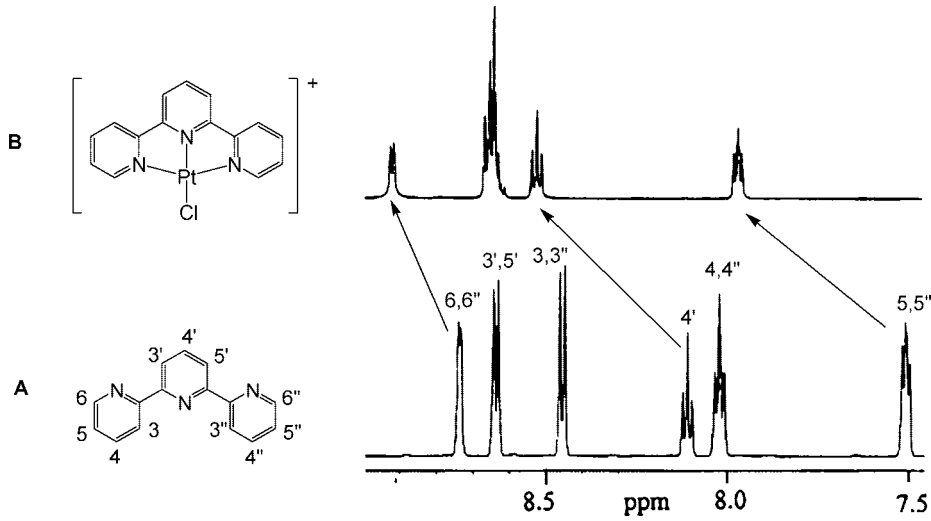

Figure 1. ^{1}H NMR of (A) terpyridine and (B) $[Pt(tpy)(Cl)]^+$ in DMSO-d_6. (Reprinted with permission from ref 41. Copyright 2001 Elsevier).

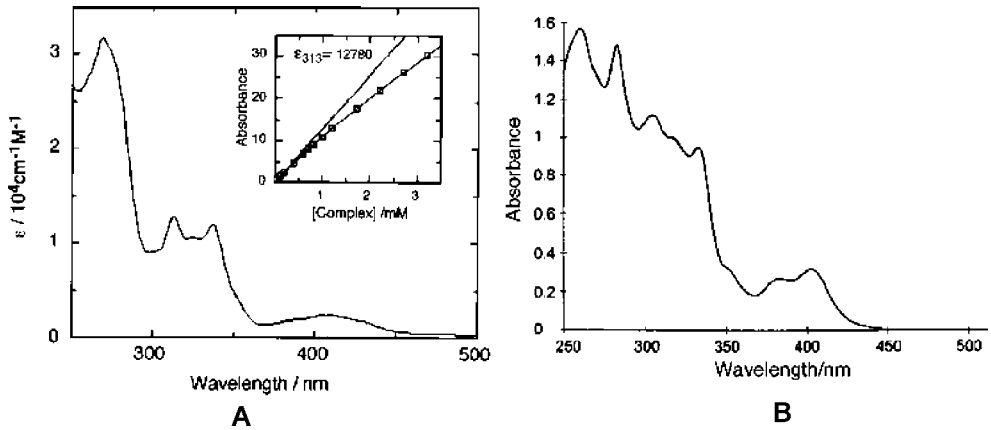

Figure 2. The UV−vis spectra of (A) {[Pt(tpy)(Me)][BPh_4]} in MeCN at 25 °C. In the inset, the straight line represents the theoretical concentration dependence of absorbance at 313 nm with ϵ_{313} = 12 780 M^{-1} cm^{-1} according to Beer's law, and the line connected with open squares represents the experimental result. (Reprinted with permission from ref 73. Copyright 2000 Elsevier). (B) [Pt(4′-Ph-tpy)(Cl)][SbF_6] in MeCN at 25 °C. (Reprinted with permission from ref 44. Copyright 1999 The Royal Society of Chemistry).

plexes.[58] The ^{195}Pt NMR was also used to characterize these Pt(II) terpyridine complexes, each of which revealed a single Pt peak at ca. −3000 ppm.[72]

The UV−vis spectra of {[Pt(tpy)(Me)][BPh_4]} in MeCN revealed well-resolved peaks at 408 nm (ϵ = 2300 M^{-1} cm^{-1}), 337 (11 950), 325 (10 780), 313 (12 780), and 270 (31 150) (Figure 2A).[73] The peaks in the range of 310−340 nm were attributed to a $\pi-\pi^*$ intraligand (IL) transition of terpyridine, whereas the peak at 408 nm was assigned to either a d$\pi-\pi^*$ transition or "metal-to-ligand charge-transfer" (MLCT) transition.[54] Similar bands were observed for {[Pt(4′-Ph-tpy)(Cl)][SbF_6]} (Figure 2B)[44] and $[Pt(4'\text{-}R^1\text{-}tpy)(R^2)]^+$ (R^1 = H, Ph; R^2 = Cl, Me, Ph) in MeCN.[37] The MLCT peak of these complexes displayed significant red shifts in DCM compared to MeCN due to higher dipole moment of the MLCT excited-state in DCM.[49] The UV−vis absorption of $[Pt(tpy)(R)]^{+n}$ [R (n) = [Cl, Br, I, NCS, OH, OMe, N_3] (1), NH_3 (2)] complexes displayed a similar behavior to that depicted in Figure 2.[35,54]

The absorption peaks of {[Pt(tpy)(Me)][BPh_4]} did not change with increased concentration; however, an increase in the intensity of the absorption displayed a nonlinear curve that did not obey Beer's law (inset in Figure 2A).[73] This nonlinear behavior was interpreted as an aggregation of complexes through $\pi-\pi$ interaction of terpyridine ligands and $d_{z^2}-d_{z^2}$ orbital interactions of the Pt−Pt metals; ^{1}H NMR data supported this conclusion.[37] In the case of the terpyridine possessing three bulky *t*-butyl groups, aggregation of the Pt complexes was circumvented.[74]

Absorption spectra of $[Pd(tpy)(Cl)]^+$ showed peaks at 362 nm (ϵ = 8180 M^{-1} cm^{-1}), 345 (9050), 328 (8670), 279 (23 900), 246 (25 800), and 205 (57 500). Peaks between 200 and 280 nm were assigned to the $\pi-\pi^*$ IL transitions and the 300−370 nm absorptions to the MLCT bands, which are in agreement with other Pd(II) terpyridine complexes.[60,68] However, $[Au(t\text{-}Bu_3tpy)(Cl)]^{2+}$ did not display any MLCT bands due to electrophilicity of the Au(III) center and the ligand-to-metal charge-transfer (LMCT) absorption that was possibly mixed with the high energy bands below 300 nm. The $\pi-\pi^*$ IL transitions of the $[Au(t\text{-}Bu_3tpy)(Cl)]^{2+}$ complex were observed between 310−370 nm with a peak at 349 nm (ϵ = 11 430 M^{-1} cm^{-1}).[36]

2.3. Single X-ray Crystal Structures and Their Molecular Packing

Single crystal X-ray structures of $[Pt(4'\text{-}R\text{-}tpy)(Cl)]^+$ (R = H, Aryl) revealed that the Pt(II) metal center is coplanar relative to the four donor atoms forming an irregular square-planar motif with a deviation[34,41,43–45] from idealized

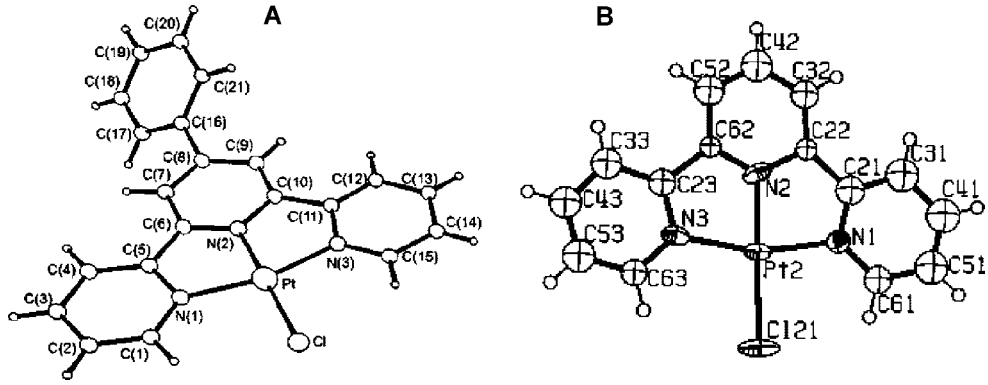

Figure 3. Crystal structures of (A) $[Pt(4'\text{-Ph-tpy})(Cl)]^+$, (Reprinted with permission from ref 44. Copyright 1999 The Royal Society of Chemistry) and (B) $[Pt(tpy)(Cl)]^+$. (Reprinted with permission from ref 41. Copyright 2001 Elsevier).

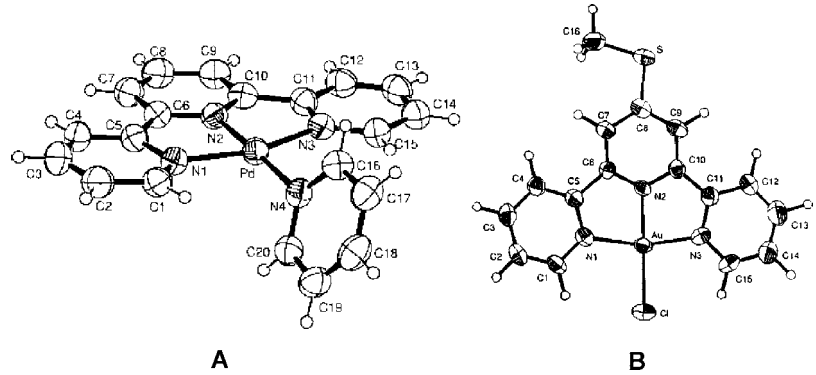

Figure 4. Crystal structure of (A) $[Pd(tpy)(pyr)]^{2+}$, (Reprinted with permission from ref 65. Copyright 2004 Elsevier) and (B) $[Au(4'\text{-MeS-tpy})(Cl)]^{2+}$. (Reprinted with permission from ref 58. Copyright 1999 The Royal Society of Chemistry).

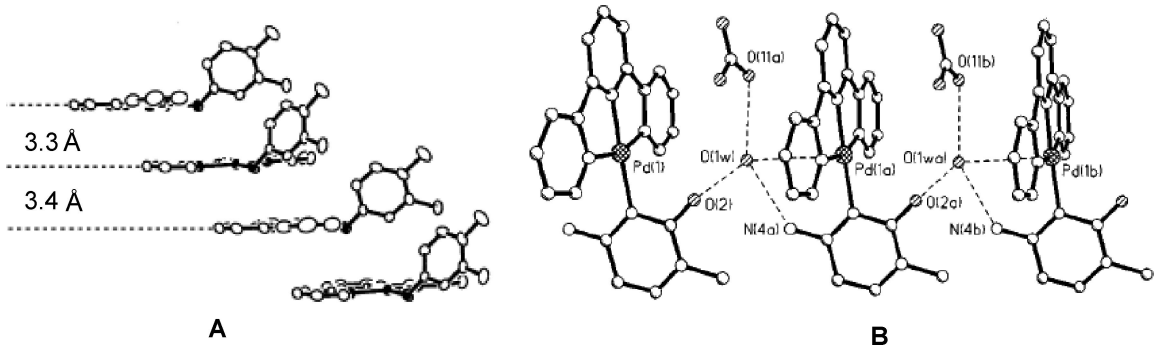

Figure 5. Molecular packing of (A) $[Pd(tpy)(O\text{-Ph-}Me_2)]^+$, (Reprinted with permission from ref 67. Copyright 2003 Elsevier) and (B) $[Pd(tpy)(1\text{-Me-cytosine-}N^3)]^{2+}$. (Reprinted with permission from ref 69. Copyright 1999 The Royal Society of Chemistry).

geometry evident in N(1)−Pt−N(2) and N(2)−Pt−N(3) possessing angles of 80−82° (Figure 3). Since there are $d_{z^2}-d_{z^2}$ orbital interactions between the Pt−Pt metals and possible $\pi-\pi$ interactions between the terpyridine moieties in the neighboring coplanar complexes with distances less than 3.8 Å, they were grouped as linear chain,[45] tetrameric,[44] dimeric,[34,41] and monomeric[43] units along the supramolecular parallel stacks of the coplanar Pt(II) complexes.

The single crystal X-ray structures of $[Pd(tpy)(pyr)]^{2+}$ and $[Au(4'\text{-R-tpy})(Cl)]^{2+}$(R = H, SMe) revealed a coplanar metal center with a distorted square-planar geometry (Figure 4).[57,58,65] Molecular packing of $[Pd(tpy)(OPhMe_2)]^+$ revealed a linear chain-like stacking of complexes through $\pi-\pi$ interactions of the terpyridine moieties with interplanar distances of 3.3−3.4 Å; the Pd−Pd distance (5.3 Å) ruled out any $d_{z^2}-d_{z^2}$ orbital interactions (Figure 5A).[67] Linear stacking of the $[Pd(tpy)(1\text{-Me-cytosine-}N^3)]^{2+}$complex was achieved through H-bonding of 1-Me-cytosine and water. There were neither $d_{z^2}-d_{z^2}$ orbital nor $\pi-\pi$ interactions in the stacks possessing Pd−Pd distances of 7.3 Å (Figure 5B).[69]

The crystal packing of $\{Pt[4'\text{-}(o\text{-Me-Ph})tpy](Cl)\}[SbF_6]$ revealed a linear chain motif with equal spacing (3.368 Å) between the Pt−Pt metals that were stacked on top of each other in a head-to-tail fashion. The torsion angle with respect to Cl(1)−Pt(1)−Pt(2)−Cl(2) was exactly 180° (Figure 6A).[45] The cationic Pt(II) complex and SbF_6^- counterion formed separate columns stacking parallel to the *c*-axis. The Pt−Pt−Pt angle was 162°, revealing that the neighboring platinum atoms were almost eclipsed when viewed down the stacking axis. The interplanar distance of successive terpyridine moieties (3.33 Å) suggested possible $\pi-\pi$ interactions. Another linear, chain-like packing was observed for $\{Pd(4'\text{-}[Ph(CH_2)_3O]tpy)(Cl)\}^+$ (Figure 6B) with equal Pd−Pd (3.46 Å) and terpyridine interplanar distances (3.1 Å).[60]

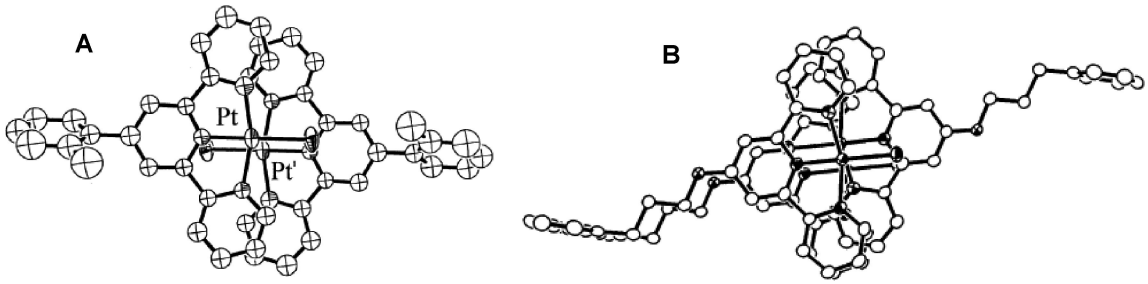

Figure 6. Linear chain packing of (A) {Pt[4′-(*o*-Me-Ph)-tpy](Cl)}[SbF_6], (Reprinted with permission from ref 45. Copyright 2002 The Royal Society of Chemistry) and (B) {Pd(4′-[Ph(CH_2)$_3$O]tpy)(Cl)}$^+$. (Reprinted with permission from ref 60. Copyright 2001 Elsevier).

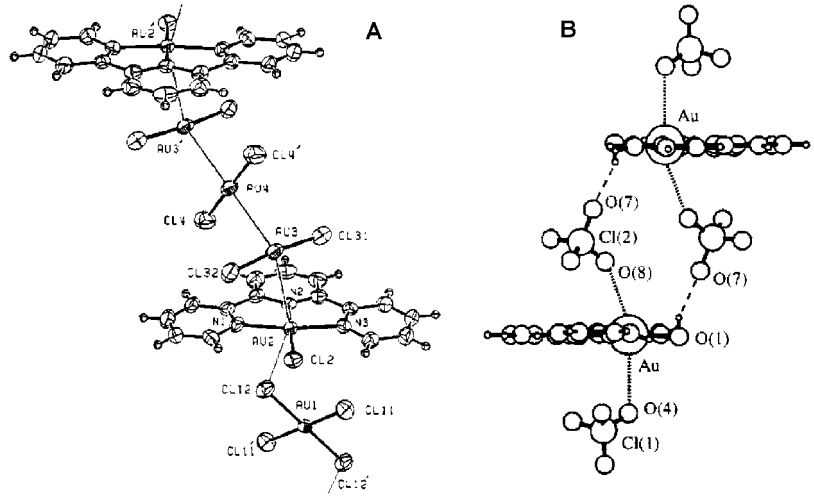

Figure 7. Crystal molecular packing of (A) [Au(tpy)(Cl)]$_2$[$AuCl_2$]$_3$[$AuCl_4$], (Reprinted with permission from ref 57. Copyright 1983 American Chemical Society) and (B) [Au(tpy)(OH)][ClO_4]. (Reprinted with permission from ref 59. Copyright 1999 The Royal Society of Chemistry).

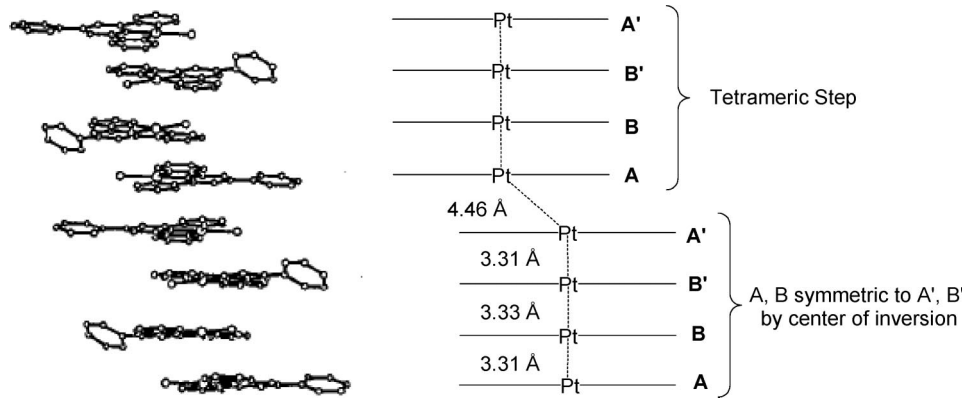

Figure 8. Stacking of [Pt(4′-Ph-tpy)(Cl)][BF_4]·MeCN. (Reprinted with permission from ref 44. Copyright 1999 The Royal Society of Chemistry).

Molecular packing of [Au(tpy)(Cl)]$_2$[$AuCl_2$]$_3$[$AuCl_4$] revealed an extended chain-like formation of [$AuCl_2$]$^-$ anions that were situated between [Au(tpy)(Cl)]$^{2+}$ cations with Au(2)−Au(3) and Au(3)−Au(4) distances of 3.3 and 3.1 Å, respectively (Figure 7A).[57] Similarly, packing of [Au(tpy)(OH)][ClO_4] revealed a dimeric formation of the [Au(tpy)(OH)]$^{2+}$ cation promoted by H-bonding of the coordinated OH groups to the ClO_4 counterions and weak Au(III)−O$^-$ interactions (Figure 7B).[59]

The crystal packing of the [Pt(4′-Ph-tpy)(Cl)][BF_4] displayed an extended chain of stepped tetramers, which were formed by σ-interaction of d_{z^2}−d_{z^2} orbitals of the Pt−Pt metals.[44] Each tetramer contains two pairs of independent cations (**A**, **B** and **A′**, **B′**; Figure 8), which are related to each other by a center-of-inversion. Stacking within the tetramer was considered to be uniform, since the Pt−Pt distance between independent pairs [Pt(B)−Pt(B′) = 3.33 Å] and cation **A** and **B** [Pt(A)−Pt(B) = 3.31 Å] is very similar. The overall angle between Pt(A)−Pt(B′)−Pt(A′) (175°) revealed a column-like stacking of Pt metals inside the tetramer, while the angle between Pt(A′)−Pt(B′)−Pt(A) (142°) explained the step-like stacking of each tetramer sliding from the edge of the previous molecule with a head-to-tail arrangement.

The crystal packing of [Pt(tpy)(Cl)][X] (X = ClO_4^-, $CF_3SO_3^-$, [Pt(DMSO)(Cl)$_3$]$^-$) revealed a continuous stack of dimers that formed by a strong Pt−Pt σ-interaction with a distance of 3.33 Å (Figure 9).[34,35,41] Furthermore, stacking of the coplanar [Pt(tpy)(Cl)]$^+$ cations with either ([ClO_4]$^-$)[34] or ([$PtCl_3$(DMSO)]$^-$)[41] displayed a similar distance between

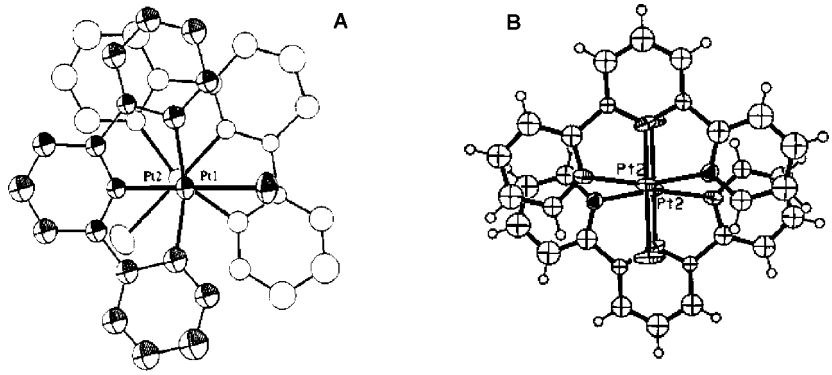

Figure 9. X-ray crystal packing diagrams of (A) $[Pt(tpy)(Cl)][ClO_4]$ dimer, (Reprinted with permission from ref 34. Copyright 1995 American Chemical Society) and (B) $[Pt(tpy)(Cl)][Pt(DMSO)(Cl)_3]$ dimer. (Reprinted with permission from ref 41. Copyright 2001 Elsevier).

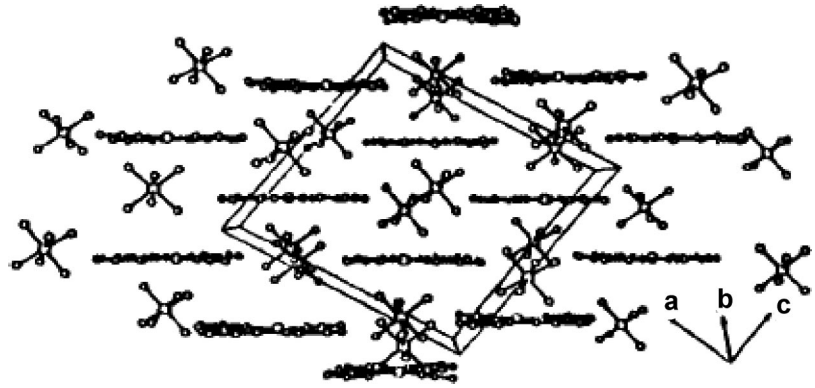

Figure 10. Crystal packing of $\{[Pt(tpy)(MeCN)][(SbF_6)_2]\}$. (Reprinted with permission from ref 43. Copyright 1997 American Chemical Society).

Pt−Pt dimers of 4.2 Å. The torsion angle of Cl(1)−Pt(1)−Pt(2)−Cl(2) inside the dimers with ClO_4^- and $[Pt(DMSO)(Cl)_3]^-$ displayed a staggered, head-to-tail arrangement, respectively (Figure 9). The Pt atoms in the stack showed a zigzag configuration with a Pt(1)−Pt(2)−Pt(1′) angle of 143° with ClO_4^- counterion and an almost linear configuration with a Pt(1)−Pt(2)−Pt(1′) angle of 167° with the $[Pt(DMSO)(Cl)_3]^-$ counterion. A similar dimerization behavior in other Pt(II)[53,73,75,76] and Pd(II)[68] terpyridine complexes has been observed.

The irregular square-planar $[Pt(tpy)(MeCN)][(SbF_6)_2]$ complex surprisingly did not display any close metal−metal or $\pi-\pi$ interactions in the crystal lattice.[43] Instead, it showed a stacking of parallel sheets consisting of cations and anions (Figure 10). The closest distance (4.9 Å) between these sheets implicated that there were no close range interactions. Furthermore, the $[Pt(tpy)(MeCN)]^{2+}$ cations form parallel sheets, where each complex is paired with two SbF_6^- anions.

Other than these four most common packing motifs, additional possible packing diagrams of coplanar, Pt-based terpyridine complexes are known, such as the crystal packing of $\{Pt[4'-(o\text{-Cl-Ph})tpy](Cl)\}[SbF_6]$ represented by a structure that is intermediate between linear chain and a stacked dimer due to an alternating close distance (3.37−3.51 Å) between Pt−Pt metal centers in successive layers.[46]

The counterion, solvent, and temperature play crucial roles in the formation of supramolecular stacks from Pt(II)-, Pd(II)-, and Au(III)-based terpyridine complexes. These supramolecular stacks possess distinct solid-state photophysical properties that will be considered later in this review.

2.4. Dimerization and Its Constant (K_D)

On the basis of the single crystal X-ray packing and UV−vis spectroscopy analyses, Jennette et al.[53] suggested that the aggregation of Pt(II) terpyridine complexes would occur in a dimeric formation. The dimerization constants (K_D) of $[Pt(tpy)(Cl)][Cl]$ and $[Pt(tpy)(SCH_2CH_2OH)][NO_3]$ were calculated to be 4×10^3 and 7×10^3 M^{-1}, respectively, in aqueous 0.1 M NaCl solution. Later, Bailey et al.[34] gave another explanation for the dimerization process by calculating the dimerization constant of $[Pt(tpy)(Cl)][ClO_4]$, specifically based on either the $\pi-\pi$ interaction of the ligands or d−d interaction of the metal centers, as 1.3×10^3 and 1.0×10^3 M^{-1}, respectively, in aqueous 0.1 M NaCl solution at 25 °C. Romeo et al.[73] reported the dimerization constants of $[Pt(tpy)(Me)][BPh_4]$ in MeCN and water by means of a UV−vis spectroscopy analysis as 180 M^{-1} and 1.0×10^4 M^{-1}, respectively. The notable difference in K_D was caused by the low dielectric constant of MeCN. Other dimerization constants of both mono- and dinuclear Pt(II) complexes have been reported.[13,77]

2.5. Photophysical Properties

The Pt(II) terpyridine complexes were expected to show luminescent properties, since their planar geometry encourages D_{2d} distortions, thus, promoting a radiationless decay. Aldridge et al.[54] reported the first solution emission properties of Pt(II) terpyridine complexes at 25 °C. The $[Pt(tpy)(Cl)][Cl]$ complex did not show any emission at 25 °C due to efficient radiationless decay *via* its low-lying ^{3}d−d state; however, the $[Pt(tpy)(R)]^+$(R = OH, NCS, OMe) complexes

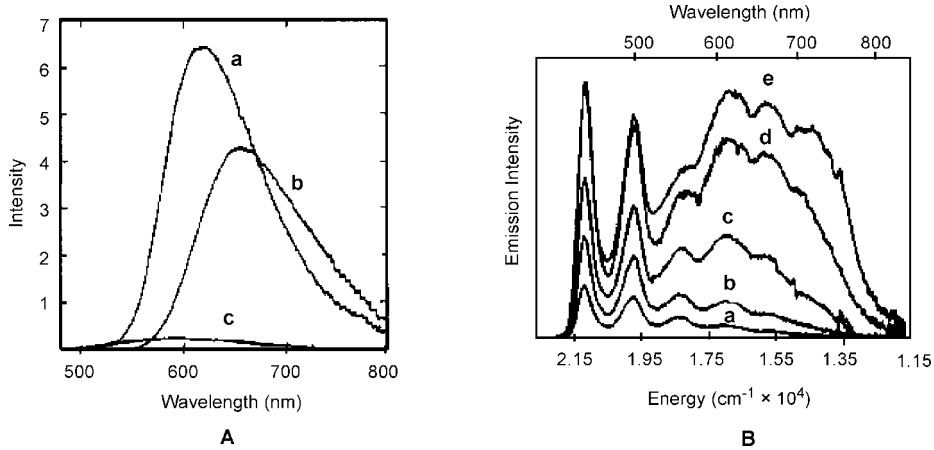

Figure 11. (A) Corrected emission spectra of $[Pt(tpy)(R)]^+$[R = (a) OH, (b) OMe, and (c) NCS]. (Reprinted with permission from ref 54. Copyright 1994 American Chemical Society). (B) Concentration dependence (mM) of emission spectrum of $[Pt(tpy)(Cl)][PF_6]$ in EtOH/MeOH/DMF (5:5:1) at 77 K (366 nm excitation) (a) 0.006, (b) 0.0132, (c) 0.03, (d) 0.072, (e) 0.15. (Reprinted with permission from ref 34. Copyright 1995 American Chemical Society).

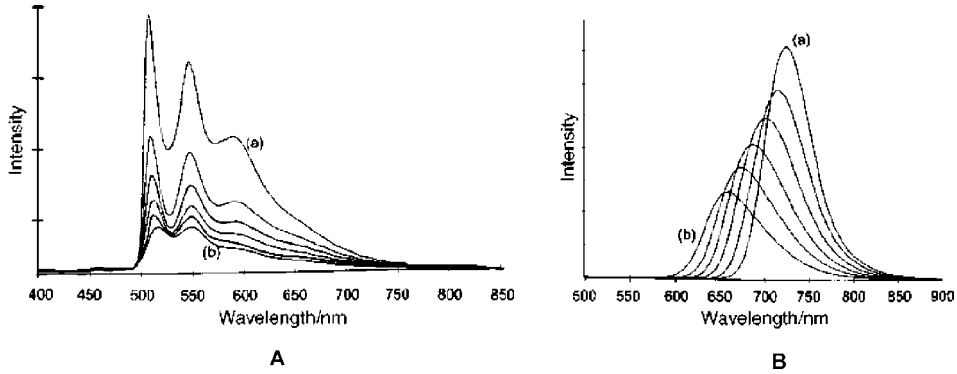

Figure 12. Solid-state emission of $[Pt(4'\text{-Ph-tpy})(Cl)][BF_4]$ (A) yellow and (B) red form recorded at 40 K intervals over the range of (a) 80 K to (b) 280 K upon excitation at 340 nm. (Reprinted with permission from ref 44. Copyright 1999 The Royal Society of Chemistry).

did display broad, structureless emissions at ca. 621, 588, and 654 nm, respectively, in MeCN at 30 °C (Figure 11A). The $[Pt(tpy)(R)]^+$(R = OH, NCS) complexes showed emissions in DCM at 610 and 594 nm, respectively, at 30 °C. These emissions were suggested to arise from the ^{3}MLCT state. The concentrations of the complexes in the solution were kept in the range of 10−500 μM in order to minimize or circumvent dimerization. The $[Pt(tpy)(OH)]^+$ gave the highest excited-state lifetime of 2 μs compared to $[Pt(tpy)(R)]^+$(R = OMe, NCS).

The $[Pt(tpy)(Cl)]^+$ complex showed a highly structured luminescence at ca. 470 nm, assigned to a $^3(\pi^* \rightarrow \pi)$ transition, upon excitation at 366 nm in a dilute (6 μM) glassy solution of butyronitrile at 77 K (Figure 11B[a]).[34] Emission behavior of this complex showed a concentration dependence; a narrow, unstructured, low-energy emission band appeared at ca. 720 nm, which was attributed to triplet metal-to-metal-to-ligand charge-transfer (^{3}MMLCT) $\pi^* \rightarrow d\sigma^*$ transitions caused by possible dimerization (Figure 11B[e]). Other $[Pt(tpy)R]^+$(R = Br, I, NH_3, N_3, SCN and CH_2NO_2) complexes also showed luminescence in a butyronitrile glass at 77 K.[35,75]

Yip et al.[35] observed the first solid-state structureless emission from the microcrystalline $[Pt(tpy)(Cl)][ClO_4]$ complex at ca. 700 nm at 25 °C. This emission was assigned to a ^{3}MMLCT transition due to dimer formation of the complex in extended linear stacks, which was observed in the single crystal X-ray structure. Most of the Pt(II) terpyridine complexes displayed strong solid-state emissions at 25 °C and were highly dependent on the counterion, as well as the crystallization solvent. For example, $[Pt(tpy)(Cl)][X]$ (X = ClO_4^-, Cl^-, and PF_6^-) complexes formed deep red, orange, and yellow colored crystals, respectively, from aqueous solutions; whereas, the $[Pt(tpy)(Cl)][ClO_4]$ complex formed rust-orange crystals from a DMF/Et_2O solution.[34] The $[Pt(tpy)(Cl)][X]$ (X = ClO_4^-, Cl^-, PF_6^-, SbF_6^-, and $CF_3SO_3^-$) complexes displayed ^{3}MMLCT emissions in the 630−730 nm range depending on the counterion and crystallization solvent.[34,43,75] The $[Pt(4'\text{-(R-Ph)tpy})(Cl)][X]$ (R = H, *o*-OMe, *o*-CF_3; X = BF_4^-, SbF_6^-) complexes showed solid-state luminescence at ca. 630 nm at 25 °C.[44,45] The $[Pt(4'\text{-Ph-tpy})(Cl)][BF_4]$ complex was crystallized in two different (red and yellow) crystal packing forms, which determined their solid-state emission properties.[44] The yellow form was in a monomeric environment based on its packing pattern and displayed only triplet intraligand (^{3}IL) emissions, whereas the red form packed as dimers and displayed ^{3}MMLCT emissions (Figure 12). Monomeric crystal packing of $[Pt(tpy)(MeCN)][(SbF_6)_2]$ showed an emission spectrum similar to the yellow form of the $[Pt(4'\text{-Ph-tpy})(Cl)][BF_4]$.[43] Solid-state emissions of all these complexes were observed to be temperature-dependent. For example, ^{3}MMLCT emission of $[Pt(4'\text{-Ph-tpy})(Cl)][BF_4]$ complex (red form) displayed a red shift and an intensity increase in emission upon decreasing the temperature causing decreased Pt−Pt packing (Figure 12B).[44] The excited-state lifetimes of these solids were in the range of 0.1−1 μs at 25 °C (298 K) and increased up to 14 μs at 77 K.[43]

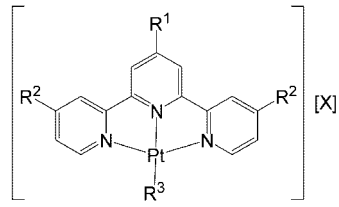

Number	R^1	R^2	R^3
2	Cl	Cl	Cl
3	t-Bu	t-Bu	CH_2COMe
4	t-Bu	t-Bu	CH_2COPhe
5	CN	H	Cl
6	NMe_2	H	Cl
7	SMe	H	Cl
8	H	H	CN
9	CN	H	CN
10	NMe_2	H	CN
11	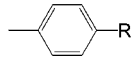	H	CN

R = H, Me, Cl, CF_3

Number	R^1 (R^2 = H; R^3 = Cl)
12	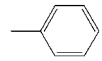
13	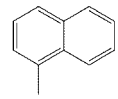
14	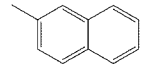
15	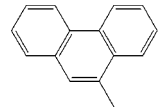

Number	R^1 (R^2 = H; R^3 = Cl)
16	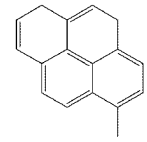
17	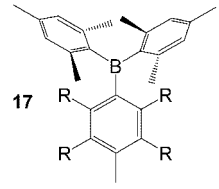

R = H, Me

Figure 13. Selected luminescent Pt(II) terpyridine complexes **2**−**17** in DCM, MeCN, or DMF solutions at 25 °C.[36,49–51,81,82]

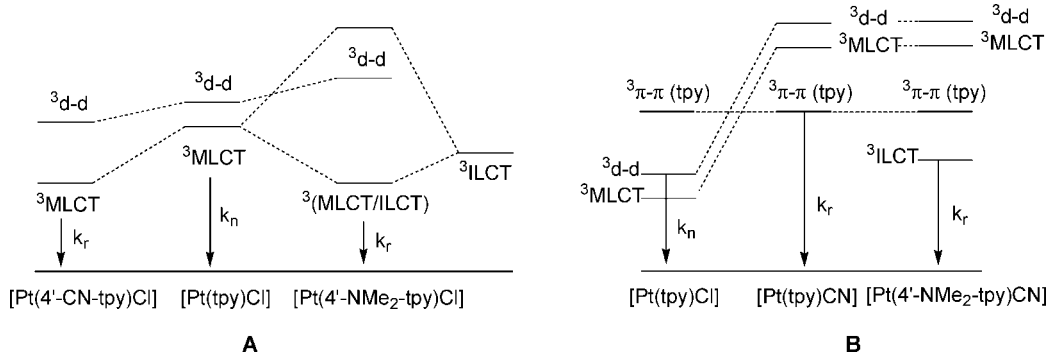

Figure 14. Energy level diagrams of Pt(II) complexes with either (A) [Cl][2] or (B) [C≡N][78,79] as co-ligand, k_r and k_n as radiative and nonradiative decay, respectively.

Various functional groups were introduced onto the terpyridine ligand with the goal to fine-tune the luminescence properties of the resultant Pt(II) terpyridine complexes **2**−**17** at 25 °C (Figure 13). Trichloro-substituted **2** displayed an ambient temperature luminescence in degassed MeCN at ca. 620 nm that was assigned to the ^{3}MLCT with a 1.9 μs excited-state lifetime.[50] Similar long-lived ^{3}MLCT transitions at ca. 600 nm for ketonic complexes **3** and **4** were reported with 3.3 and 6.4 μs excited lifetimes, respectively.[36] It was suggested that greater stabilization of the Pt(II) d(x^2-y^2) orbitals led to an increase in the energy gap between ^{3}d−d and ^{3}MLCT, thereby decreasing the radiationless decay.

Complexes **5**−**7** containing the electron-withdrawing cyano moiety and electron-donating NMe_2 and SMe groups exhibited luminescence at 25 °C with excited-state lifetimes of 116, 1920, and 146 ns, respectively.[49] It was proposed that the cyano group in complex **5** activated the ^{3}MLCT band by decreasing its energy level and increasing the gap between ^{3}d-d and ^{3}MLCT, whereas the NMe_2 group in **6** induced the luminescence *via* mixing the ^{3}MLCT and triplet intraligand charge-transfer (^{3}ILCT) transitions (Figure 14A).[2] The cyano group was utilized as co-ligand in complexes **8**−**11**, which exhibited photoluminescence at 25 °C.[78,79] Photophysical studies of complexes **8**−**11** revealed that the cyano group, as a co-ligand, deactivated the ^{3}MLCT by increasing its energy level over the $^3\pi-\pi^*$ of the terpyridine ligand resulting in a weak phosphorescence from $^3\pi-\pi^*$ band (Figure 14B). Complex **10** displayed a remarkable emission, largely based on ^{3}ILCT, with an excited-state lifetime of 22 μs and quantum yield of 0.26.[78] Emissions of complexes **5**−**7** were successfully quenched *via* exciplex formation with Lewis bases.[80]

Aromatic groups were introduced onto the terpyridine ligand, as in complexes **12**−**17** (R = H) that were shown to display remarkably long-lived emissions at 25 °C with 0.085, 16.5, 12.1, 21, 64, and 0.6 μs excited lifetimes, respectively, attributed to their orbital parentage excited-state that has significant intraligand character.[51,81,82] Complex **16** showed emissions from ^{1}ILCT, ^{3}ILCT, $^3\pi-\pi^*$ (pyrene), and ^{3}MLCT.[51] Furthermore, solvents can influence the absorption and emission spectra *via* their polarity that can effect the MLCT state and/or quenching of the emission. The emission

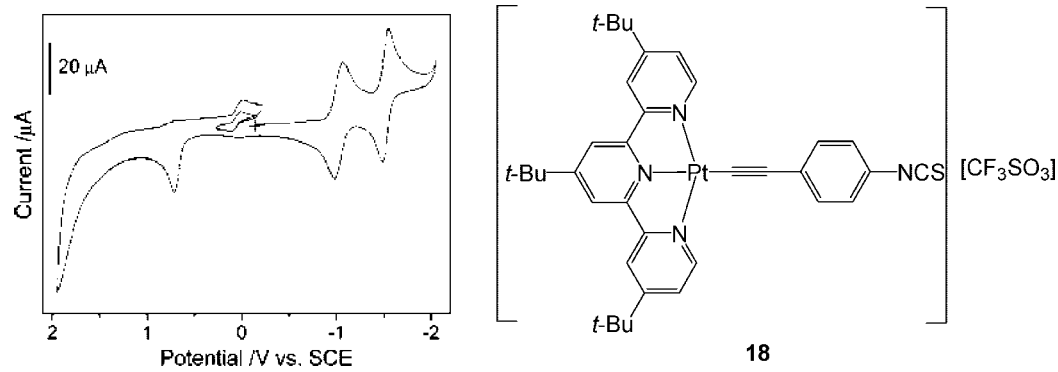

Figure 15. Cyclic voltammogram of complex **18** in MeCN with 0.1 M n-Bu_4NPF_6. (Reprinted with permission from ref 83. Copyright 2004 American Chemical Society).

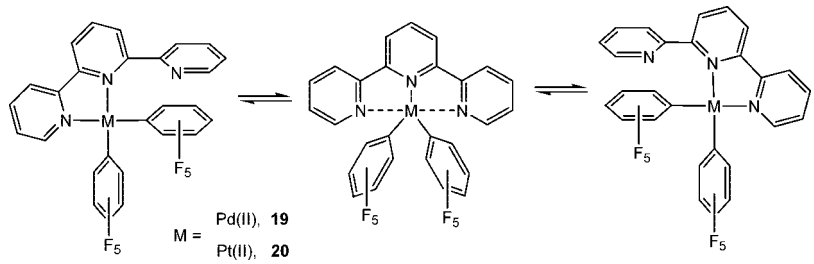

Figure 16. Interconverting structures of *cis*-[M(tpy)(C_6F_5)$_2$] complexes as a result of the 1,4-metallotropic fluxional shift *via* a 'tick-tock' twist mechanism.[86]

of **17** (R = H) was affected by the synergic effects of the MLCT, π(aryl)−p(B) charge-transfer interactions, and electron communication between the Pt(II)-tpy and arylborane moiety, which was confirmed by comparison to the non-emissive complex **17** (R = Me).[82]

2.6. Electrochemical Properties

The cyclic voltammogram of **18** displayed two quasi-reversible reductions at −0.99 and −1.46 V (vs SCE) and one irreversible oxidation at +1.41 V (Figure 15).[83] Two successive reductions were assigned to the terpyridine moiety mixed with some Pt(II) character. The irreversible oxidation was attributed to Pt(II) → Pt(III). It was suggested that this was caused by a quick decomposition of the unstable Pt(III) metal. Similar assignments have been reported for other Pt(II) terpyridine complexes.[3,49,51,56] Introducing different chemical groups to the terpyridine ligand did not affect the reduction potentials of the ligand, whereas a co-ligand connected to Pt(II) with higher electron-donating ability and aromaticity decreased the oxidation potential of the irreversible Pt(II) → Pt(III) reaction.[3,51,56,83]

The cyclic voltammogram of [Pt(tpy)(Cl)][PF_6] displayed two chemically reversible reductions (− 0.74 and − 1.30 V), followed by an irreversible process at − 2.2 V (vs AgCl/Ag).[84] The irreversible reduction at − 2.2 V became quasi-reversible at − 20 °C with − 2.1 V. Spectroelectrochemical studies and EPR spectroscopy of $[Pt(tpy)(Cl)]^+$ suggested that the unusual positive reduction potential shifts, when compared to similar Pt(II) complexes, were attributed to dimer formation stabilizing the reduced products relative to the monomeric $[Pt(tpy)Cl]^0$. The Pd(II) terpyridine complexes displayed only two irreversible terpyridine reductions.[60,85]

2.7. Fluxionality

Square-planar *cis*-[M(tpy)(C_6F_5)$_2$] [M = Pd(II) and Pt(II)], in which the terpyridine ligand acts as a bidentate chelator, displayed fluxional behavior with the terpyridine oscillating between equivalent bidentate modes described as a 'tick-tock' twist mechanism (Figure 16).[86] The ^{1}H NMR spectra of the Pd(II) **19** and Pt(II) **20** complexes at 0 and 70 °C, respectively, exhibited well-resolved absorptions that were fully assigned by selective decoupling experiments, thereby proving them to be bidentate terpyridine complexes. Moreover, the ambient temperature ^{19}F NMR experiments gave well-resolved spectra revealing two different C_6F_5 groups. The ^{1}H and ^{19}F NMR studies in the 0−140 °C range for the Pd(II) complex displayed extensive changes characteristic of the previously reported fluxional process associated with bidentate terpyridine complexes using Ru(II), Re(I), Pt(IV), Mo(0), and W(0) metals.[87–89]

New Pt(II) and Pd(II) complexes of 4′-substituted terpyridines were investigated to shed additional light on this mechanism and to give a better understanding to the fluxional process in these complexes.[90] The ^{1}H NMR spectrum of complex **21** revealed two different isomers **21a** and **21b**, as a result of its fluxional process, with a ratio of 65:35, respectively (Figure 17). The ^{1}H and ^{19}F 2D-NMR studies further supported the proposed 'tick-tock' twist mechanism.

The energy barriers, as $\Delta G^{\ddagger}$ values, for the fluxion processes for **19**−**21** were calculated to be 71, 94, and 100.6 kJ·mol^{-1}, respectively, with the aid of high temperature ^{1}H and ^{19}F NMR studies; simpler spectra were observed at higher temperatures further confirming a rapid fluxional process on the NMR time scale.[86,90]

Low-temperature ^{19}F NMR studies of **19**−**21** displayed splitting of the peaks that was interpreted to be due to the varying rates of rotation of the uncoordinated pyridine ring parallel to the C_6F_5 ring and orthogonal to the rest of the terpyridine moiety resulting in two different degenerate rotamers (Figure 18).[86,90] Furthermore, fluxional properties of the Pt(II) complex with a bis-terpyridine ligand were reported.[91] Fluxional behavior, *via* an oscillatory process, was observed in the Pd(II) complex with t-Bu_3-terpyridine,

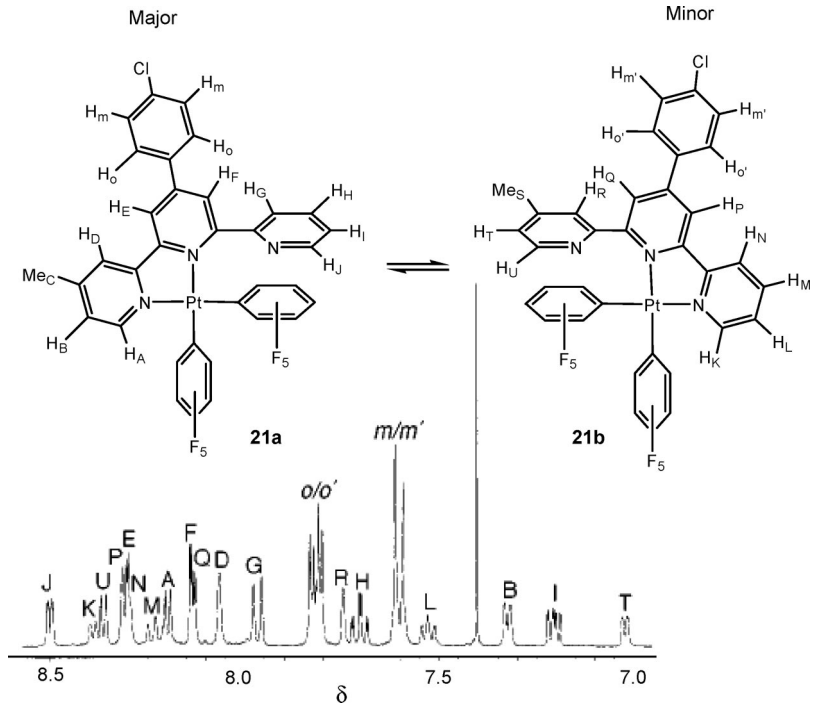

Figure 17. [1]H NMR spectrum (aromatic region) of complex **21** in $(CDCl_2)_2$ at 313 K. (Reprinted with permission from ref 90. Copyright 1998 The Royal Society of Chemistry).

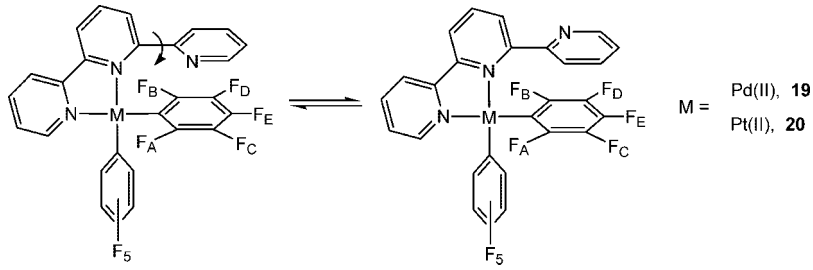

Figure 18. Proposed solution rotamers for complexes **19** and **20**.[86,92]

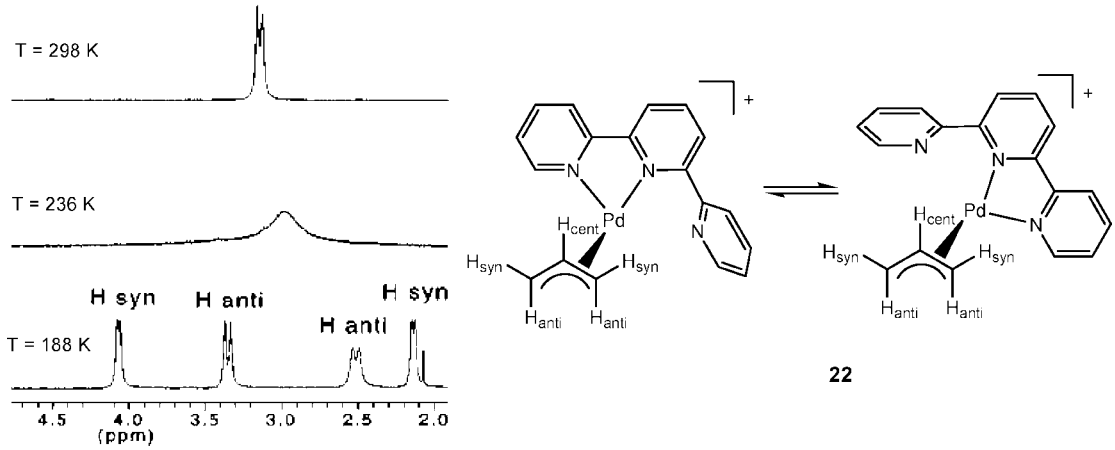

Figure 19. [1]H NMR and fluxional process of complex **22**. (Reprinted with permission from ref 93. Copyright 1996 American Chemical Society).

as a bidentate chelator, and two pentafluorophenyl rings were connected to Pd(II) metal through a tetrazenido moiety.[92] Rotation of both C_6F_5 rings was hindered with an energy barrier of 53.9 kJ·mol^{-1} at 293 K; this agreed with that of complexes **19** (47.0 kJ·mol^{-1}) and **20** (55.9 kJ·mol^{-1}).[86,92]

Another fluxional process promoted *via* a proposed 'tick-tock' twist mechanism in Pd(II) allyl complex **22** was detected by the coalescence of *syn* and *anti* allyl peaks into one doublet in the [1]H NMR in the range of 188−298 K and single crystal X-ray analysis (Figures 19A and 20).[93] However, the *syn*/*anti* interconversion in **23** and **24** suggested that it occurred *via* a classical η^3-η^1-η^3 mechanism (Figure 20B).[94]

The activation barriers ($\Delta G^{\ddagger} = 44-48$ kJ mol^{-1}) for an allyl-to-ring hydrogen exchange in complexes **22**−**24** were similar to $\Delta G^{\ddagger}$ of pyridyl hydrogen exchange suggesting that the two fluxional processes are possibly concerted.[93,94]

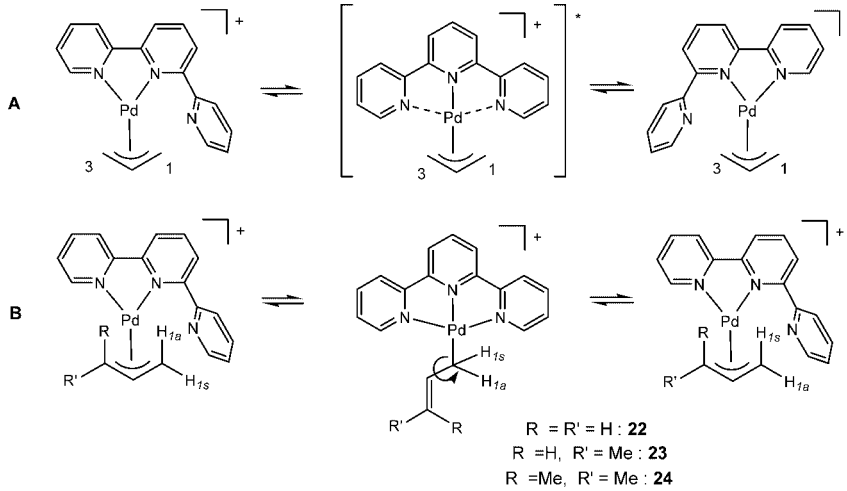

Figure 20. Fluxional process in complexes **22**−**24** occurred *via* (A) an oscillatory or 'tick-tock' twist and (B) classical η^3-η^1-η^3 mechanisms.[94]

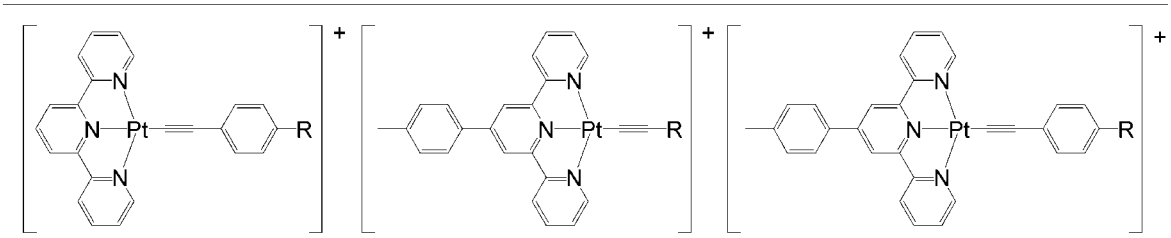

Number	R	Number	R	Number	R
25	H	**29**	CH_2OH	**33**	H
		30	$CH_2CH_2CH_3$	**34**	Cl
26	Cl			**35**	Br
		31		**36**	Me
27	Me			**37**	OMe
		32		**38**	NO_2
28	NO_2			**39**	NMe_2

Figure 21. Luminescent Pt(II) terpyridine complexes **25**−**39** with alkynyl moieties.[3,56,95]

3. Applications of Mononuclear Terpyridine Complexes

Structure−property relationships in square-planar terpyridine complexes possessing Pt(II), Pd(II), and Au(III) metals are contingent upon substituents that are introduced to the terpyridine ligand and/or the metal center, as a co-ligand, such as electron-donating and withdrawing, aromatic, H-bonding, cyclic, and biomolecules. As a result, novel photophysical, electrochemical, and optical properties can be accessed, thereby promoting new applications in optical limiting, molecular sensing, and switches, as well as construction of supramolecular architectures.

3.1. Luminescent Pt−Terpyridine Complexes

A new generation of remarkable photoluminescent Pt(II) terpyridine complexes **25**−**39** consisting of alkynyl groups, as co-ligands, has been described (Figure 21).[3,56,95] Absorption spectra of these complexes (at concentrations of 10^{-5}−10^{-2} M) displayed unique MLCT bands mixed with alkyne-to-terpyridine charge transfer (LLCT) bands in the range of 410−480 nm, which were confirmed by computational studies.[96] Emission spectra of complexes **25**−**39** revealed ^{3}MLCT/^{3}LLCT bands[96] at ca. 550−670 nm in MeCN or DCM at 25 °C.[3,56,95] Excited-state lifetimes (τ) and quantum yields (Φ_{em}) of **25** and **33** were significantly decreased by solvent change from DCM to MeCN revealing a solvent quenching process. The highest τ and Φ_{em} were observed for **29** and **30** in degassed DCM, that is, 14.6 μs and 0.30, and 10.3 μs and 0.25, respectively; it was postulated that the electron-donating alkynyl ligands increase the energy gap between ^{3}d−d and ^{3}MLCT excited states, and as a result, the radiationless decay of the ^{3}MLCT state, mediated by a low-lying ^{3}d−d state, became less prevalent.[56] The Pt(II) acetylene terpyridine complexes containing naphthalene groups, that is, **31**, displayed a similar emission behavior to the parent complex **25** but did not improve its excited-state lifetime.[47] Even though the acetylene bearing Pt(II) complexes proved to be luminescent at 25 °C, pendant groups and solvent were observed to have a dramatic effect on their excited-state lifetimes and quantum efficiencies.

Novel Pt(II) complexes **40**−**42** with aryl-modified and fused terpyridine ligands have been reported along with their luminescent properties at ambient temperature (Figure 22).[97–99]

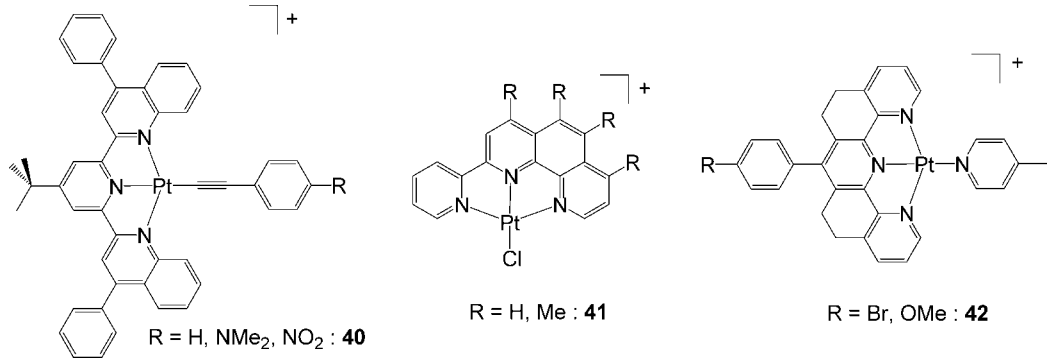

Figure 22. Structures of aryl-modified and fused terpyridine complexes **40**−**42**.[97–99]

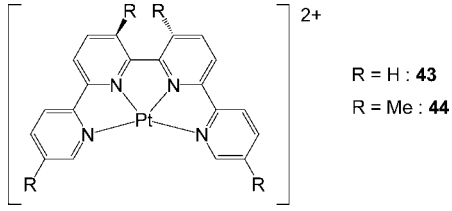

Figure 23. Quaterpyridine-based structures of complexes **43** and **44**.[100] The twisting motion in **44** is limited.

Complexes based on the architectures of **40** exhibited ^{3}MLCT/^{3}LLCT emissions similar to those of alkynyl-containing complexes **25**−**39**; the strongest emission was derived from complex **40** where R = NMe_2 (Φ_{Em} = 0.11 and τ = 2.4 μs).[99] All complexes of motif **41** possessing 0−4 methyl groups displayed photoluminescence in the range of 530−670 nm at 25 °C that was assigned to a combination of ^{3}ILCT/^{3}MLCT bands.[97] The quantum yield (Φ_{Em}) and excited-state lifetime (τ) of complex **41** dramatically increased from Φ_{Em} = 0.0031 and τ = 0.23 μs (R = H_4) to Φ_{Em} = 0.055 and τ = 9.3 μs (R = Me_4) in degassed DCM at 25 °C, which was rationalized by MO calculations, thereby unveiling the substituent effect on the HOMO and LUMO energy levels. It was suggested that luminescent complexes **41** and **42** could be useful as spectroscopic probes for biomacromolecules, while the architectures of **42** could serve as antitumor agents.[97,98]

Two unusually distorted square-planar Pt(II) quaterpyridine complexes **43** and **44** were each reported to possess N(1)−Pt−N(4, 1A) angles of 116° (Figure 23), and they both exhibited solid-state luminescence at ca. 700 nm with 0.24 μs excited-state lifetimes.[100] However, complex **44** exhibited a long-lived luminescence in degassed MeCN with an excited lifetime of τ = 7.0 μs at 25 °C, due to a hindered twisting motion in the ligand.

3.2. Molecular Stacking and Induced Self-Assembly

Among *N*-heterocyclic thiones, 2,5-dimercapto-1,3,4-thiadiazole (H_2dmct) and 2-amino-5-mercapto-1,3,4-thiazolate (Hamct) having five donor atoms in protonated and deprotonated forms can facilitate construction of mono- and multinuclear metal complexes. The Pd(II) complex **45** formed a dimeric structure through NH_2−NH H-bonding of Hamct, which was established by its single crystal structure (Figure 24A).[85] Moreover, the Pt(II) complex **46** formed a similar dimeric structure through NH−N H-bonding of the H_2dmct moiety, displayed possible π−π interaction between terpyridines, and did not have a strong Pt−Pt interaction (4.92 Å) (Figure 24B).[101] Complex **46** demonstrated an emission at ca. 620 nm that was attributed to a ^{3}LLCT band, whereas the Pd(II) complex **45** was nonemissive.[85,101] The cyclic voltammogram of **46** revealed an oxidation peak at +0.31 V, which was associated with the thiolate-dithio redox process.[101] It was suggested that these metal complexes might be useful redox reagents, since H_2dmct and Hamct were utilized as cathode material in high-performance lithium batteries.[102]

The novel linear chain-like structure consisting of one neutral [Pt(8-QNS)$_2$] (8-QNS = 8-quinolinethiolate) and two cationic [Pt(tpy)(Cl)]$^+$ units possesses a sandwich-like stacking of alternating strong Pt(II)−Pt(II) (3.35 Å) and weak Pt(II)−S (3.85 Å) interactions, where π−π (3.42 Å) interactions were distributed throughout the columnar structure (Figure 25A).[103] This particular structure did not exhibit an emission, since the stacked luminescent [Pt(tpy)Cl]$^+$ was quenched *via* charge-transfer to [Pt(8-QNS)$_2$].

A unique bis-terpyridine ligand in which two terpyridines were connected through a 2,7-di-*tert*-butyl-9,9-dimethylxanthene residue was complexed with only 1 equiv of Pt(II) metal in order to construct the mononuclear **47**, which was assembled as head-to-head columns *via* intermolecular Pt−Pt (3.42 Å) and π−π (3.69 Å) interactions (Figure 25B).[104] In general, the intramolecular distance of 4.0 Å did not appear to contribute to the stacking. The dinuclear complexes of this bis-terpyridine ligand with Pt−Pt and Pt−Ru metals will be considered later in this review.

Hatoun et al.[105] reported the synthesis of double salts **48**−**54** *via* treatment of [Pt(tpy)(Cl)][Cl] with salts containing Au(III) or Au(I) metals (Scheme 7). The products **48**−**54** were recrystallized in polar organic solvents and displayed an extended linear chain-like structure through 'metallophilic' interactions in their crystal packing, forming single-atom-wide wires. For example, the double salts **49** and **53** packed by means of Pt(II)−Au(I) metal interactions with distances of 3.28 and 3.34 Å, respectively (Figure 26). It was proposed that these salts could display interesting solid-state luminescent and conductive properties.

Yu et al.[106] reported that (n-Bu)$_4$NOH (TBAH) deprotonated poly(acrylic acid) (PAA) induced the self-assembly of complexes **25** and **55** *via* Pt−Pt and π−π interactions, which were supported by unique changes in their absorption and emission spectra (Figure 27). Color changes in solutions of **25** and **55** from yellow to light-brown and light-yellow to pink/red, respectively, were attributed to new MMLCT bands appearing at ca. 480/580 and 543 nm, respectively (Figure 27). New emission bands for complexes **25** and **55** at ca. 800 nm were assigned to a ^{3}MMLCT luminescence. The maximum intensity for the absorption and emission spectra of **25** and **55** was obtained with a ratio of 1:3:3

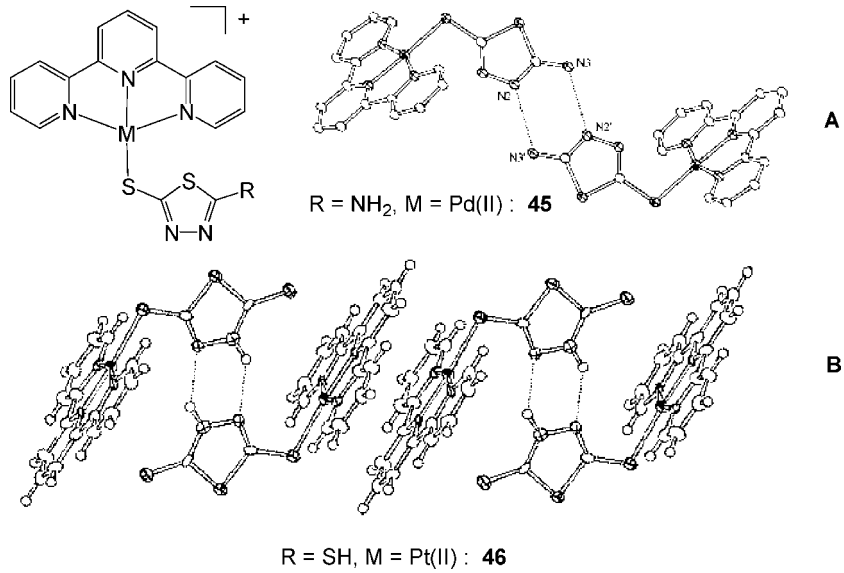

Figure 24. Single crystal structure of (A) H-bonded dimer **45**. (Reprinted with permission from ref 85. Copyright 2006 The Chemical Society of Japan); and (B) **46**. (Reprinted with permission from ref 101. Copyright 2003 The Royal Society of Chemistry).

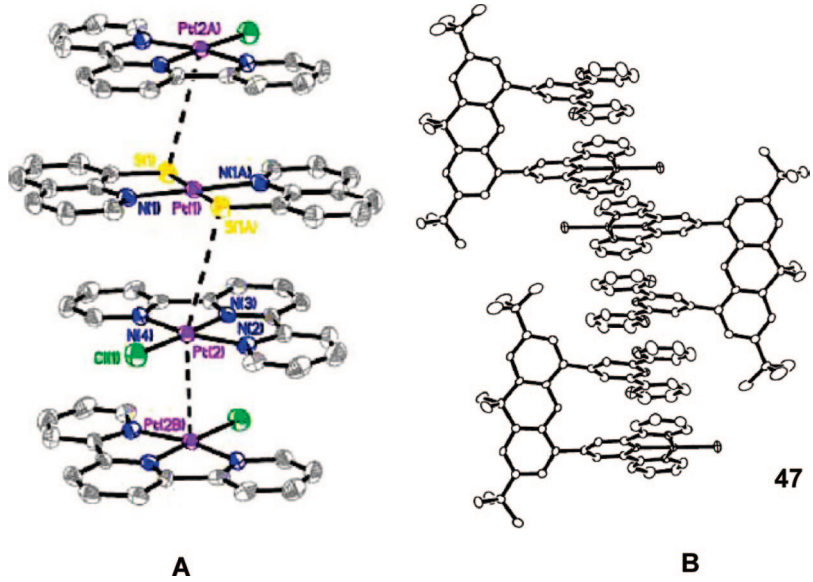

Figure 25. Molecular stacking of (A) linear chain-like $[Pt(8\text{-}QNS)_2][Pt(tpy)(Cl)]_2[(ClO_4)_2]$. (Reprinted with permission from ref 103. Copyright 2003 Elsevier). And (B) mononuclear bis-terpyridine complex **47**. (Reprinted with permission from ref 104. Copyright 2004 American Chemical Society).

Scheme 7. Synthesis of Double Salts with Metallophilic Interactions[105]

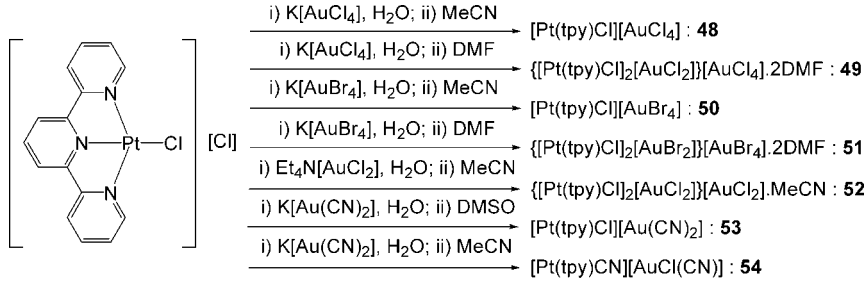

(complex/PAA/TBAH). No color changes were observed for **25** and **55** in only PAA or TBAH and mono-, di-, and tricarboxylic acids with TBAH, which suggested the need for high molecular weight and negatively charged promoters. Complex **56** with bulky *t*-butyl groups did not aggregate in PAA with TBAH.

Single-stranded nucleic acids, poly(L-glutamate), and poly(L-aspartate), which carry multiple negative charges in aqueous solution at pH = 7.5, were also utilized as templates to self-assemble complexes **55** and **57** that subsequently exhibited new MMLCT absorption and ^{3}MMLCT emissions bands.[107] It was suggested that, as the local concentration of the complex increased, the aggregation of these complexes was induced by d−d and $\pi-\pi$ interactions. Helical self-assembly of **55** and **57** associated with polynucleotides and poly(amino acids) displayed an induced circular dichroism (ICD) in

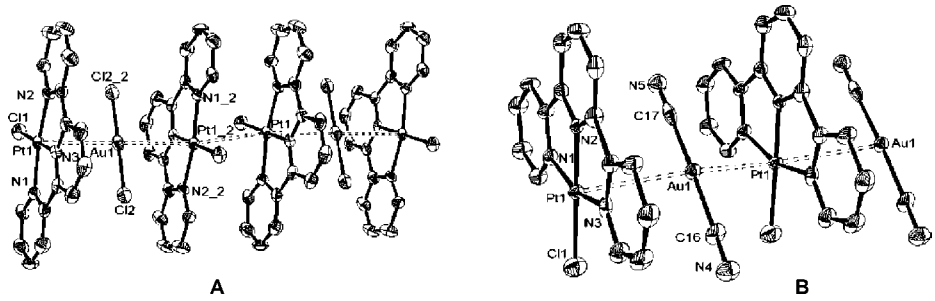

Figure 26. Crystal packing diagrams of (A) **49** and (B) **53**. (Reprinted with permission from ref 105. Copyright 2006 American Chemical Society).

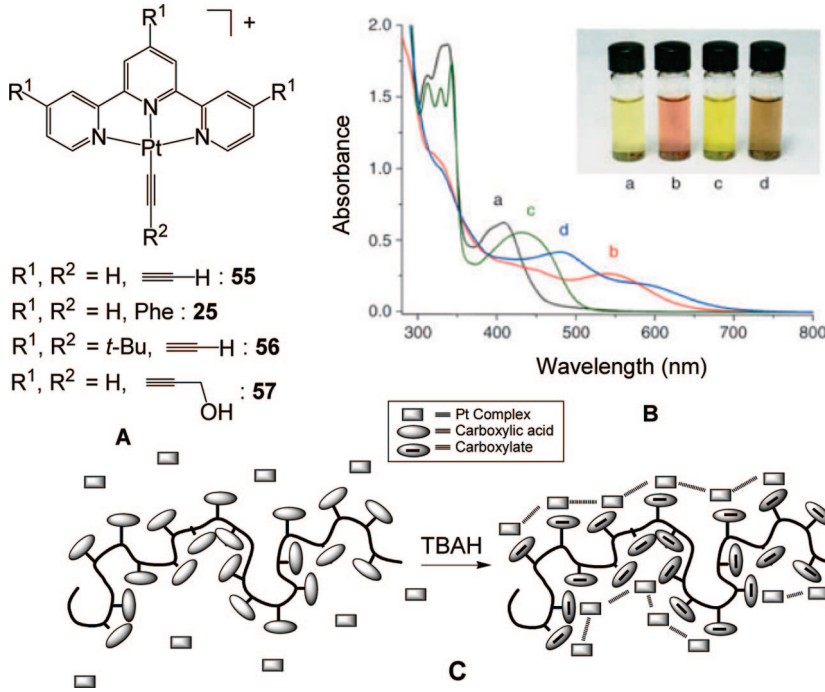

Figure 27. (A) Structure of **25** and **55**−**57**, (B) UV−vis spectra of (a) **55**, (b) **55** + PAA + TBAH, (c) **25**, (d) **25** + PAA + TBAH, and (C) aggregation of Pt(II) complexes. (Reprinted with permission from ref 106. Copyright 2005 Wiley-VCH).

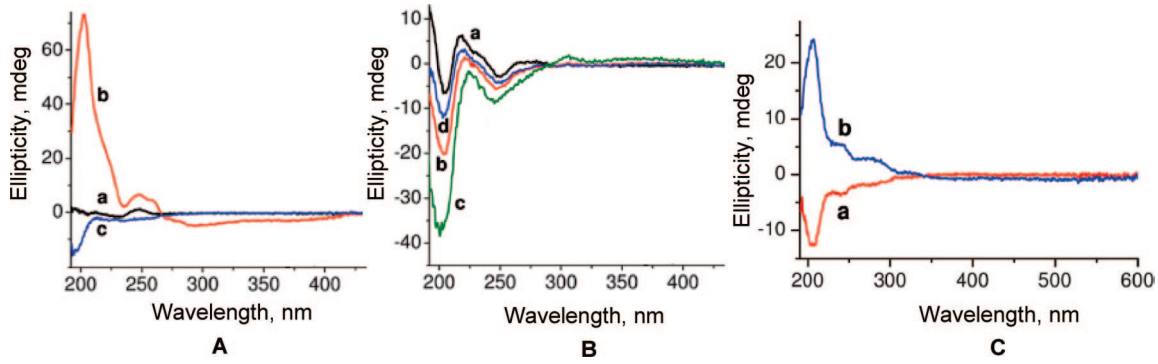

Figure 28. CD spectrum of (A) 90 μM of poly(dT)$_{25}$ (a) and its binding with 30 μM of complexes **57** (b) and **55** (c); (B) 90 μM of poly(dC)$_{25}$ (a) and its binding with 30 and 45 μM of complex **57** (b and c) and 30 μM of complex **55** (d); (C) 30 μM of complex **57** binding to 90 μM of poly(L-aspartate) (a) and poly(L-aspartate) (b) in 5 mM Tris·HCl buffer with 10 mM NaCl at pH = 7.5. (Reprinted with permission from ref 107. Copyright 2006 National Academy of Sciences, U.S.A.).

which its shape and intensity depended on the primary and secondary structures of the biopolymers (Figure 28). As an exception, aggregation of **57** was only observed at low concentrations with DNA, in that as the concentration of **57** increased the new MMLCT absorption and the emission bands disappeared, suggesting that the complex intercalated into DNA instead of electrostatic binding. Supramolecular self-assembly of $[Pt(tpy)Me]^+$ was also achieved by its electrostatic interaction with α-helical form of poly(L-glutamic acid) at pH = 4.5 as proven by ICD.[108]

Single crystal packing of complex **55** displayed dimorphism in dark-green and red forms, in which the former was crystallized from the slow diffusion of Et_2O vapor into MeCN solution of **55** and the latter into a diluted acetone solution (Figure 29).[109] The dark-green form of **55** revealed an extended, nearly perfect linear chain-like structure with

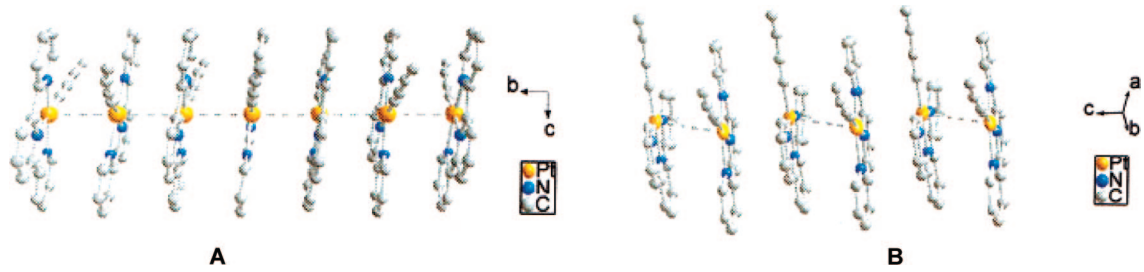

Figure 29. Perspective view of complex cation of **55** in (A) its dark-green form with an extended linear chain packing and (B) its red form with a dimeric zigzag arrangement. (Reprinted with permission from ref 109. Copyright 2002 American Chemical Society).

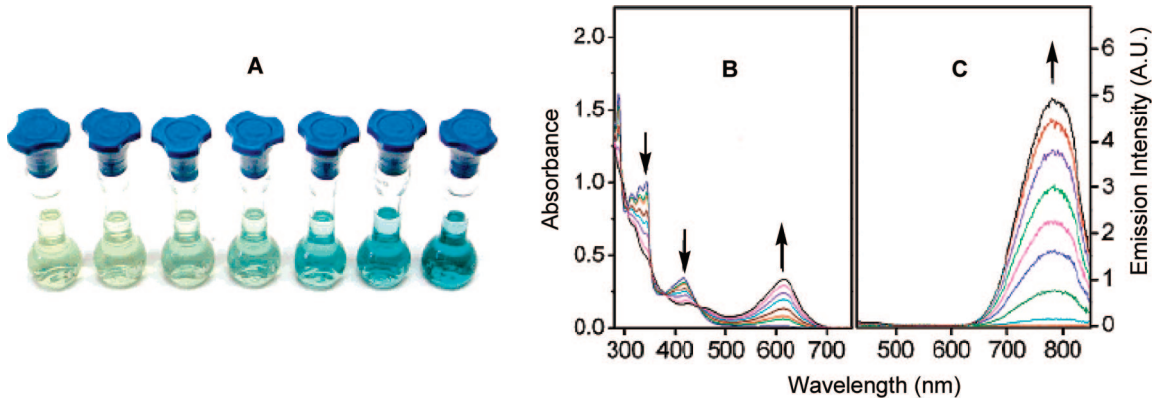

Figure 30. (A) Solution of **55** (1.47×10^{-4} M) in MeCN/Et_2O mixture displaying color changes upon increasing Et_2O composition (from left to right): 64, 68, 72, 74, 76, 78, and 80%, and (B) absorption and (C) emission spectra of those solutions. Darker blue solutions exhibit stronger emission. (Reprinted with permission from ref 109. Copyright 2002 American Chemical Society).

a Pt−Pt−Pt angle of 179.2° *via* equally distanced Pt−Pt interactions (3.388 Å) and partial stacking of terpyridine moieties (Figure 29A); however, the corresponding red form stacked as dimeric units with alternating Pt−Pt distances of 3.396 and 3.648 Å in a zigzag arrangement with Pt−Pt−Pt angle of 154.3° (Figure 29B). The single crystal structure of complex **56** was obtained but it did not show any short-range interactions due to the presence of the bulky *t*-Bu groups. Dimorphism of [Pt(tpy)(Cl)][Cl], which was crystallized in a yellow colored form from EtOH and a less-stable red form from 1 M HCl, was detected *via* X-ray powder diffraction.[110]

3.3. Molecular Sensors and Switches

Luminescent and colored Pt(II) terpyridine complexes, which are sensitive to their environment, such as concentration, solvent, acidity, and counter-ions, have been utilized as sensors for pH, ions, and solvents. The reversible responsive behavior of these complexes also suggests their potential use as molecular switches.

Yam et al.[109] reported remarkable color changes for complex **55** upon increasing the Et_2O content in either MeCN or acetone (Figure 30A). The absorption spectra revealed an intensity drop in the MLCT band at 415 nm and an incidental advancement of a new low energy band at 615 nm, in which the intensity was dramatically enhanced upon increasing the Et_2O composition (Figure 30B). Since **55** is insoluble in Et_2O, it was proposed that it aggregated into oligomeric forms that were confirmed by a new MMLCT absorption band at ca. 600 nm (Figure 30B) and ^{3}MMLCT emission band at ca. 785 nm (Figure 30C). These unique solvatochromic effects *via* the assembly of **55** can promote applications as adaptable probes of environmental changes.

In an elegant work, Wadas et al.[5] reported a nicotinamide Pt(II) terpyridine complex **58**, which possesses a reversible vapochromic behavior by changing its color from red to orange and displaying a shift in the emission band to higher energy upon exposure to MeOH vapors. These two forms of **58**, detected in the *same* single crystal, exhibited a dimeric form *via* H-bonding of nicotinamide residues (Figure 31A); however, they showed different packing arrangements (Figure 31B,C). The orange form of **58** revealed molecules of MeOH in the lattice and packed as a chain-like structure with a zigzag conformation of metal centers, in which the Pt−Pt−Pt angle was 126.7°; moreover, molecules of **58** were arranged in a head-to-tail fashion. However, the red form of **58** did not contain any MeOH residues in the lattice and packed as a pseudolinear extended chain structure, in which the Pt−Pt−Pt angle was 171.9° with a head-to-tail orientation. The distances of Pt−Pt metals and terpyridine moieties in the red form were 3.3 and 3.5 Å, respectively, revealing strong d−d and $\pi-\pi$ interactions, whereas the orange form of **58** possessed weak interactions since those distances were more than 3.6 Å.

The red form showed a solid-state emission band at 660 nm at 25 °C, which was assigned to the ^{3}MMLCT; however, the orange form displayed an emission at 630 nm that was attributed to ^{3}MLCT since it had only weak d−d and $\pi-\pi$ interactions.[5] The emission band of the red form was at 660 nm, which shifted to higher energy at 630 nm upon exposure to MeOH, whereas upon *in vacuo* heating, the emission band shifted back to its original position (Figure 32A). This reversible vapochromic response cycle was repeated (five times) with no noticeable chemical decomposition of **58**. Moreover, complex **58** was immobilized on filter paper and irradiated with long-wave UV light at ambient temperature; color changes from pink to yellow were visually observed in the presence as well as in the absence of MeOH (Figure 32B). This notable vapochromic behavior of complex **58**

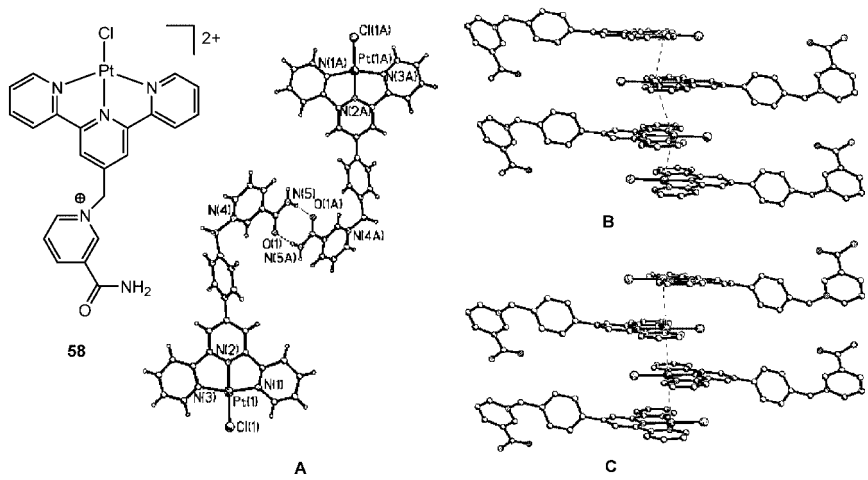

Figure 31. (A) H-bonded dimer, (B) zigzag stacking of orange form, and (C) nearly linear packing of red form of complex **58**. (Reprinted with permission from ref 5. Copyright 2004 American Chemical Society).

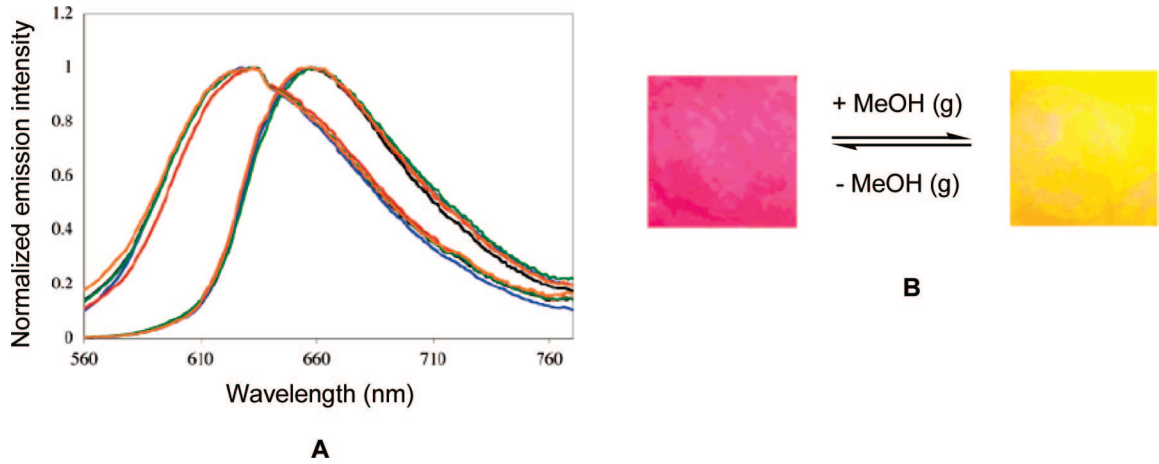

Figure 32. (A) Solid-state emission of **58** acquired from cycling through exposure and removal of MeOH in air multiple times. (B) Luminescence of **58** observed by eye in the presence and absence of MeOH. (Reprinted with permission from ref 5. Copyright 2004 American Chemical Society).

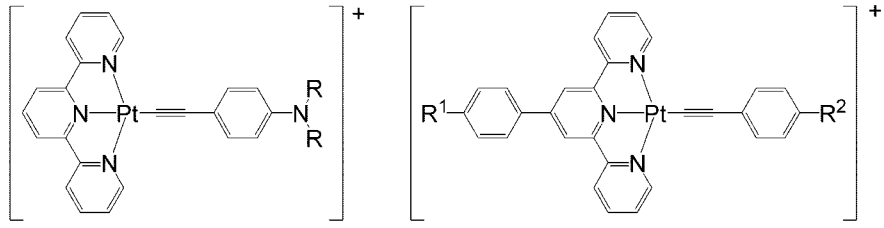

Number	R	Number	R^1	R^2
59	H	**39**	Me	NMe_2
		62	NMe_2	H
60	Me	**63**	NMe_2	NMe_2
61	$CH_2CH_2OCH_3$	**64**	NMe_2	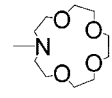

Figure 33. Chemical structures of pH sensitive complexes **39** and **59**−**64**.[111–113]

could be utilized as a chemosensor or MeOH-induced molecular switch.

Wong et al.[111] reported a remarkable reversible color changes in complexes **59**−**61** (Figure 33) upon consecutive addition of *p*-toluenesulfonic acid and NEt_3 (Figure 34A). The absorption spectra of **61** displayed a low energy band at 546 nm that was assigned to the LLCT of amine-containing acetylene moiety-to-terpyridine mixed with some

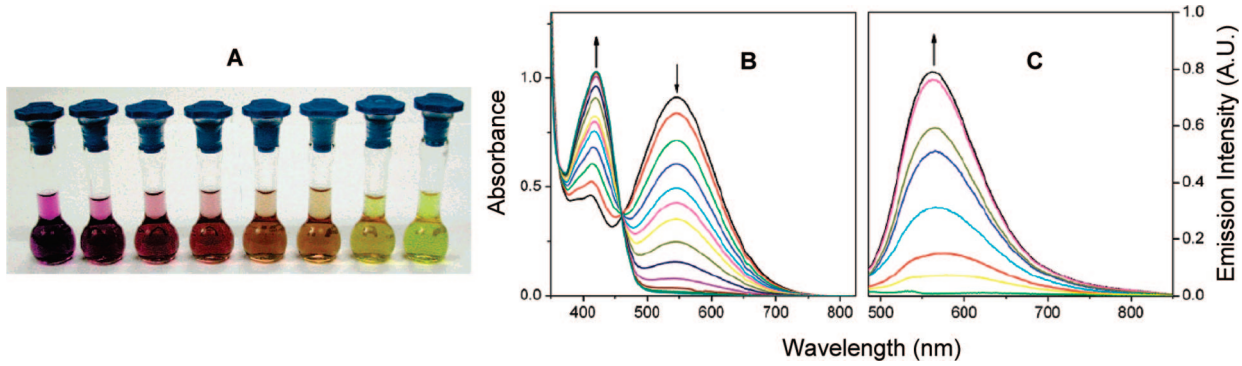

Figure 34. (A) Solution of **61** (1.8×10^{-4} M) in MeCN with various concentrations of *p*-toluenesulfonic acid (from left to right): 0, 0.11, 0.16, 0.18, 0.22, 0.27, 0.33, and 44 mM, displaying dramatic color changes, and (B) absorption and (C) emission spectra of those solutions. (Reprinted with permission from ref 111. Copyright 2005 American Chemical Society).

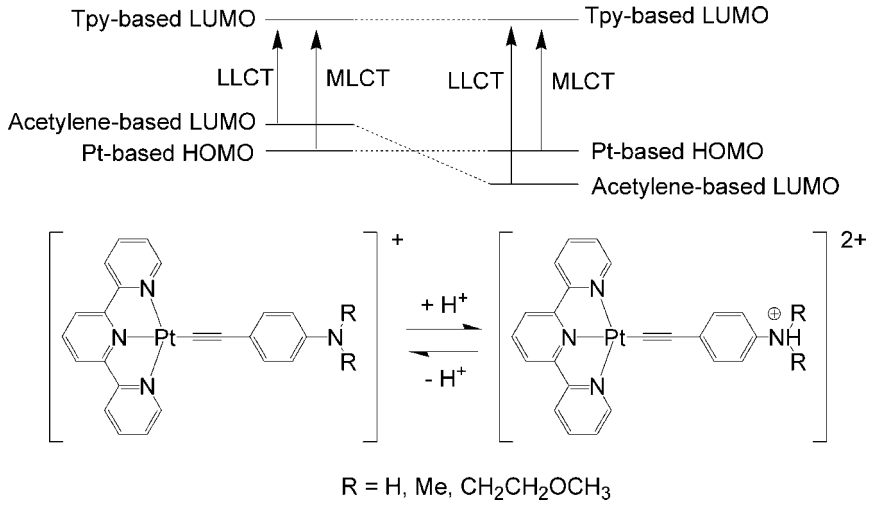

Figure 35. Proton-induced deactivation of LLCT in complexes **39** and **59**−**61**.[111–113]

MLCT character and a high energy band at 412 nm that was attributed to MLCT. Upon addition of *p*-toluenesulfonic acid, the intensity of the LLCT band was dramatically decreased and the intensity of the MLCT band was increased with a clear isobestic point at 460 nm indicative of complete conversion of the complexes to their corresponding protonated forms (Figure 34B). Moreover, upon protonation of complexes **59**−**61**, a new emission band was observed at ca. 600 nm, which was attributed to the ^{3}MLCT band.

Yang et al.[112,113] observed similar reversible absorption and emission behavior for complexes **59**−**61**, as those of complex **39**, upon sequential addition of [HBF_4], as a proton source, and NEt_3, as base. It was suggested that the low energy LLCT state was deactivated *via* protonation, which led to a dominant MLCT absorption in the UV−vis spectra and the formation of the formerly quenched ^{3}MLCT emission band by low energy nonemissive ^{3}LLCT (Figure 35). Furthermore, complex **62** containing a -NMe_2 group, which was positioned on the terpyridine moiety instead of the alkynyl co-ligand, as in **39**, displayed a new low energy ILCT band from the amino-substituted phenyl to the terpyridine mixed with the MLCT band at 490 nm. Upon addition of acid, the intensity of the ILCT band of **62** was monotonically decreased, leaving a less intense MLCT band at 450 nm; moreover, the formation of a new ^{3}MLCT emission band was also observed.[113]

Introducing an amino group on both the terpyridine ligand and acetylene co-ligand as in complex **63** promoted a mixed ILCT/LLCT absorption band, which was subsequently deactivated *via* addition of [HBF_4].[113] The UV−vis titration spectra of **63** with 1 equiv of acid revealed that the LLCT excited-state was deactivated, showing a decrease in absorbance at the low energy band $\lambda > 520$ nm with well-defined isobestic points at 445 and 520 nm (Figure 36A), then 1 additional equiv of the acid deactivated the ILCT excited state, displaying a decrease in absorbance at 490 nm with a well-defined isobestic point at 430 nm and leaving a MLCT band in the range of 380−550 nm (Figure 36B). Furthermore, even though the ^{3}LLCT and ^{3}ILCT states of **63** were not emissive, the fully protonated form of **63** exhibited luminescence from its ^{3}MLCT band at 575 nm. Transient absorption spectroscopy of **39**, **62**, and **63** confirmed the LLCT, ILCT, and MLCT excited states as well as their reversible interconversion to each other under acidic and basic conditions. These studies suggested new promising applications as calorimetric, luminescent pH sensors, and proton-driven molecular switches could be developed by tuning spectroscopic properties of these type of acetylene- and amino-containing Pt(II) terpyridine complexes.

Tang et al.[8] and Yang[112] et al. attached an azacrown ether group to the alkynyl co-ligand of the Pt(II) complex **65** (Figure 37) and investigated its ion binding properties. Significant color changes were observed for azacrown **65** upon addition of Li^+, Na^+, Mg^{2+}, Ca^{2+}, Cd^{2+}, and Zn^{2+} metal ions, depicted in Figure 38A.[8] The absortion spectra of **65** displayed a low energy band at 548 nm, which was assigned to a combination of the LLCT band possessing mixed MLCT character. Upon addition of Cd^{2+} and Ca^{2+} ions, the LLCT absorption disappeared and an increased intensity of MLCT was observed (Figure 38 B,C). It was

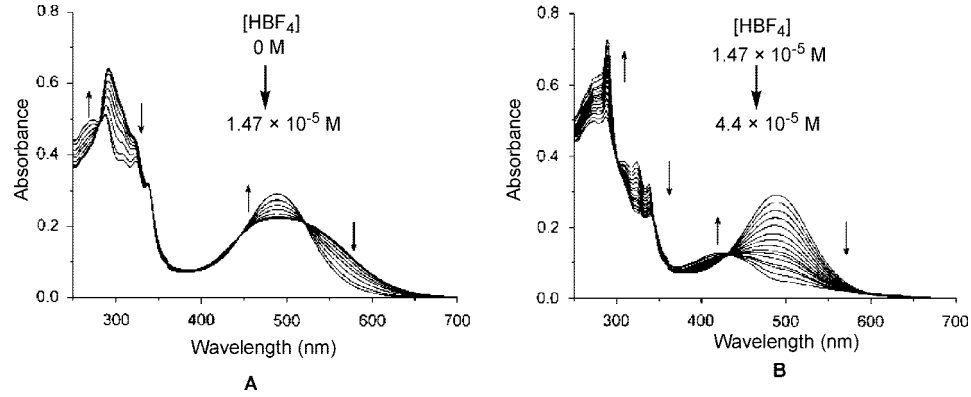

Figure 36. Changes in absorption of complex **63** (1.47×10^{-5} M) upon addition of various concentration of $[HBF_4]$ in MeCN. (A) $[HBF_4]$, $0-1.47 \times 10^{-5}$ M; (B) $[HBF_4]$, $1.4-4.4 \times 10^{-5}$ M. (Reprinted with permission from ref 113. Copyright 2007 Wiley-VCH).

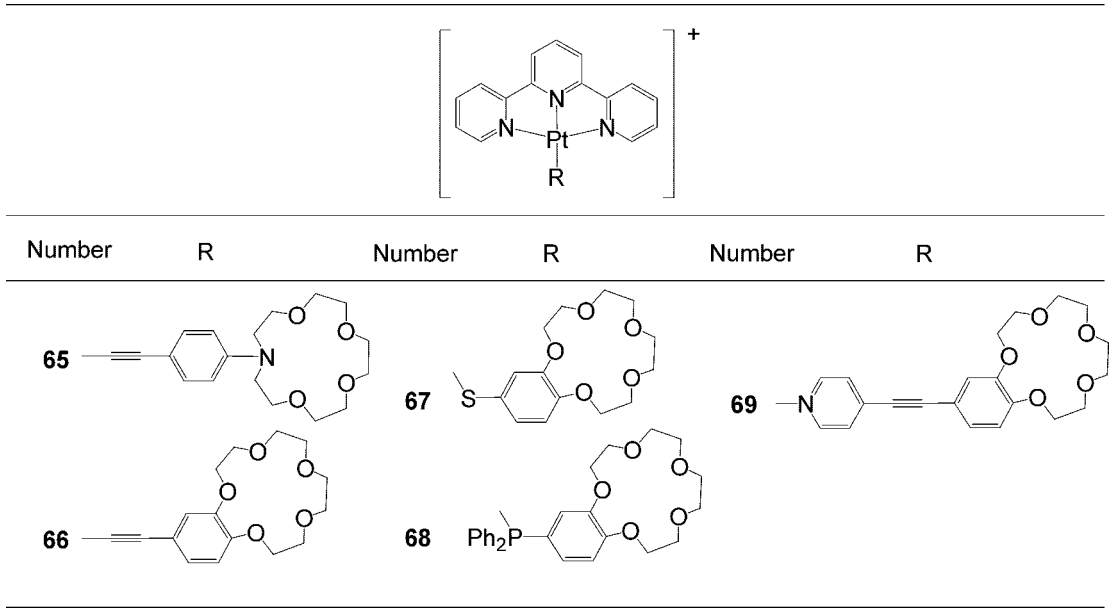

Figure 37. Chemical structures of ion binding complexes **65**−**69**.[3,8,114,115]

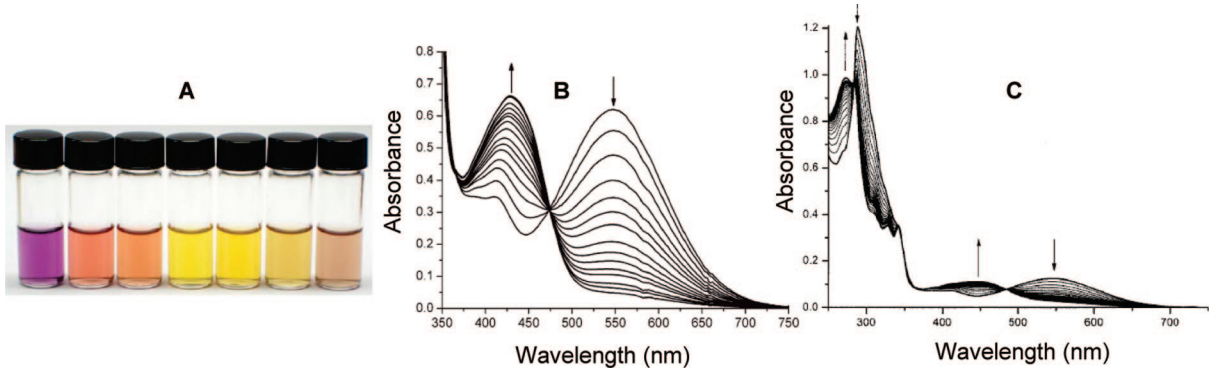

Figure 38. (A) Solution of **65** (2.2×10^{-4} M) in MeCN with variety of metal ions (from left to right): no metal, Li^+, Na^+, Mg^{2+}, Ca^{2+}, Cd^{2+}, and Zn^{2+}; (B) changes in absorption of **65** upon addition of various concentrations of Cd^{2+}. (Both reprinted with permission from ref 8. Copyright 2005 The Royal Society of Chemistry); and (C) Ca^{2+}. (Reprinted with permission from ref 112. Copyright 2004 Wiley-VCH).

suggested that ions, bound to the azacrown moiety, decreased its electron-donating ability and eventually switched the LLCT band of **65** to higher energy where the ion's charge density played an important role in the switching process. For example, the Li^+ ion did not cause complete deactivation of LLCT but rather caused the band to blue-shift due to its low charge density. Complex **65** did not show any emission upon ion binding, which was explained by possible ion dissociation caused by the excited Pt(III) center being more electrophilic than Pt(II).[112] Binding stoichiometry and stability constants of the ions were also reported.

Han et al.[113] introduced an azacrown ether to the alkynyl co-ligand and an amino group to the terpyridine ligand, as in complex **64**. The UV−vis spectra of **64** revealed an alkyne-based LLCT and aminophenyl-to-terpyridine-based ILCT absorptions, which were deactivated by successive additions of Ca^{2+} cation and $[HBF_4]$, respectively, showing similar behavior to complex **63**.

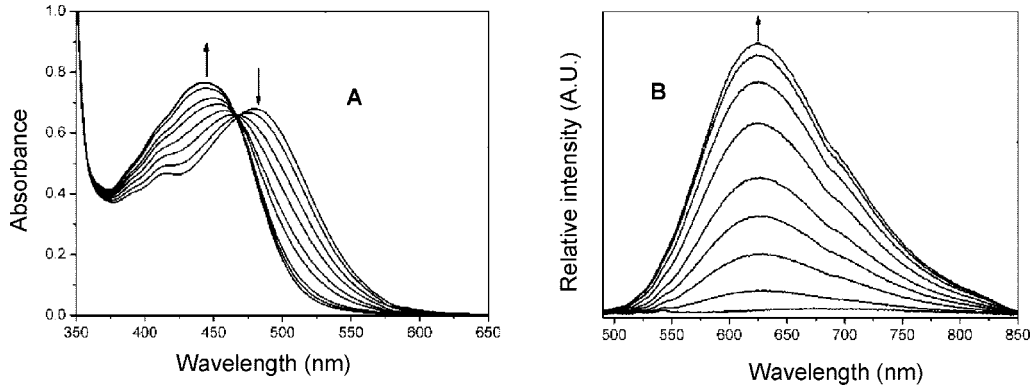

Figure 39. (A) Changes in absorption of **66** with various concentrations of Ca^{2+} and (B) changes in emission of **66** with various concentrations of Mg^{2+}. (Reprinted with permission from ref 8. Copyright 2005 The Royal Society of Chemistry).

Scheme 8. Synthesis of Pseudorotaxane 74, Proton-Induced Interchange of 71 and 72[70]

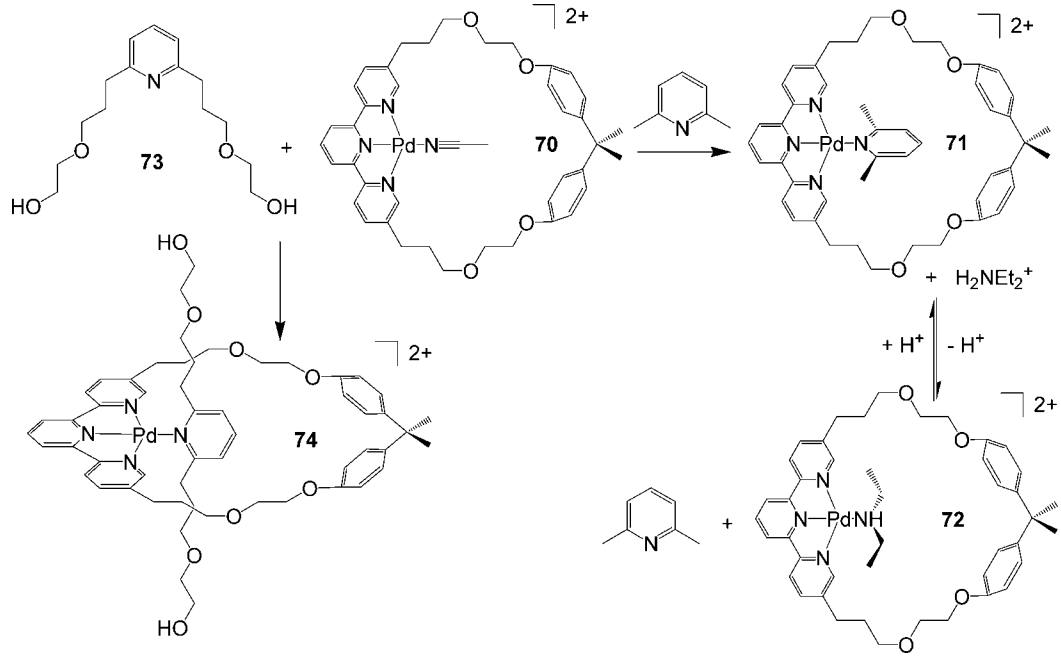

The novel benzo-15-crown-5 demonstrating strong binding affinity toward alkali and earth alkali metal ions was connected to Pt(II) terpyridine complexes **66**−**69** through a variety of bridging co-ligands.[3,8,114,115] Complex **66**, containing an acetylene coligand, displayed a low energy LLCT band with some MLCT mixing, which was blue-shifted upon the addition of Ca^{2+} ion (Figure 39A).[8] A new emission band at ca. 650 nm was observed for **66** upon addition of Mg^{2+} ion, which was assigned as ^{3}MLCT band that was previously quenched by photoinduced electron transfer from ^{3}LLCT. The Li^+, Na^+, K^+, Mg^{2+}, Ca^{2+}, Cd^{2+}, and Zn^{2+} ions were all proven to bind to the benzo-crown moiety of complex **66** by mass, UV−vis, and NMR spectroscopy.[3,8] The ion binding ability of benzo-crown and azacrown containing Pt(II) complexes offered novel approaches to ion sensors for alkali and earth alkali metals.

Hamann et al.[70] reported the preparation of pseudorotaxane **74** *via* threading a string-like molecule **73** through a 35-membered macrocycle **70** that contained a terpyridine moiety with a square-planar Pd(II) metal center, as the template (Scheme 8). Macrocycle **71** containing 2,6-lutidine, as a co-ligand, was converted to macrocycle **72** containing $HNEt_2$, as a co-ligand, in acidic media and *vice versa*. It was proposed that an interexchange of the macrocycles by controlling the acidity of the media could open a new avenue to proton-driven molecular machines.

Yutaka et al.[116] reported the azobenzene-conjugated Pt(II) terpyridine complexes **75** and **76** with pyridine and Cl as co-ligands, respectively (Figure 40A). The azobenzene moiety in **75** and **76** was shown to be trans in the single crystal structures; isomerization to the cis-orientation was easily accomplished upon irradiation with visible light. Photoinduced trans-to-cis isomerization was clearly observed in absorption spectra of **76** by formation of low energy azo $n \rightarrow \pi^*$ band at 470 nm with two isobestic points, indicative of complete isomerization (Figure 40B). Moreover, a new emission band for **75** was observed at ca. 600 nm at 77 K upon photoirradiation, which confirmed the formation of the *cis*-isomer, since the *trans*-isomer did not show any emission at 77 K. It was proposed that these complexes could be utilized as multifunctional materials, since their emission spectral and *trans*−*cis* conformation changes are closely related.

3.4. Photocatalytic Activities

Zhang et al.[117] incorporated a photoluminescent complex **77** (Figure 41) into a Nafion membrane (Nafion-Na^+) and

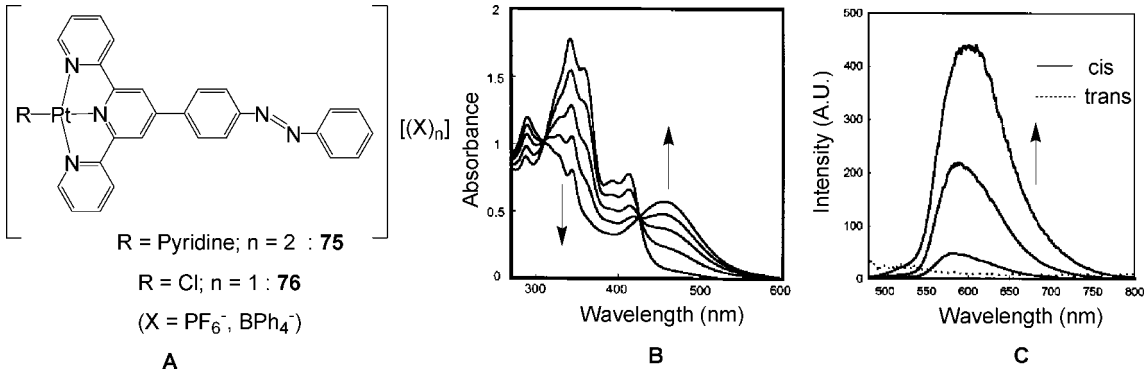

Figure 40. (A) Chemical structures of azobenzene containing **75** and **76**; (B) changes in absorption of **76** in DMF (4.2×10^{-5} M) upon irradiation at 366 nm light for 25 min; (C) changes in emission of **75** in EtOH/MeOH/DMF = 5:5:1 (v/v) at 77 K upon irradiation with 366 nm light for 8 min. (Reprinted with permission from ref 116. Copyright 2002 American Chemical Society).

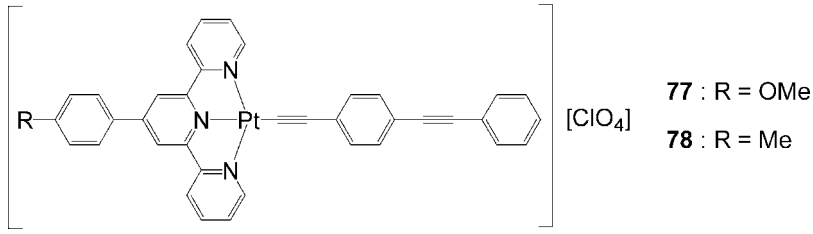

Figure 41. Chemical structures of photosensitizers **77** and **78**.[117]

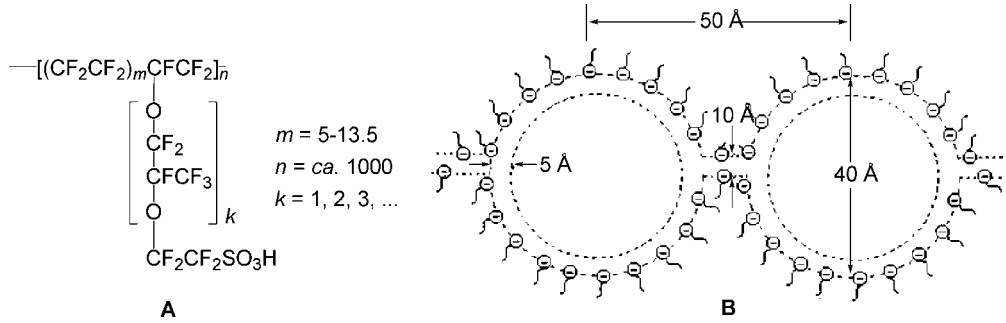

Figure 42. (A) Chemical structures of Nafion membranes and (B) their two-phase cluster network model. (Reprinted with permission from ref 118. Copyright 1980 American Chemical Society).

utilized this system as a photosensitizer to generate transient singlet oxygen ($^1O_2$) for the oxidation of alkenes in aqueous or organic solutions. The Nafion membrane possesses a perfluorinated backbone and short pendant chains terminated by sulfonic acid groups (Figure 42).[118] When Nafion is swollen in H_2O or MeOH, the structure of Nafion resembles that of an inverse micelle. The hydrated R-SO_3^- (R = alkyl) headgroups are clustered within H_2O-containing pockets (ca. 40 Å in diameter) that are interconnected with each other by short channels within the perfluorocarbon matrix. This H_2O-swollen Nafion can incorporate high concentrations of aromatic hydrocarbons and organic dyes;[119,120] as well, the oxygen concentration in this Nafion is 10 times greater than in organic solvents.[121,122] Complex **77** was chosen as the photosensitizer, since it can absorb light in the visible region, photochemically generate $^1O_2$, is positively charged, and contains aromatic ligands, which can easily be incorporated into Nafion membrane *via* hydrophobic and electrostatic interactions.[117] Thus, this **77**/Nafion system was specifically designed for photooxidation purposes.

The detection of $^1O_2$ production from the **77**/Nafion system was established by its immersion in O_2-saturated MeOH and then the addition of a radical scavenger 2,2,6,6-tetramethylpiperidine (TMP), followed by irradiation ($\lambda > 450$ nm) for 100 s. The formation of $^1O_2$ occurred *via* energy transfer between molecular O_2 and triplet excited-state of **77**; then, the corresponding stable free radical nitroxide (TMPO) product was detected by EPR spectroscopy (Figure 43).[117]

Three substrates, 7-dehydrocholesterol (**79**), α-pinene (**82**), and cyclopentadiene (**85**), were oxidized *via* $^1O_2$, generated by the **77**/Nafion system in aqueous and organic solutions (Scheme 9).[117] The cholesterol **79** was converted to **80** in 95% yield along with traces of **81** based on the consumption (20%) of the starting material *via* **77**/Nafion immersed in MeOH. It was suggested that solvent quenching of $^1O_2$ caused the low quantum yield, so changing the solvent to CD_3OD and D_2O increased up to 95% the consumption of the starting material. To reduce the cost of the deuterated solvent used in the process, **77**/Nafion system was swollen in the deuterated solvents and the reactions were performed in DCM. As a result, α-pinene (**82**) was converted to **83** in DCM with D_2O-swollen **77**/Nafion in 90% yield, based on the consumption of **82**, and then treating the peroxy **83** with $NaHSO_3$ afforded alcohol **84**. Furthermore, cyclopentadiene (**85**) underwent [4 + 2] cycloaddition with $^1O_2$, generated by D_2O-swollen **77**/Nafion in DCM, to give epidioxide **86** with quantitative yield based on the consumption of **85**; **86** was readily converted to diol **87** upon addition of thiourea. Advantages of this photocatalyst are that products were easily

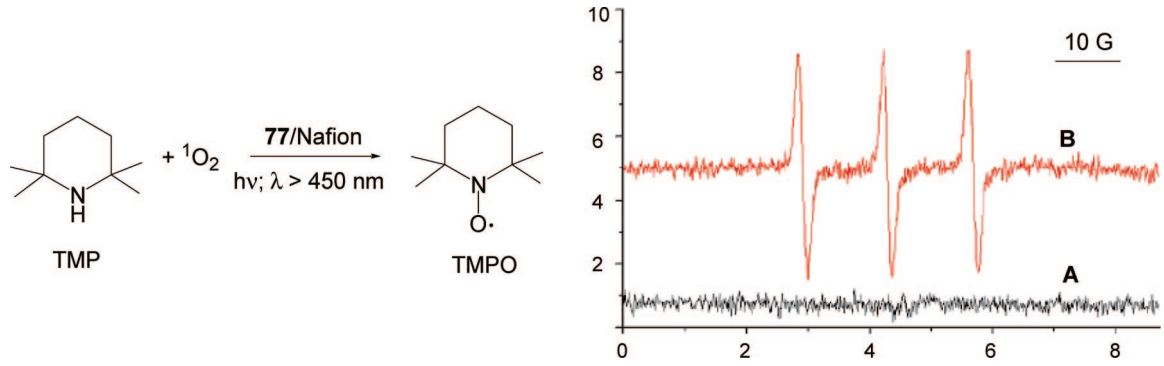

Figure 43. EPR spectrum of nitroxide radical generated of O_2-saturated TMP/MeOH solution, where **77**-incorporated Nafion was immersed (A) in the dark and (B) after the sample was irradiated for 100 s. (Reprinted with permission from ref 117. Copyright 2003 American Chemical Society).

Scheme 9. Photooxidation of Alkenes 79, 82, and 85 by 77/Nafion System[117]

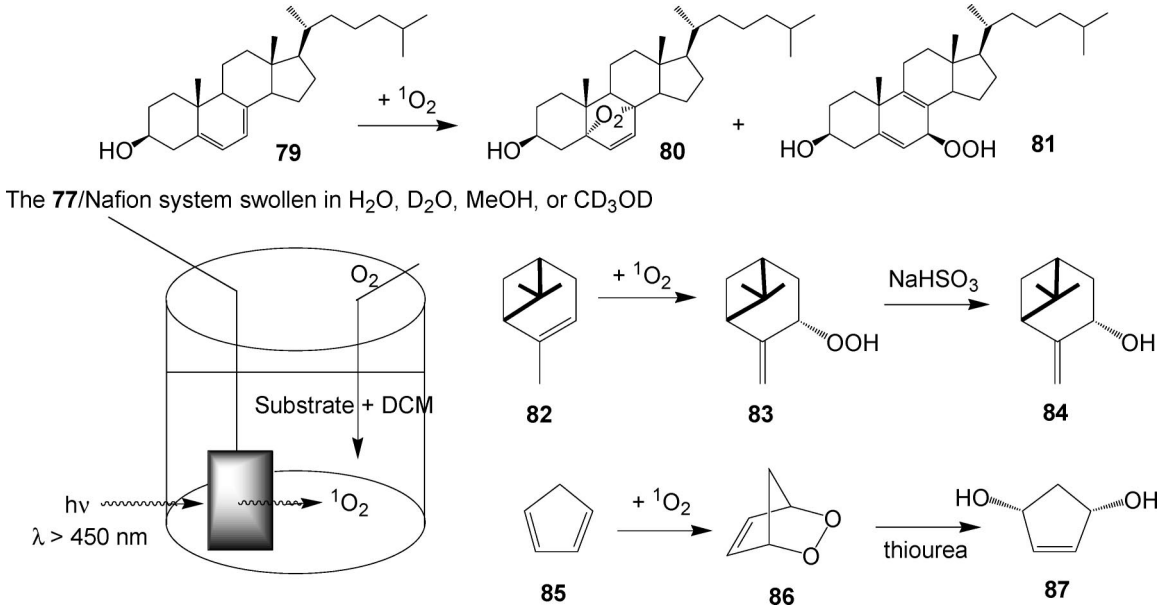

Scheme 10. Proposed Mechanism for Ketone Deprotection[123]

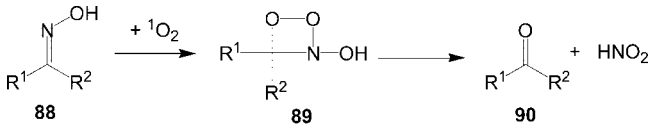

separated from the reaction mixture and the catalyst can be recycled without any significant loss of activity.

Yang et al.[123] reported that D_2O-swollen **77**/Nafion system in oxygen saturated DCM and MeCN successfully removed the oxime protecting groups **88**, affording the corresponding carbonyl derivatives **90** in good to excellent yields (57−94%, Scheme 10). It was suggested that oxime deprotection occurred through an $^1O_2$ mechanism. The oximes **88** underwent [2 + 2] cycloaddition with $^1O_2$ to give the unstable dioxetane intermediates **89**, which decomposed under the reaction condition to give desired **90**. The nitrite byproduct was detected using acidic ferrous sulfate. A possible direct electron-transfer mechanism for this deprotection was not possible since none of the oximes used in that study could quench the strong ^{3}MLCT-based photoluminescence of **77** at ca. 620 nm in degassed MeCN at 25 °C.

Li et al.[124] reported that the nonemissive Pt(II)-quaterpyridine complex **43** displayed a ^{3}IL-based strong photoluminescence upon incorporation to the Nafion membrane (Nafion-Na^+) at 25 °C, suggesting that oligomerization of **43** was possible *via* partial $\pi-\pi$ stacking of quaterpyridine ligands. A significant decrease in absorption was observed for **43** upon photoirradiation at 25 °C in aerated MeCN; however, the photochemically unstable **43**, when attached to Nafion matrix, did not display any change in absorption spectra upon photolysis in MeCN for 10 h. The **43**/Nafion system was utilized as a photosensitizer to generate $^1O_2$, which oxidized *trans*-stilbene to PhCHO and *trans*-1,2-dimethoxystilbene to $PhCO_2Me$ in quantitative yields.

Abe et al.[125] reported the electrochemical and photochemical reduction of H^+ to H_2 *via* the $[Pt(tpy)(Cl)]^+$ complex. In an electrochemical process, the BPG or ITO electrode-coated Nafion membrane, incorporating the $[Pt(tpy)(Cl)]^+$, was analyzed by potentiometric electrolysis at an applied potential of −0.95 V (vs Ag/AgCl) in H_2O at pH 5.9; moreover, CV, UV, and XPS studies confirmed the reduction process. In the case of the photochemical process, a system consisting of (1) $[Pt(tpy)(Cl)]^+$, as an active catalyst, (2) $[Ru(bpy)_3]^{2+}$, as sensitizer, (3) methyl viologen (MV^{2+}), as an acceptor, and (4) EDTA, as a sacrificial donor, was utilized to reduce H^+ to H_2. In that the reduction mechanism is not clearly understood, it was suggested that a methyl

Scheme 11. Mechanism for H_2 Formation from H_2O *via* 33/MV^{2+}/TEOA/Colloidal Pt[9]

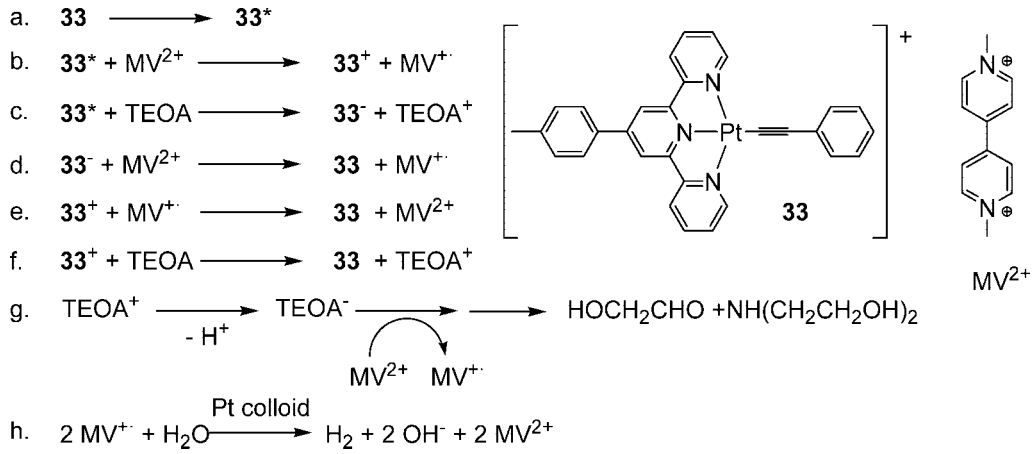

Scheme 12. Photooxidation of Hantzsch Dihydropyridines by Pt(II) Complexes[126]

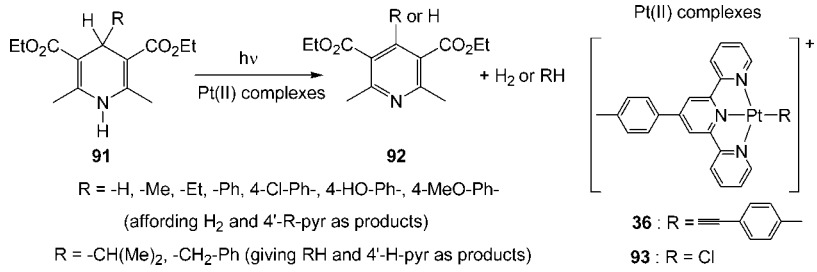

viologen radical cation ($MV^{+\bullet}$) was involved in the process, since the reduction potential of H^+/H_2 (−0.54 V vs Ag/AgCl at pH = 5.9) is slightly lower than $MV^{2+}/MV^{+\bullet}$ (−0.64 V vs Ag/AgCl); this radical was observed throughout the reaction.

Du et al.[9] reported the photocatalytic generation of H_2 from H_2O using complex **33**, as a sensitizer, MV^{2+}, as an acceptor, triethanolamine (TEOA), as a donor, and colloidal Pt (5−7 nm size stabilized by sodium polyacrylate), as a catalyst. Both MV^{2+} and TEOA successfully quenched the strong photoluminescence of **33** at ca. 500−800 nm *via* oxidative (Scheme 11[b]) and reductive (Scheme 11[c]) processes, respectively, in degassed MeCN. The degassed solution of **33** with MV^{2+} was colorless after irradiation suggesting the rapid and efficient back-electron-transfer (Scheme 11[e]) from $MV^{+\bullet}$ to MV^{2+} upon quenching. However, when both quenchers were mixed with **33**, a deep blue color solution was generated indicating the formation of the methyl viologen radical ($MV^{+\bullet}$) *via* reductive quenching (Scheme 11[c],[d]), followed by an oxidative decomposition (Scheme 11[g]) of TEOA and another electron-transfer from $MV^{+\bullet}$, which afforded glycoaldehyde and diethanolamine. Addition of colloidal Pt particles to the **33**/ MV^{2+}/TEOA mixture caused an electron transfer from $MV^{+\bullet}$ to the colloidal catalyst, and then, proton reduction at the Pt surface generated H_2 from H_2O at different pHs; the best yield was obtained at pH 7 with extended irradiation times up to 4 h (Scheme 11[h]).

Zhang et al.[126] reported a remarkable photocatalytic oxidation of the Hantzsch 1,4-dihydropyridine (DHP) and its 4-alkyl- and 4-aryl- derivatives **91** *via* the Pt(II) complexes **36**, **77**, **78**, and **93** producing pyridines **92** and H_2 or RH in quantitative yields with high catalytic turnover (Scheme 12). Although the mechanism of this photooxidation is not well-understood, in a mechanistic study by Narayana-Prabhu and Schmehl,[127] the transient absorption spectroscopy of **34** with various quenchers (NEt_3, *N*-methylphenothiazine, DHP, etc.) in degassed MeCN gave convincing evidence for the production of a one-electron-reduced Pt(II) intermediate; however, it was previously suggested[126] that DHP behaves as a H-atom donor in its photooxidation.

3.5. Miscellaneous Applications

Unique long-lived emissions with high quantum yields of complexes **31**−**33**, **35**, **37**−**39**,[95,128] **77** and **78**,[128] and **94**−**97** (Figure 44)[95,129] attracted a great deal of interest as optical limiting materials since the structurally analogous Pt-ethynyl[130–132] complexes displayed such properties. The linear absorption spectrum of these complexes revealed the lowest energy MLCT/LLCT band at ca. 560 nm and their transient absorption difference spectrum (e.g., Figure 45A) exhibited a positive band over 500 nm, suggesting a stronger excited-state absorption than that of the ground state, which can promote a reversible saturable absorption and is beneficial for optical limiting of nanosecond laser pulses.[95,128,129] To demonstrate this phenomena, nonlinear transmission measurements were conducted at 532 nm using 4.1 ns (fwhm) laser pulses with concentrations of the solution calibrated to achieve the same linear transmission of 70% for complexes **77**, **78** and **94**−**97**.[95,129] Significant deviation from a linear absorption curve for these complexes proved the existence of optical limiting properties in which **97** displayed the strongest optical limiting for nanosecond laser pulses at 532

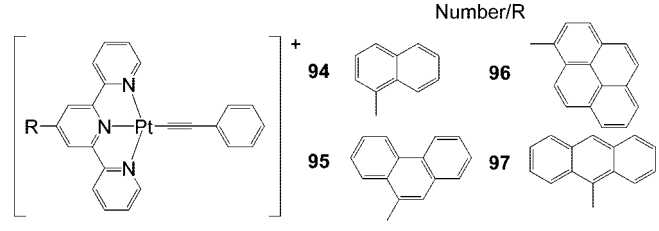

Figure 44. Chemical structures of optical limiting complexes **94**−**97**.[95,129]

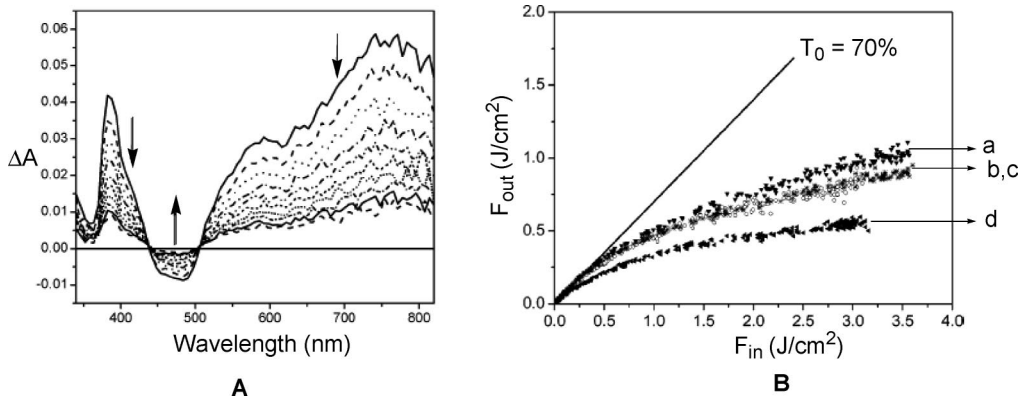

Figure 45. (A) Transient absorption difference spectra of complex **33** in Ar degassed MeCN solution at 25 °C following 355 nm excitation with 160 ns time increments, (Reprinted with permission from ref 95. Copyright 2005 American Chemical Society) and (B) optical limiting of complexes (a) **95**, (b) **94**, (c) **96**, and (d) **97** in a 2 mm cell for 532 nm, 4.2 ns laser pulses with linear transmission of the solutions as 70%. (Reprinted with permission from ref 129. Copyright 2006 American Chemical Society).

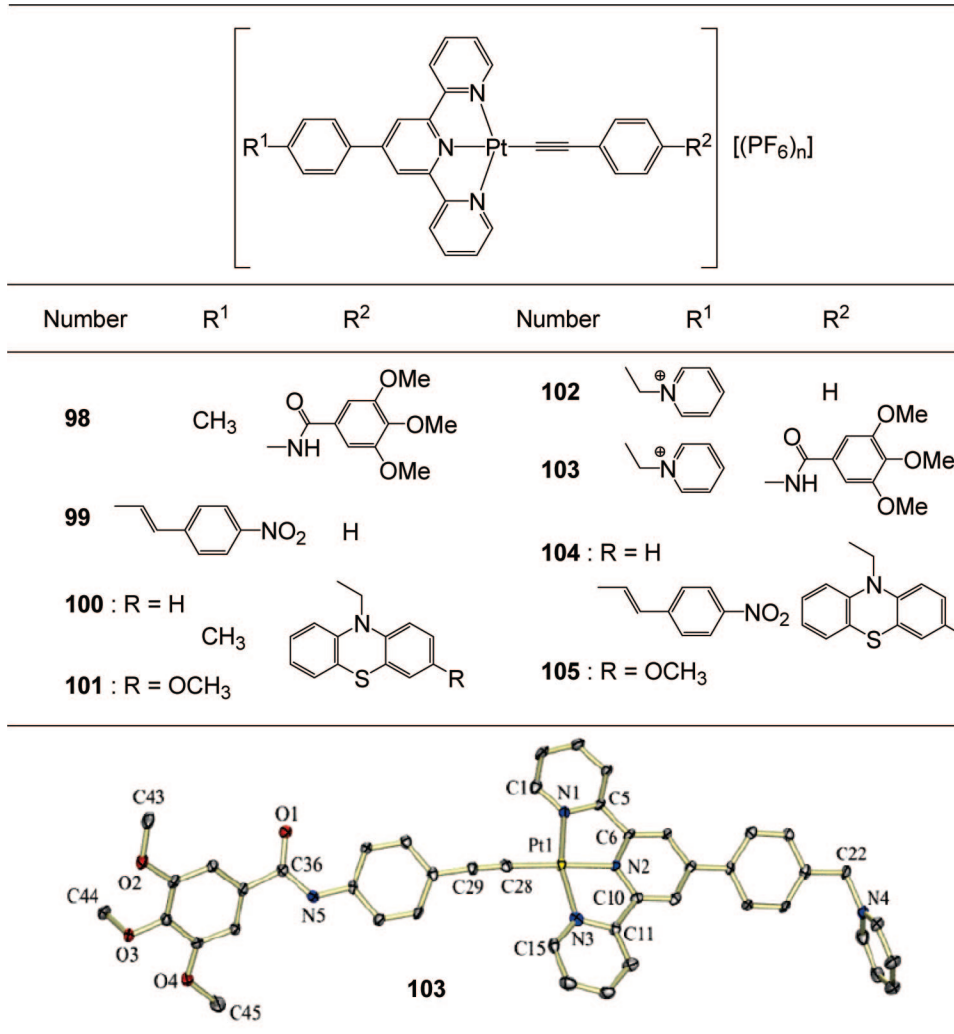

Figure 46. Structures of complexes **98**−**105** and single crystal structure of **103**. (Reprinted with permission from ref 38. Copyright 2005 American Chemical Society).

nm (Figure 45B), thus, offering it as a promising material for this application.[129]

Chakraborty et al.[38,39] reported the novel donor-chromophore-like **98**, **100**, **101** (D-C), chromophore-acceptor-like **99** and **102** (C-A), and donor-chromophore-acceptor-like **103**−**105** (D-C-A) systems (Figure 46), in which the Pt(II) terpyridine complex acted as a chromophore, pyridinium and 4-nitrophenylvinyl acted as acceptors, and trimethoxybenzene, phenothiazine (PTZ), and methoxyphenothiazine (MTZ) acted as donors. Specifically, the D-C-A systems were designed to mimic a photosynthetic reaction center by achieving photoinduced charge separation. Even though the parent complex **33** is luminescent in MeCN solution at 25 °C with a 700 ns excited-state lifetime; complexes **98**−**105** displayed complete reductive quenching of the chromophore ^{3}MLCT emission, except for **99** and **102**,

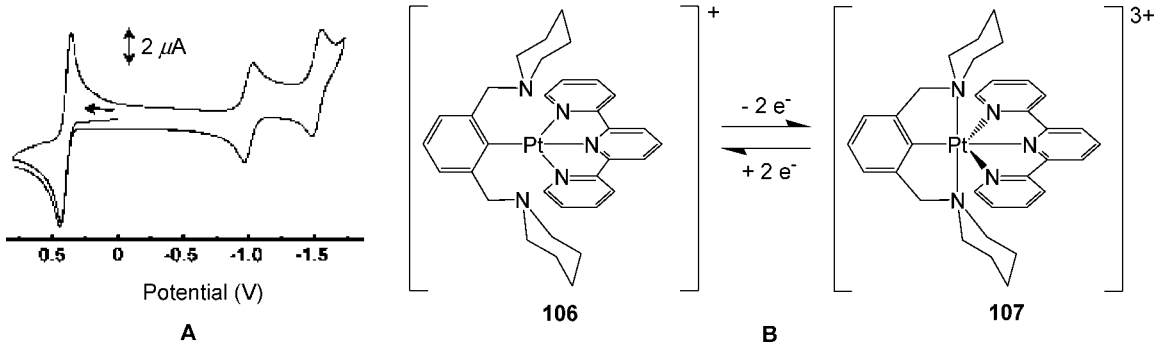

Figure 47. Cyclic voltammogram of complex **106** (A) and the potential two-electron oxidation process involved in transformation from the square-planar Pt(II) **106** to the octahedral Pt(IV) **107**. (Reprinted with permission from ref 133. Copyright 2003 American Chemical Society).

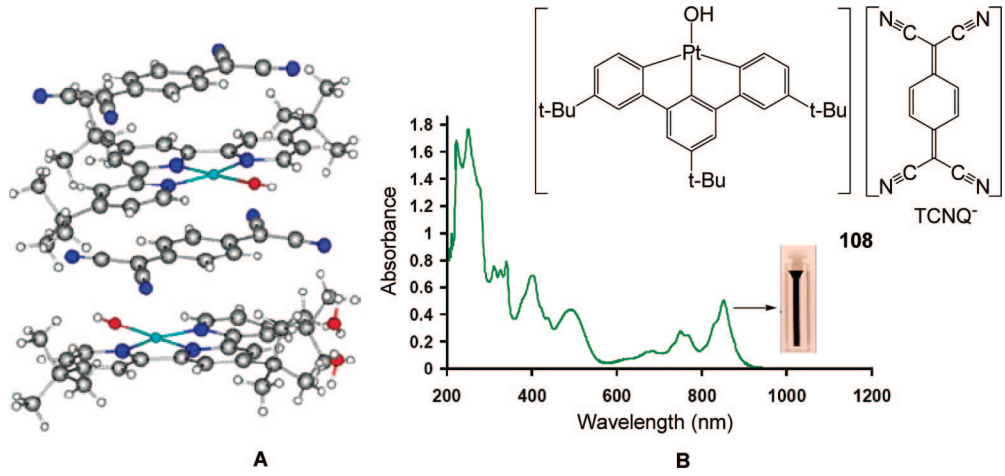

Figure 48. Single crystal packing (A) and UV−vis spectra with concentration of 5×10^{-5} M in DCM at 25 °C (B) of [Pt(*t*-Bu$_3$-tpy)(OH)][TCNQ] (**108**). (Reprinted with permission from ref 134. Copyright 2006 American Chemical Society).

which were weakly emissive. A single crystal X-ray structure of complex **103** confirmed the distorted square-planar geometry for Pt(II) atom and edge-to-edge D-A separation of 27.95 Å; however, it did not exhibit any short-range interactions.[38] Cyclic voltammograms of trimethoxybenzene, PTZ and MTZ containing **98**, **100**, **101**, and **103**−**105** revealed donor-based oxidations, whereas pyridinium- and nitro-containing **99** and **102**−**105** displayed acceptor- and terpyridine-based reductions. Transient absorption (TA) spectroscopy of complexes **98**−**103** revealed that trimethoxybenzene acted as a reductive donor; however, the pyridinium groups failed to perform as an acceptor. Finally, 230 ns long-lived charge separation in D-C-A **104** and **105** was achieved.[39]

A remarkable electrochemical, nearly reversible, two-electron oxidation of a Pt(II) metal center from square-planar bis-piperidine containing complex **106** was achieved *via* an outer-sphere oxidation mechanism giving rise to a possible octahedral Pt(IV)-containing product **107** (Figure 47).[133] The CV of bis-piperidine **106** displayed two irreversible reductions at −0.98 to −1.50 V versus Ag/AgCl, which were assigned to terpyridine reduction and the almost reversible oxidation at 0.4 V, attributed to the Pt(II) → Pt(IV) oxidation. It was suggested that the lone pair electrons of the piperidyl moieties are critical to the stabilization of the octahedral Pt(IV) metal center; this was affirmed by the irreversible oxidation of the protonated analogue of **106** under similar conditions. Moreover, the Pt(II) complexes consisting of either the terpyridyl or piperidine moieties did not yield any similar oxidation process to that of **106**.

Chen et al.[134] reported unique black absorbers with continuous UV−vis-NIR absorptions by simply changing the counterion and the co-ligand of the [Pt(*t*-Bu$_3$-tpy)(Cl)][Cl] to [Pt(*t*-Bu$_3$-tpy)(R-PhS)][TCNQ] complexes (TCNQ = 7,7,8,8-tetracyano-quinodimethane; R = 4-Me, 4-Cl, 3,4-diMe, and 2,5-diOMe) for possible conducting, magnetic, and solar cell applications. The crystal structure of **108** revealed short-range $\pi-\pi$ interactions between Pt(II) cation and TCNQ anion with interplanar distances of 3.5 Å (Figure 48A). The singly charged $TCNQ^-$ counterion was reduced to the doubly charged $TCNQ^{2-}$ anion, present in the crystal structure, which was confirmed by a new absorption band at 490 nm (Figure 48B). Thus, a charge delocalization was proposed in **108** *via* the partial oxidation of the Pt(II) cation and reduction of the TCNQ anion. The UV−vis spectra of **108** revealed a MLCT band at ca. 400 nm and $TCNQ^-$ structured absorption in the NIR region. Moreover, the aromatic thiol containing Pt(II) complexes exhibited dramatic red-shifted LLCT absorption bands at ca. 560 nm when compared to MLCT band of **108**.

Ziessel et al.[135,136] reported a new generation of Pt(II) terpyridine complexes **109**−**122** in which the Pt(II) metal was connected to different aromatic groups *via* an acetylene bridge (Figure 49). A simple and straightforward CuI-catalyzed reaction between $[Pt(R_3\text{-tpy})(Cl)]^+$ (R = H, *t*-Bu) and the acetylene connected to the aromatic ligands afforded

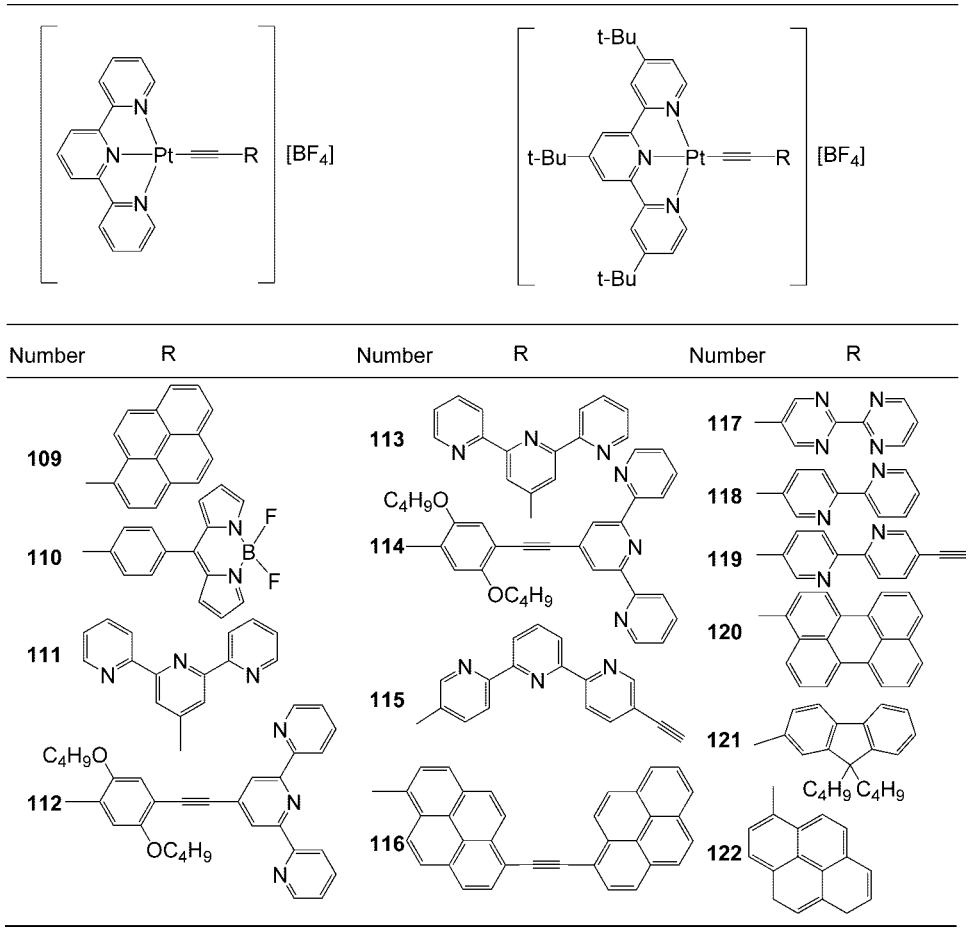

Figure 49. Chemical structures of **109**−**122**.[135,136]

the desired complexes **109**−**122**, except for complex **110**, which was prepared by a reaction of trimethylsilyl (TMS)-protected acetylene, attached to boraindacene, with $[Pt(tpy)(Cl)]^+$ in the presence of anhydrous K_2CO_3. Solubility problems with **109** and **111** were overcome by either introducing *t*-Bu groups on the terpyridine moieties or 1,4-bis-(*n*-butoxy)benzene, as a connector. The single crystal X-ray structure of **112** revealed noticeable $\pi-\pi$ interactions between different aromatic rings separated by ca. 3.6 Å.[136] The low energy absorption bands of **109**−**122** were attributed to MLCT and LLCT bands.

Cyclic voltammograms of **114**, **118**, and **121** exhibited two quasi-reversible reductions in the range from −0.97 to −1.56 V versus ferrocene (+0.38 V) in DCM, which were assigned to terpyridine reduction that was slightly mixed with some Pt(II) metal character.[135,136] The Pt(II) complexes **111**−**114** containing free terpyridines were later coordinated with Fe(II) or Zn(II) forming octahedral complexes in order to construct trinuclear molecular rods; similarly, **115** and **119** attached to free acetylenes were reacted with another $[Pt(tpy)Cl]^+$ to form the homonuclear dimetallic Pt−Pt structures.

4. Metallo-Supramolecular Terpyridine Architectures

Different multinuclear supramolecular systems were achieved using square-planar Pd(II) and Pt(II) complexes with properly designed mono- and bis-terpyridine ligands. Evident $\pi-\pi$ interactions between aromatic moieties and d−d orbital interaction between metal centers in these systems promoted interesting solid-state packing, remarkable photophysical, and optical properties. Some of the multimetallic complexes were further utilized as molecular building blocks to construct higher-ordered two- and three-dimensional supramolecular self-assemblies, for example, rectangles and trigonal prisms. Cavities inside the supramolecular architectures offered possible molecular recognition centers by means of reversible host−guest interactions leading to the construction of molecular switches.

4.1. Dyads and Triads

Yam et al.[137] reported luminescent acetylene-containing molecular rods **123** (n = 1, 2, 4) capped with Pt(II) terpyridine complexes (Figure 50). The *t*-Bu groups were introduced onto the terpyridines to overcome solubility problems. Single crystal structures revealed the Pt−Pt distances in **123**, proceeding from the molecular to nanoscale, as 5.16 (n = 1), 7.71 (n = 2), and 12.83 Å (n = 4). The absorption spectra of **123** displayed low energy MLCT bands mixed with some LLCT character and high energy IL $\pi-\pi^*$ bands attributed to the acetylene and terpyridine ligands. Emission spectra of **123** exhibited a strong luminescence in the range of 550−625 nm in the solid-state and solution upon excitation at λ > 400 nm; this was assigned to the dominant ^{3}MLCT mixed with ^{3}LLCT/^{3}IL bands. Ziessel et al.[135] connected two Pt(II) terpyridine complexes through a linear diacetylene linker, consisting of 2,2′-bipyridine, as in **125**, and a 120° juxtaposed diacetylene bridge, attached to the terpyridine 5,5″-position, as in **126**, to investigate their energy and electron transfer abilities.

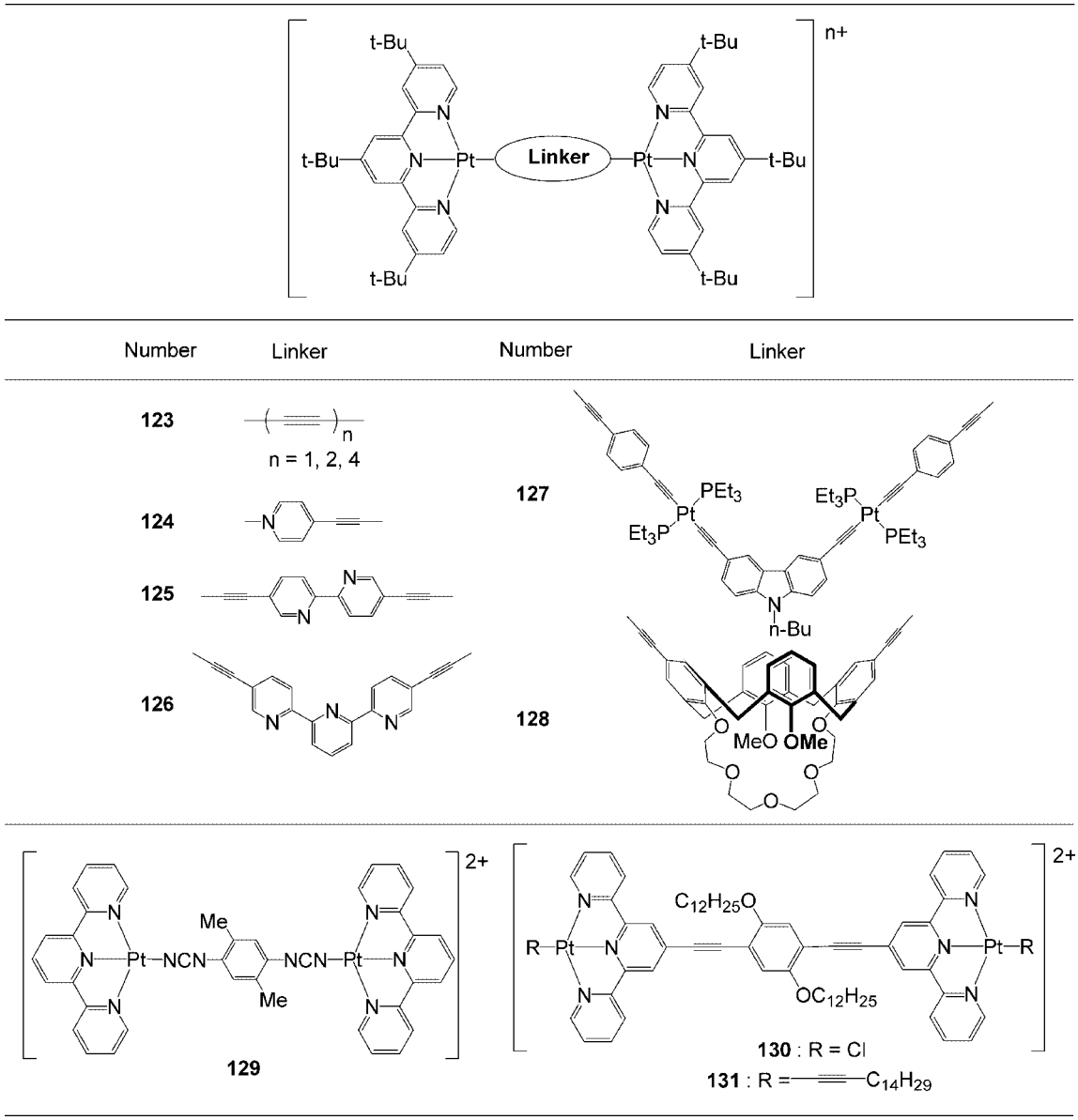

Figure 50. Dinuclear Pt(II) complexes **123**−**131** with rigid linkers.[135,137–141]

Yam et al.[138] also utilized 4-acetylenylpyridine, as a connector, which was attached to two Pt(II) terpyridine complexes as in **124**. The single crystal X-ray structure of **124** revealed that the Pt−Pt distance was 9.4 Å and did not show any short-range interactions due to the bulky *t*-Bu groups (Figure 51). The CV of **124** demonstrated four quasi-reversible reduction couples with two at ca. −0.82 to −0.93 and two at −1.33 to −1.42 V versus SCE, which were attributed to successive one electron reductions of the two terpyridines, since the co-ligand connected to Pt(II) is different.

A luminescent tetranuclear supramolecule **127** was assembled by formation of two Pt−acetylene linkages between 2 equiv of a Pt(II)-tpy complex with an *n*-Bu-carbazole-containing core.[139] Electrochemical, absorption, and emission properties of **127** exhibited similar features to other acetylene-containing dinuclear complexes **123**−**126**.[135,137–139]

Lo et al.[140] reported a unique dinuclear **128** containing alkynylcalix[4]crown-5 ligand. The single crystal X-ray structure did not show any short-range interactions; the Pt−Pt metal centers were separated by 8.54 Å due to bulky *t*-Bu groups attached to the terpyridine moieties. Upon excitation

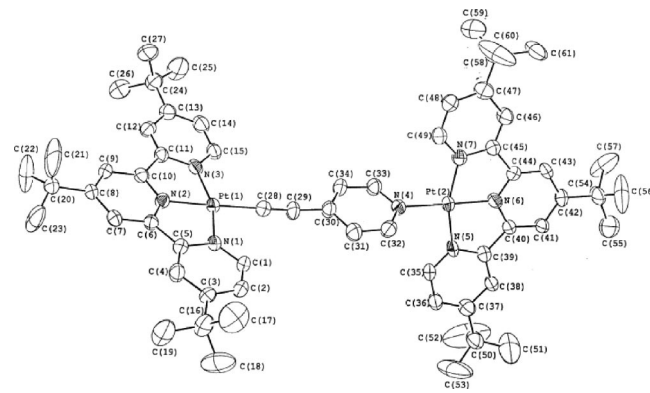

Figure 51. Single crystal X-ray structures of **124**. (Reprinted with permission from ref 138. Copyright 2004 American Chemical Society).

at $\lambda > 400$ nm, the calixcrown **128** displayed a weak ^{3}MLCT emission mixed with ^{3}LLCT band at 738 nm due to possible reductive quenching by photoinduced electron transfer in which the electron-donating calixcrown moiety acted as a quencher. The macrocyclic cavity within the calixcrown was

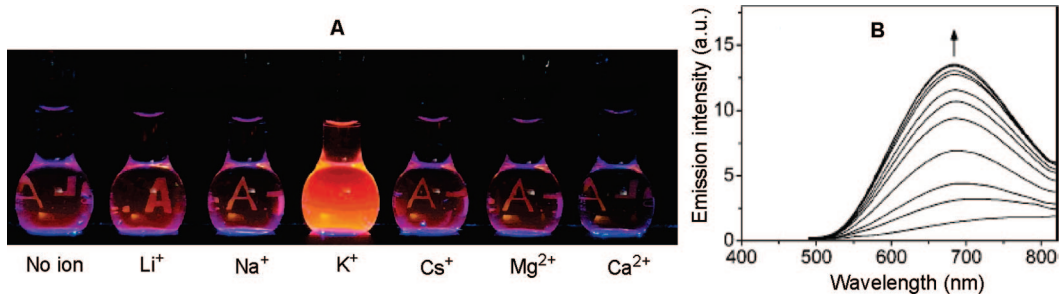

Figure 52. (A) Effect of various metal ions (5.0×10^{-5} M) on emission intensities of **128** and (B) emission spectra of calixcrown **128** with K^+ ion. (Reprinted with permission from ref 140. Copyright 2006 American Chemical Society).

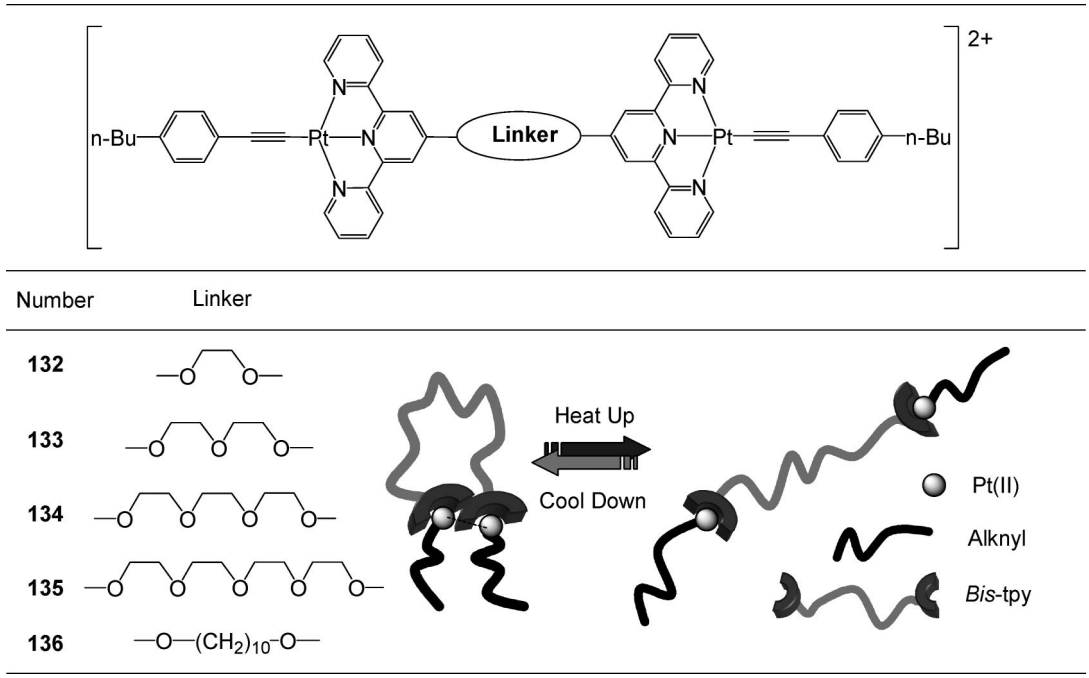

Figure 53. Chemical structures of dinuclear complexes **132**−**136** with flexible linkers and their aggregation/deaggregation behavior (bottom right corner).[145]

utilized as a molecular recognition center for alkali and alkaline earth metals. Binding of Li^+, Na^+, K^+, Cs^+, Ca^{2+}, and Mg^{2+} ions was detected with a blue shift of the MLCT band and a well-defined isobestic point in its absorption spectrum. Moreover, a notable increase in emission intensity at ca. 700 nm was observed upon binding of K^+ ion, which is favored over the other alkali and alkaline earth metal ions, thereby suggesting a possible application as a luminescent chemosensor (Figure 52).

Derosa et al.[141] utilized 2,5-dimethyl-*N*,*N*′-dicyanoquinonediimine dianion (Me_2-dicyd^{2-}) as a bridge to connect two Pt(II) terpyridines, as in **129** (Figure 50). It was proposed that the Me_2-dicyd^{2-} moieties would stack *via* $\pi-\pi$ interactions and could promote conductivity upon doping similar to related structures.[142,143] Even though **129** was not crystalline; it could still be doped with iodine to form a radical anion of Me_2-dicyd^{2-} and I_3^-, which led to its 100 times weaker powder conductivity compared to a crystal conductivity,[144] as $\sigma = 39\ \mu S\ cm^{-1}$ ($x = 1.3$ as in **129**$\cdot[I_3^-]_x$).[141]

To circumvent the solubility problems, Ziessel et al.[135] prepared a linear bis-terpyridine ligand with two dodecyloxy chains that was reacted with 2 equiv of K_2PtCl_4 to afford **130**, which was later capped by acetylene containing $C_{14}H_{29}$ alkyl chain to give desired **131** (Figure 50).

Dinuclear Pt(II) bis-terpyridines **132**−**136**, connected through flexible bridges, were reported for their intramolecular self-assembly in solution (Figure 53).[145] The ^{1}H NMR of **132** and **133** with short linkers revealed well-defined peaks at 25 °C; however, **134**−**136** with longer flexible connectors showed poorly resolved broad peaks, which sharpened and shifted downfield upon heating (Figure 54A). Absorption spectra of **135** displayed an MMLCT band as a shoulder at 535 nm at −40 °C, which disappeared upon heating (Figure 54B). Upon excitation at $\lambda > 400$ nm, complex **136** exhibited a ^{3}MMLCT band at 830 nm at 5 °C that also disappeared upon heating (Figure 54C). The Pt−Pt and $\pi-\pi$ interactions were proposed to be the driving force for this particular reversible self-aggregation process.

Various dinuclear Pt(II) and Pd(II) complexes with short linkers such as pyrazole in **137**,[146] diphenylformamidine in **138**,[146,147] azaindole in **139**,[146] guanidine in **140**,[35,148] 2-mercaptoimidazole in **141**,[149] 1-methylcytosine in **142** and **143**,[69] acetamide in **144** and **145**,[67,150,151] canavanine in **146**,[152] and arginine in **147**[146,152] favoring intramolecular interactions between metal centers (d−d) and terpyridine moieties ($\pi-\pi$) were reported for their crystal packing and photophysical properties (Figure 55). Dewan et al.[153] accidentally discovered **148** from the crystallization of $[Pt(tpy)(SCH_2CH_2NH_3)]^{2+}$ with two-base DNA single strand T-A [deoxymethoxythyminyl-(3′,5′)-deoxyadenosine]. The trinuclear **148** was crystallized in two diastereomeric structures, which affected an overlap between parallel terpy-

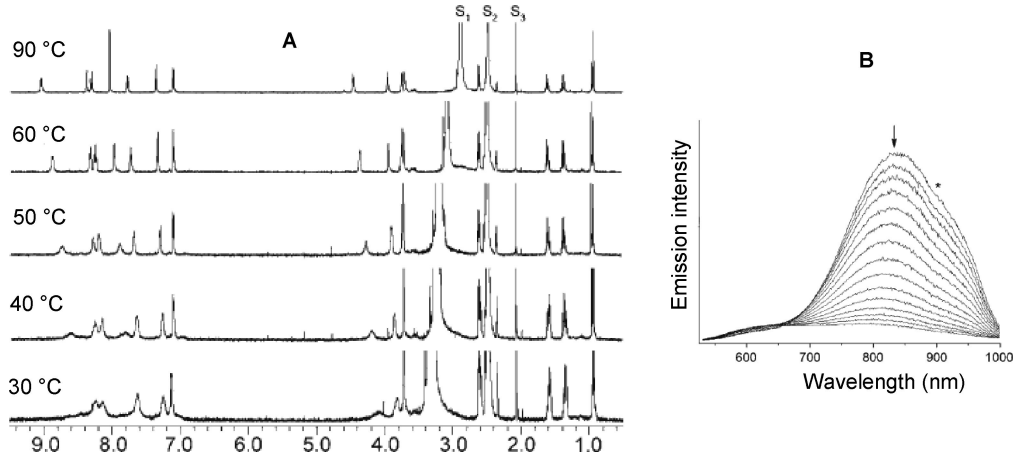

Figure 54. (A) High-temperature ^{1}H NMR of **135** in DMSO-d_6, S_1-S_3 represents H_2O, DMSO and MeCN solvents, respectively; (B) changes in emission of **136** upon heating from 5 to 75 °C. (Reprinted with permission from ref 145. Copyright 2006 Wiley-VCH).

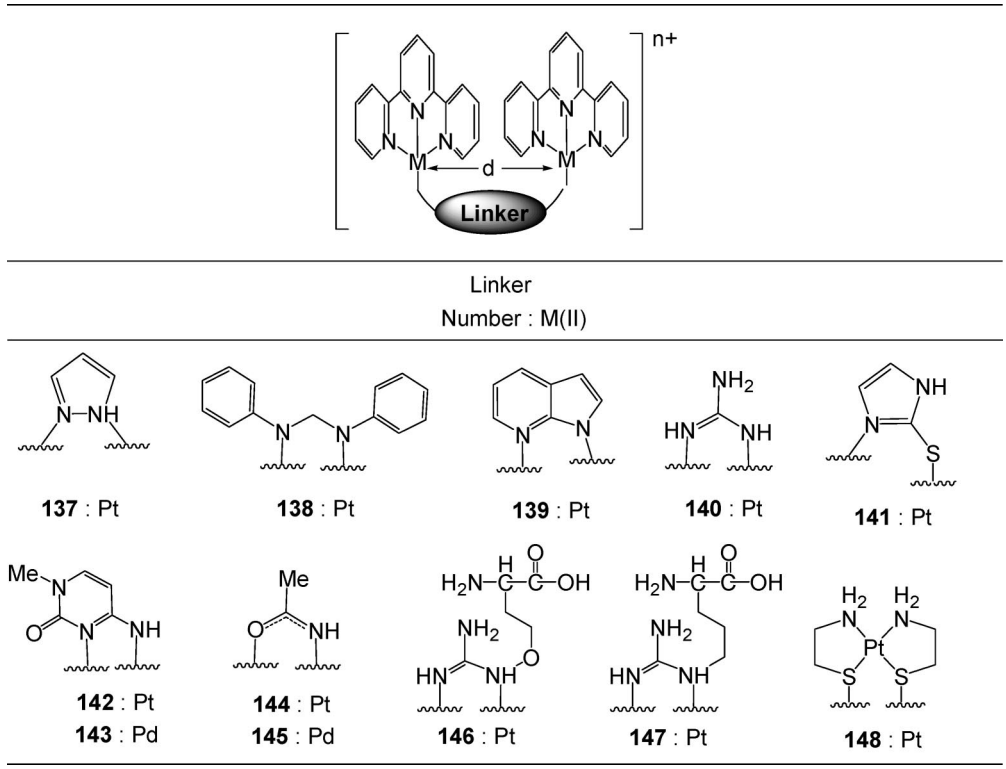

Figure 55. Structures of dinuclear **137**−**148** with short intramolecular distances between metal centers (Pt−Pt and Pd−Pd) and terpyridine moieties.[35,67,69,146–153]

ridines; further, only weak short-range (distances > 3.88 Å) interactions were observed between Pt metal centers and terpyridine moieties (Figure 56).

Single crystal X-ray structures of **138** and **140**−**146** were reported;[35,67,69,146–152] however, only complexes **141**,[149] **143**,[69] and **145**[67] are depicted in Figure 57. These crystal structures revealed that the distances between metal centers were in the range of 2.99−3.23 Å; the terpyridine moieties were found to be parallel to each other with intraplanar distances in the range of 2.8−3.5 Å. A new low energy MMLCT absorption and ^{3}MMLCT emission bands in solution were observed for these dinuclear complexes, which were associated with short-range intramolecular Pt−Pt and $\pi-\pi$ interactions.[35,67,69,146–152]

Wong et al.[151] prepared the dinuclear complex **144** with an acetamide bridge from a suspension of [Pt(tpy)(MeCN)] in acetone. Upon slow evaporation of solvent, dark crystals of **144** formed, then were redissolved in hot acetone and recrystallized to give the red form of **144** (Figure 58A). Single crystal X-ray structure of **144** (red) contained acetone molecules in the lattice and displayed short intramolecular Pt−Pt and $\pi-\pi$ interactions with distances of 3.12 and 3.48 Å, respectively; it stacked as an extended linear chain-like structure in head-to-tail fashion with alternating intermolecular Pt−Pt distances of 3.65 and 4.45 Å (Figure 58B). On the other hand, the dark form of **144** exhibited shorter intramolecular Pt−Pt distances of 3.06 Å and stacked as dimers of **144** with intermolecular Pt−Pt distances of 3.26 Å (Figure 58C). The solid-state emissions of dark and red form of **144** displayed ^{3}MMLCT emissions at 710 and 690 nm, respectively, at 25 °C. Complex **144** showed a MMLCT absorption at ca. 426−478 and a ^{3}MMLCT emission at 600 nm at low concentration. The emission spectra at higher concentrations revealed a new emission band at 790 nm,

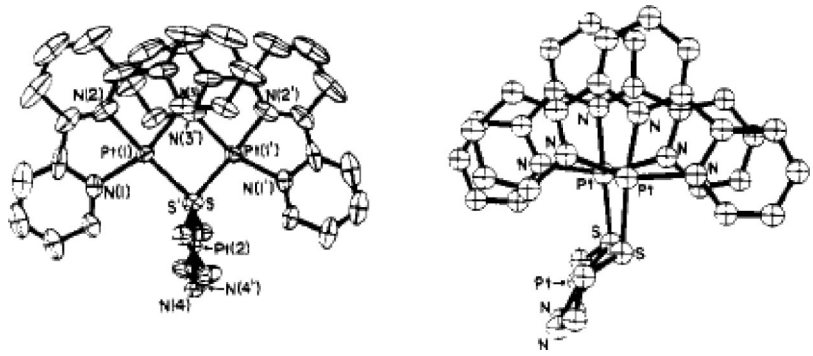

Figure 56. Crystal structures of trinuclear **148** in its two different diastereomers. (Reprinted with permission from ref 153. Copyright 1980 American Chemical Society).

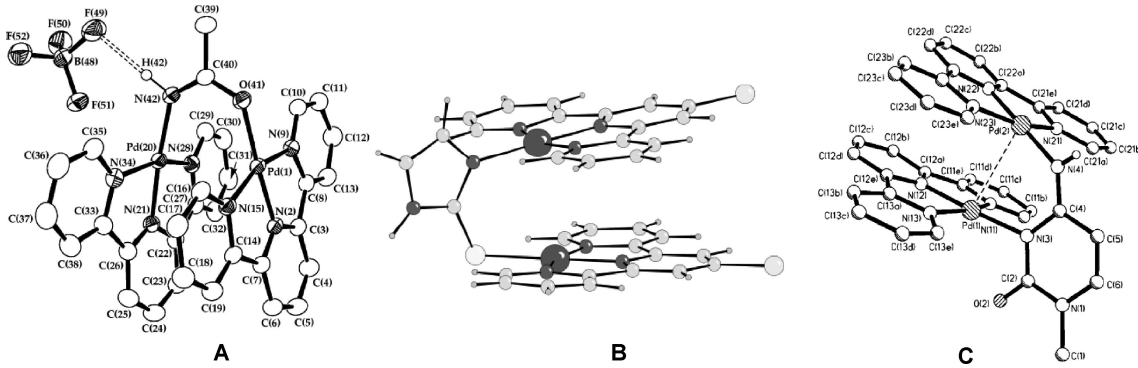

Figure 57. Single crystal structures of (A) **145**, (Reprinted with permission from ref 67. Copyright 2003 Elsevier); (B) **141**, (Reprinted with permission from ref 149. Copyright 2001 The Royal Society of Chemistry); and (C) **143**. (Reprinted with permission from ref 69. Copyright 1999 The Royal Society of Chemistry).

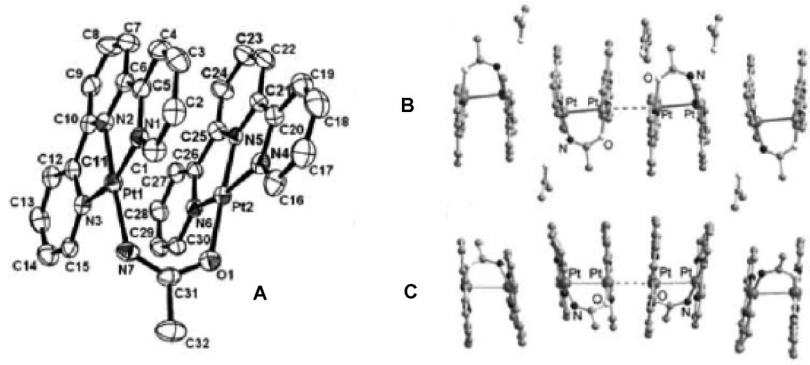

Figure 58. Crystal structure of (A) molecular clip-like **144** (red form) and packing of its (B) red form and (C) dark form. (Reprinted with permission from ref 151. Copyright 2006 The Royal Society of Chemistry).

which was attributed to dimer formation of **144** similar to the dark crystal packing.

Lowe et al.[149] prepared a dinuclear complex **149** with a thioacetamine linker, which slowly decomposed in water to form intermediate **150**, which abstracted an extra sulfur with a Pt(II) terpyridine moiety of **149** and was converted to a crystalline trinuclear propeller-like complex **151** (Scheme 13). Both enantiomeric forms of **151** possessing both right- and left-handed propeller helicity were observed in the crystal structure.

Tannai et al.[85,101] reported dimetallic homonuclear **152** and **153** as well as heteronuclear **154** that were connected through a 2,5-dimercapto-1,3,4-thiadiazole (H_2dmct) moiety. Single crystal X-ray structures of **152**−**154** revealed that the terpyridines are parallel with an inversion center in a trans configuration and did not display any inter- or intramolecular short-range interactions (Figure 59). Dinuclear complexes **152**−**154** did not show any luminescence and their cyclic voltammograms suggested that there was no metal center interaction.

Sommer et al.[71] prepared the bis-terpyridine ligands **155** and **156** connected by partial and full aromatic spacers, respectively (Scheme 14). The 3,5-di-*tert*-butylphenyl group was introduced to the linker to circumvent solubility problems. Two equivalents of Pd(II) and Pt(II) salts was added to bis-terpyridines **155** and **156** in MeCN to form molecular clefts **157**−**164** consisting of two cofacially separated square-planar complexes (Figure 60).[71,154–163] The distance (∼7 Å) between two parallel terpyridine moieties was specifically designed to offer potential $\pi-\pi$ interactions (<3.5 Å) for planar aromatic molecules, which would intercalate in the cleft to create molecular recognition centers.

Suitable single crystals of the bis-Pd(II) complex **157** for X-ray analysis were obtained patiently maintaining the

Scheme 13. Formation of Crystalline Propeller-like 151 from Dinuclear 149[a]

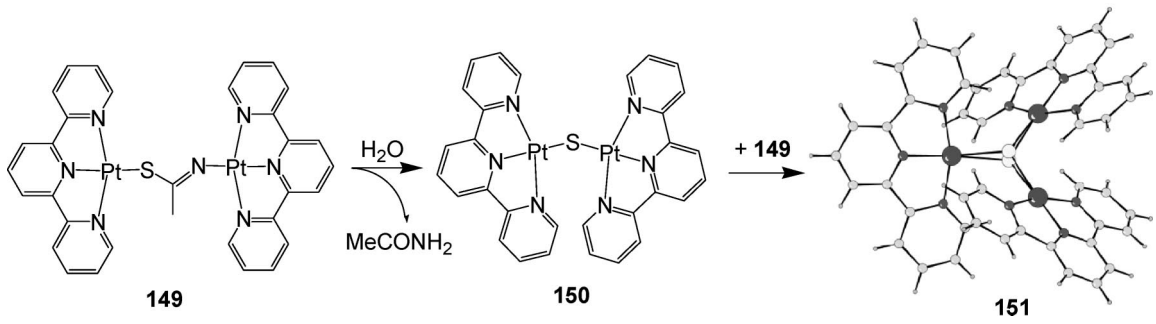

[a] Reprinted with permission from ref 149. Copyright 2001 The Royal Society of Chemistry.

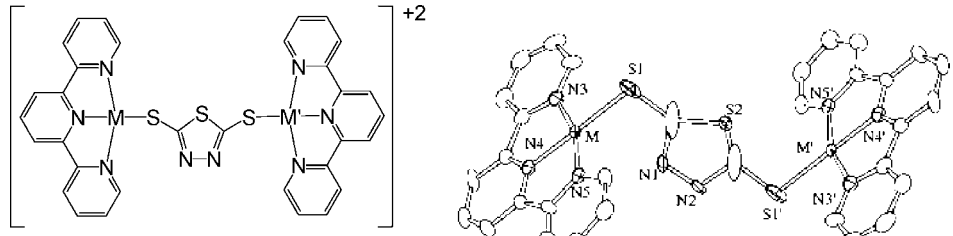

Figure 59. Structures of **152**−**154** and single crystal X-ray structure of **154**. (Reprinted with permission from ref 85. Copyright 2006 The Chemical Society of Japan).

Scheme 14. Partially Aromatic 155 and Oxidized to Fully Aromatic 156 Bis-tpy Ligand[71]

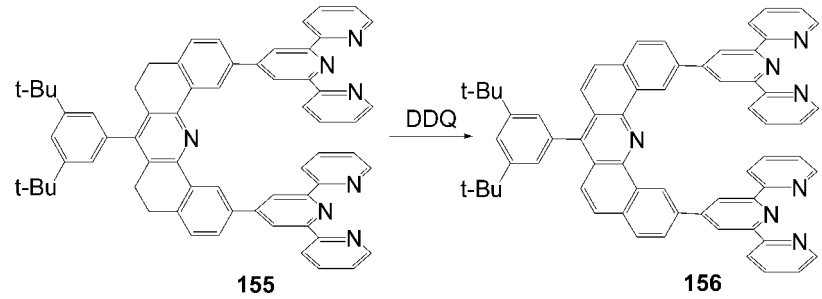

complex in MeCN at −20 °C *for 2 years* in a sealed vial.[161] The crystal packing revealed that two molecules of **157** interpenetrated through the [tpy-Pd-Cl] moieties. The distances between the interplanes (Figure 61A) and Pd−Pd metals were < 3.5 Å; the rationale for packing was the $\pi-\pi$ interaction between terpyridines and d−d orbital interaction between Pd−Pd metal centers (Figure 61B). The crystal packing of bis-Pt(II) complex **160** (Figure 62A), crystallized in DMF, revealed the same interpenetration pattern as **157** with an interplanar distance of < 3.5 Å displaying possible

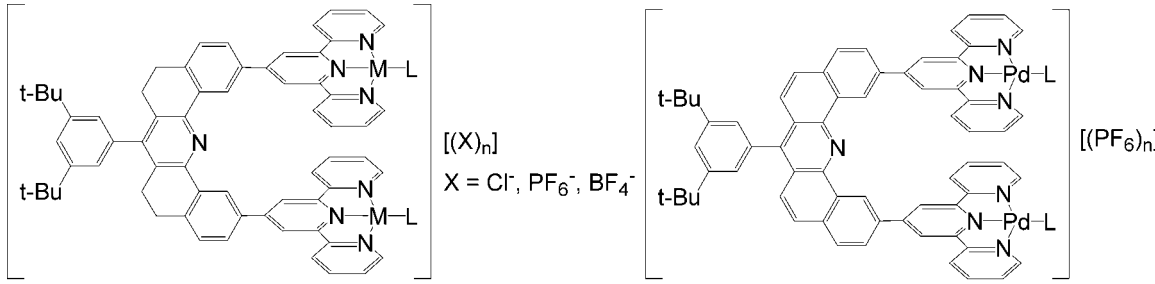

157 : M = Pd(II), L = Cl, n = 1
158 : M = Pd(II), L = MeCN, n = 2
159 : M = Pd(II), L = Pyridine, n = 2
160 : M = Pt(II), L = Cl, n = 1
161 : M = Pt(II), L = Acetone, n = 2
162 : M = Pt(II), L = Pyridine, n = 2

163 : L = Cl, n = 1
164 : L = MeCN, n = 2

Figure 60. Dinuclear molecular clefts **157**−**164**.[71,154−163]

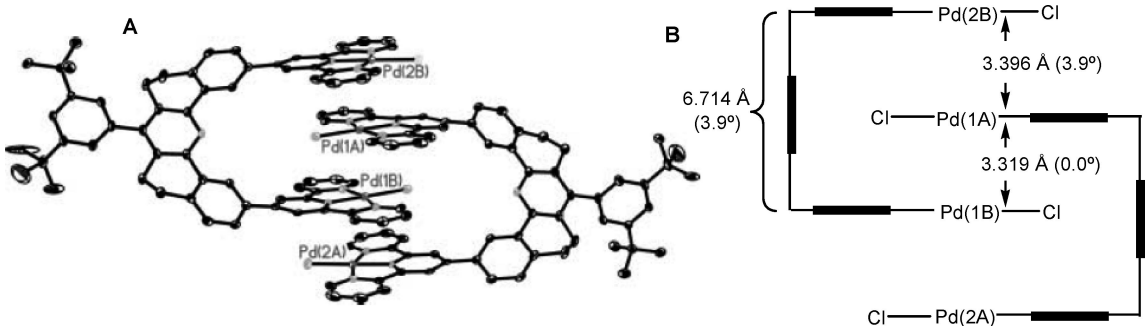

Figure 61. (A) Single crystal structure and (B) schematic representation of interplanar distances and angles of bis-Pt(II) complex **157**. (Reprinted with permission from ref 161. Copyright 2004 Wiley-VCH).

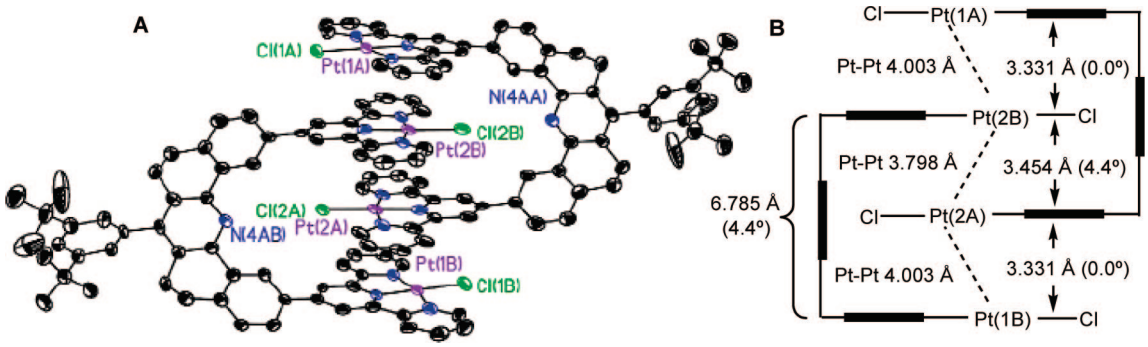

Figure 62. (A) Single crystal X-ray structure and (B) schematic representation of interplanar distances and angles of bis-Pt(II) complex **160**. (Reprinted with permission from ref 162. Copyright 2005 American Chemical Society).

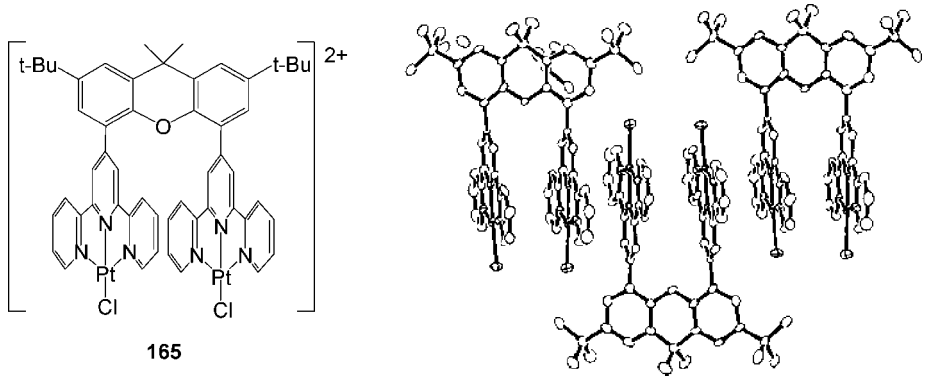

Figure 63. Structure of **165** and its molecular crystal packing. (Reprinted with permission from ref 104. Copyright 2004 American Chemical Society).

$\pi-\pi$ interaction; however, the distances between Pt−Pt metal centers were > 3.8 Å suggesting weaker d−d orbital interactions (Figure 62B).[162]

Okamura et al.[104] reported a dinuclear Pt(II) complex **165**, in which the terpyridine moieties were separated by an intraplanar distance of 4.4 Å (Figure 63). This distance did not permit **165** to interpenetrate, as in **157** and **160**;[161,162] instead, it stacked as an extended linear chain-like structure with a zigzag configuration of Pt metal centers that displayed only weak intermolecular interactions with distances of 4.2−4.4 Å.[104] The cyclic voltammogram of **165** displayed concentration-independent reversible redox couples, which were split into two, suggesting possible intramolecular interactions between Pt(II) metal centers.

Heterodimetallic Pt(II)−Ru(II) complexes **166**−**169**, containing 3,5-di-*tert*-butylsemiquinone (SQ) moiety with a radical anion, were reported to possess interesting electrochemical properties (Figure 64).[104,164] Cyclic voltammograms of **166**−**169** revealed three reversible redox couples assigned to Ru(III)/Ru(II), SQ/catechol and Pt(tpy)/Pt(tpy$^-$) that were strongly dependent on the co-ligand connected to metal centers (Table 1). The redox properties of **166**−**169** did not show any electronic interactions between metal centers even in the case of **169** in which metal centers were covalently connected. Spectroelectrochemical studies of **166**−**169** displayed a reversible shift between the absorption bands at ca. 600 and 850 nm, which was attributed to Ru(III)-SQ and Ru(II)-SQ bands, respectively. It was suggested that these complexes could be utilized as water-oxidation catalysts like their analogous bis-[Ru(tpy)(OH)(R)] (R = SQ, bipyridine) complexes.[165,166]

Heterodinuclear dyads **170**−**175**, containing Pt(II) terpyridine moieties that were connected to porphyrin units through a phenyl-acetylene bridge, displayed photoinduced electron transfers (2−20 ps) from an excited singlet state of porphyrin unit to the Pt(II) complex (Figure 65).[167] This quenching process of porphyrin fluorescence *via* ultrafast charge recombination overcame the possible charge separation state of the dyads. Cyclic voltammograms revealed weak interactions between metal centers. Further, the photophysical

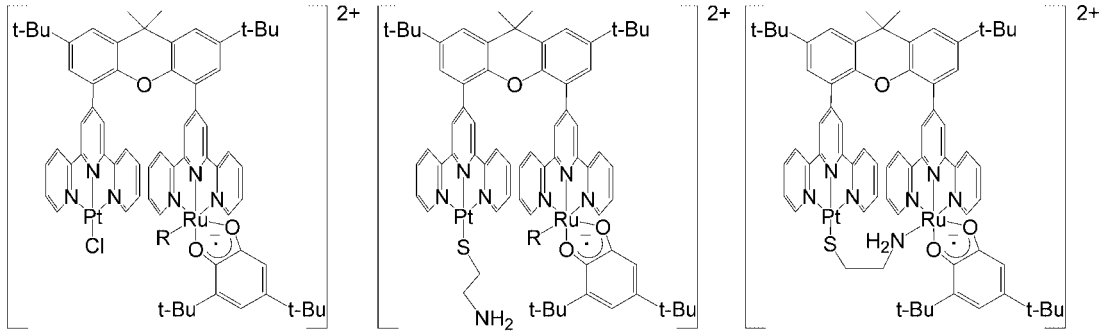

Figure 64. Chemical structures of heteronuclear complexes **166**−**169**.[104,164]

Table 1. CV Data of Complexes 166−169 in DCM[104,164]

	$E_{1/2}$/V vs SCE		
complexes	Ru(III)/Ru(II)	SQ/catechol	Pt(tpy)/Pt(tpy$^-$)
166	+0.17	−0.41	−0.61/−0.70
167	+0.64	−0.33	−0.74
168	+0.71	−0.17	−1.01
169	+0.44	−0.42	−0.99

studies of **170**−**175** were conducted *via* steady-state, time-resolved, and femtosecond transient absorption spectroscopy in DMF in which the rate constants of the electron transfer of the dyads were consistent with Marcus theory. It was suggested that the electron transfer occurred through the conjugated phenyl-acetylene bridge in **170**−**175**.

Lam et al.[168] reported heteronuclear molecular rods **176**−**181**, consisting of a Pt(II) terpyridine complex, which was connected to a Re(I) bipyridine moiety *via* phenyl-acetylene linkers (Figure 66). Single crystal X-ray structures of **176** and **178** displayed a distorted square-planar geometry for the Pt(II) terpyridine complex and did not show any short-range interactions due to the bulky *t*-butyl groups on terpyridine ligand. Absorption spectra of dyads **176**−**181** exhibited a low energy band at ca. 404−486 nm, which was attributed to a mixture of MLCT bands of [dπ(Pt) → π^*(terpyridine)], [dπ(Re) → π^*(bipyridine)], and LLCT band of [π(acetylene) → π^*(terpyridine)]; moreover upon excitation λ > 380 nm, intense orange-red emission bands at ca. 570−580 nm were observed for dyads **176**−**181** with an excited-state lifetime of 0.52−0.94 μs in MeCN solutions at 25 °C. Additional electrochemical studies and extended Hückel molecular orbital (EHMO) calculations revealed that low energy emissions originating from the ^{3}MLCT band [dπ(Pt) → π^*(terpyridine)] were actually mixed with either LLCT of [π(acetylene) → π^*(terpyridine)] or unexpectedly metalloligand-to-ligand charge-transfer of <π{C≡C-(C$_6$H$_4$)-C≡C-[Re]} → π^*(terpyridine)>.

Ziessel et al.[136] reported the first octahedral Fe(II) and Zn(II) bis-terpyridine complexes, which were connected to square-planar Pt(II) terpyridine complexes, as triads **182**−**184** (Figure 67). Either *t*-Bu groups introduced on terpyridine in **182** and **183** or 1,4-dialkoxyphenyl acetylene used as a connector in **184** helped to circumvent the solubility problems. Absorption spectra of triads **182** and **184** displayed a Fe(II)-based MLCT band at ca. 580 nm and the Pt(II)-based MLCT bands mixed with LLCT band at ca. 425 nm; however, Pt−Zn−Pt complex **183** showed only a Pt(II)-based MLCT band. Cyclic voltammograms of **182** and **184** revealed successive reductions of four terpyridine moieties connected to Fe(II) and Pt (II) metals at −1.27, −1.40 V, and −0.96, −1.54 V, respectively.

4.2. Supramolecular Self-Assemblies

Bosnich's group[71,154–158] utilized the Pd(II)- and Pt(II)-based molecular clefts **158**, **161**, and **164** as molecular building blocks to self-assemble higher ordered supramolecular architectures. Dinuclear Pd(II) complexes **158** and **164**, which are kinetically more labile and thermodynamically less stable than their analogous dinuclear Pt(II) complex **161**, exclusively formed rectangles **185**−**188** and trigonal prisms **189** and **190** with linear bidentate **191** and **192**, and trigonal tridentate spacers **193** and **194** at 25 °C within hours, respectively (Figure 68). The chemical structure of the tetranuclear Pd(II)-based molecular rectangle **187** containing a fully aromatic bis-terpyridine ligand **156** is depicted in Figure 69. The dinuclear Pt(II) cleft **161** was able to self-assemble into molecular rectangles **186** and **188** at high reaction temperatures.[163] The single crystal X-ray structure of tetranuclear **186** is depicted in Figure 70 (hydrogens, counterions, and part of the bis-terpyridine ligand were omitted for clarity).

The rectangular **186** displayed a meso conformation with one spacer in the *R*,*R*- and the other in the *S*,*S*-configuration.[163] The pair of 4,4′-bipyridyl (**191**) spacers, used to connect the Pt(II) metals, are buckled and nearly perpendicular to the coplanar Pt-terpyridine moieties, thus, almost parallel to each other in the same cleft at a distance of 6.9 Å. The closest distance between two 4,4′-bipyridyl spacers is 1.9 Å allowing appropriate guests to intercalate within the resultant void region. These supramolecular self-assemblies were utilized as molecular recognition centers for small planar molecules to be considered later in this review.

Hui et al.[169] reported a hexanuclear Pt(II) acetylene complex **196**, which was assembled *via* the reaction of the face-to-face dinuclear Pt(II) acetylene complex **195** with 4 equiv of [Pt(tpy)(MeCN)]$^{2+}$ (Figure 71). The single crystal X-ray structure of **195** revealed two Pt(II) metals connected through two diphenylphosphino ligands forming an eight membered-ring in a face-to-face arrangement with a distance of 3.28 Å, suggesting a possible Pt−Pt interaction. The single crystal structure of **196** displayed a shorter Pt−Pt core distance (3.18 Å) compared to **195** (3.28 Å), which was attributed to the decreased electron density of the Pt metals in the core upon formation of four peripheral Pt-terpyridine complexes. The two adjacent Pt(II) terpyridine moieties remained parallel with an interplanar distance of 3.67 Å, suggesting possible weak π−π interactions; however, the

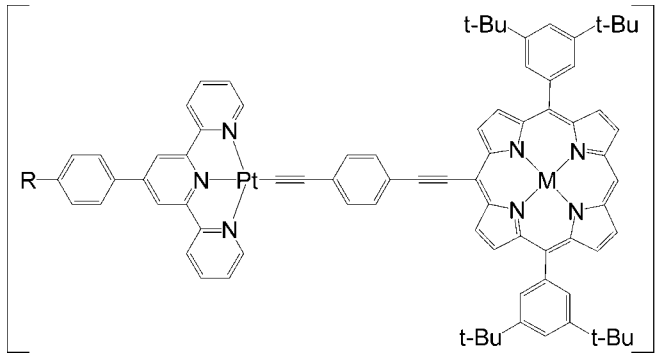

170 : M = Zn(II); R = PO_3Et_2
171 : M = Zn(II); R = H
172 : M = Zn(II); R = OC_2H_{15}
173 : M = Mg(II); R = PO_3Et_2
174 : M = Mg(II); R = H
175 : M = Mg(II); R = OC_2H_{15}

Figure 65. Structures of heterodinuclear complexes **170**−**175**.[167]

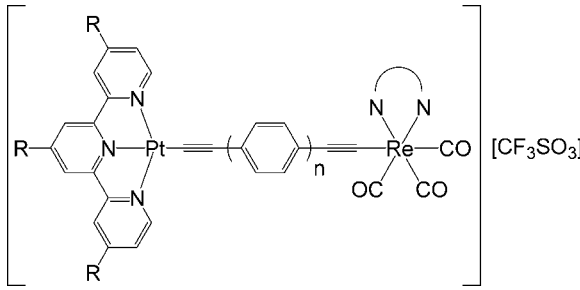

176 : N^N = bipyridine; R = t-Bu; n = 1
177 : N^N = t-Bu_2-bipyridine; R = t-Bu; n = 1
178 : N^N = $(CF_3)_2$-bipyridine; R = t-Bu; n = 1
179 : N^N = NO_2-phenanthroline; R = t-Bu; n = 1
180 : N^N = t-Bu_2-bipyridine; R = H; n = 1
181 : N^N = t-Bu_2-bipyridine; R = t-Bu; n = 0

Figure 66. Chemical structures of dyads **176**−**181**.[168]

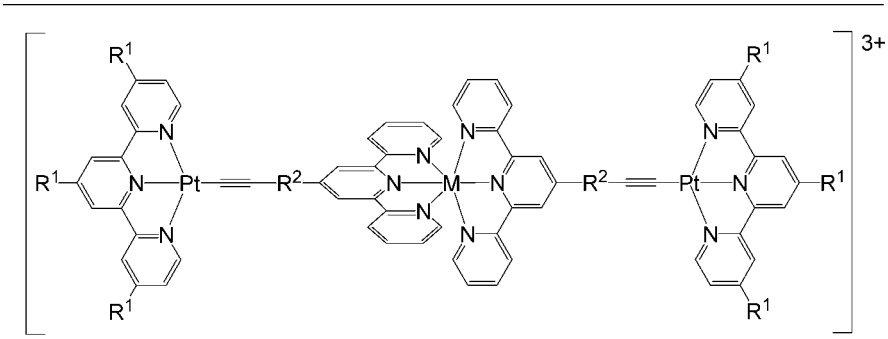

Number	M(II)	R^1	R^2
182	Fe	t-Bu	Nothing
183	Zn	t-Bu	Nothing
184	Fe	H	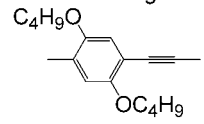

Figure 67. Chemical structures of triads **182**−**184**.[136]

Pt−Pt distances between these moieties, being 5.08 Å, did not show any Pt−Pt interaction. The hexanuclear **196** showed a low energy absorption band at 416 nm, which was assigned as MLCT. The solution and solid-state emissions at 520 and 620 nm, respectively, at 77 K were attributed to ligand-centered phosphorescence and ^{3}MMLCT, respectively.

4.3. Molecular Recognition by Host−Guest Interaction

Bosnich's group[71,154–163] investigated the Pd(II)- and Pt(II)-based molecular clefts (**157**−**164**), rectangular and trigonal prism shaped (**185**−**190**) supramolecular assemblies, as molecular recognition centers for different planar, aromatic, transition metal containing, neutral, positively, and negatively charged molecular guests (**197**−**225**, Figure 72). Since the bis-terpyridine moieties in those supramolecular architectures are separated by 7 Å, they contain molecular cavities for intercalation of guests by $\pi-\pi$ interactions with aromatic groups and d−d orbital interactions with guest metal centers.[28] Guests **217**−**222** did not display any binding properties to hosts **157**−**164**; moreover, yellow solutions of positively charged hosts **157**−**164** precipitated as red, insoluble materials upon addition of negatively charged guests **223**−**225**, suggesting the formation of host−guest complexes.[155]

9-Methylanthracene (9-MA, **197**), as a guest, displayed remarkable binding properties to most of the receptors (Table 2).[71,154,156,157,162] The yellow color of a MeCN solution of cleft **157** turned deep red upon addition of solution of 9-MA. Actual host−guest interactions and

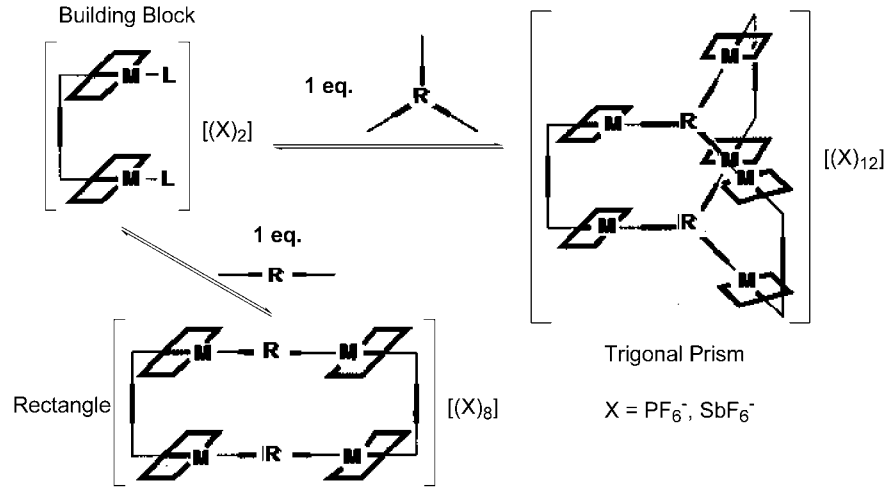

Number of the Assemby	Shape of the Assemby	Number of the Building Block	Linker (R)	Number of the Linker (R)
185	Rectangle	**158**	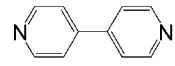	**191**
186	Rectangle	**161**		
187	Rectangle	**164**		
188	Rectangle	**161**	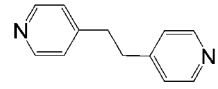	**192**
189	Trigonal Prism	**158**	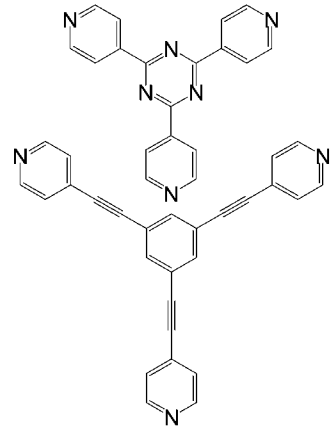	**193**
190	Trigonal Prism	**158**		**194**

Figure 68. Self-assembly of rectangular **185**−**188** and trigonal prism **189** and **190** shape architectures using molecular clefts **158**, **161**, and **164** [M = Pd(II) or Pt(II)].[28,71,154,155,157,158,163]

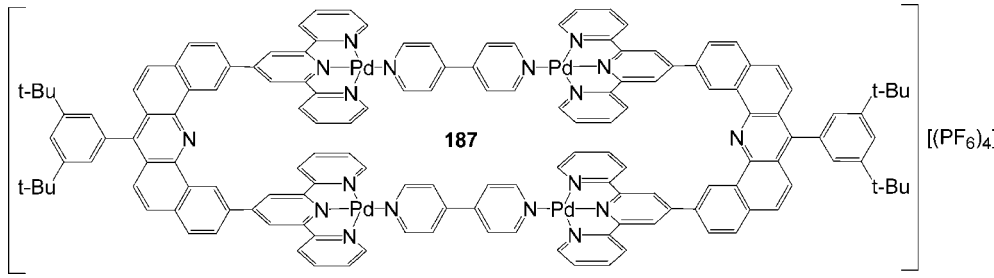

Figure 69. Chemical structure of a fully aromatic tetranuclear rectangle **187**.[71,154,155]

stoichiometry of host **157** with guest **197** (1:2) were detected by growing single crystals, which revealed that one 9-MA molecule intercalated between the [tpy-Pd-Cl] moieties by a $\pi-\pi$ interaction proven by an interplanar distance of < 3.5 Å to each side; the other 9-MA molecule lies outside the receptor **157** closely related to [tpy-Pd-Cl] moiety (Figure 73).[71,154,156]

The Pt(II)-, Pd(II)-, and Au(III)-containing square-planar complexes **198**−**205** were utilized as guests, which displayed d−d orbital interaction with the cleft's metal centers (Table 2).[71,154–163] For example, single crystal X-ray structures of guests **201** and **198,** which intercalated into **157** and **160**, respectively, with 1:1 host−guest stoichiometry, revealed that there are d−d orbital and $\pi-\pi$ interactions between Pt(II)-

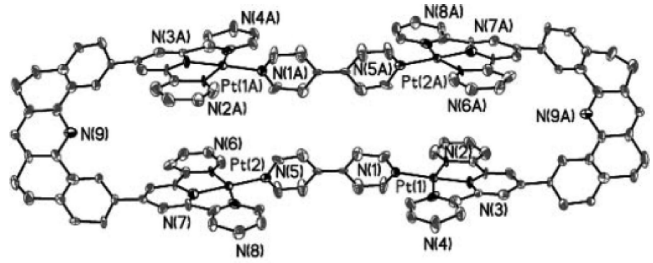

Figure 70. Single crystal structure of a tetranuclear Pt(II) molecular rectangle **186**. (Reprinted with permission from ref 163. Copyright 2005 Wiley-VCH).

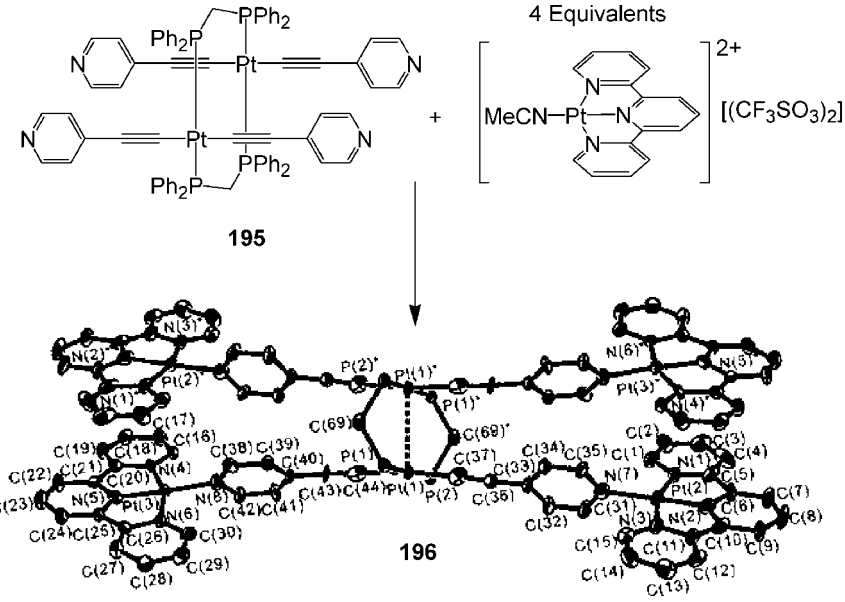

Figure 71. Assembly and crystal structure of hexanuclear Pt(II) acetylene complex **196** from dinuclear **195** and $[Pt(tpy)(MeCN)]^{2+}$. (Reprinted with permission from ref 169. Copyright 2002 American Chemical Society).

based guests and the molecular receptors, since the interplanar and metal−metal distances between hosts and guests are both <3.3 Å (Figure 74).[159–162]

Intercalation of 9-MA into the molecular clefts prompted Goshe et al.[156] to design receptor **226**, which was covalently connected to two 9-MA molecules through a pyridine-2-carboxylate spacer (Figure 75A). The single crystal X-ray structure of the covalently bound host−guest complex **226** revealed that one 9-MA molecule intercalates into the cleft and the other one lies on the top of the [tpy-Pd-Cl] moiety; moreover, **226** was stacked on the neighboring molecule to form an extended chain-like structure (Figure 75B). Since the guest molecules could fluxionally exchange the binding sites in the cleft, the dynamics of this complex were studied by low temperature ^{1}H NMR revealing symmetric, sharp peaks at 16 °C suggesting the rapid exchange of anthracenes between the accessible sites. However, these peaks were broadened upon cooling and separated into two sharp signals of equal intensity at −90 °C, suggesting that fluxional motion in **226** was frozen and statistically equal amounts of isomers were formed (Figure 75C).

The stoichiometry and intercalation of the host−guest complexes, which did not crystallize, were investigated by their dramatic ^{1}H NMR shifts of certain protons upon titration of the hosts with different mole equivalents of guests. Then, application of the "mole-ratio" method to the significant ^{1}H NMR shifts of these protons gave consistent results for the stoichiometry of host−guest complexes with single crystal X-ray structures. For example, two 9-MA guests were found to bind to the host **157** (Figure 76A).[71,154,156] Four and five 9-MA guests bound to rectangles **187** and **185**, respectively (Figure 76 B,C).[154] Trigonal prismatic shaped assemblies **189** and **190** with short and long tridentate trigonal linkers were able to contain six and seven 9-MA guests, respectively (Figure 76D).[157] It was suggested that the two larger trigonal linkers **194** in host **190** have enough room between them to accommodate an extra 9-MA.

The guest **210** intercalated into the larger trigonal prismatic supramolecule **190** as detected by ^{1}H NMR titration; however, no intercalation was observed for guest **210** with the smaller trigonal prism **189**.[157] The rigid, linear **208** and **209**, containing two guest molecules connected through a linker, were bound to molecular cleft **157** by 1:1 and 2:1 host−guest ratios, respectively (Figure 77).[158] Separation between Pt atoms of guest **208** and **209** was calculated to be 12.2 and 18.8 Å, respectively. It was suggested that electrostatic repulsion of two positively charged molecular clefts **157** was effective at distances <15 Å, which prevented the second cleft to bind to the shorter guest **208**.

Dissociation of host−guest complex {[**157**][**200**]} was achieved *via* protonation of the pyridine ring in guest **200** suggesting that the positively charged host **157** released the charged guest **200** due to electronic repulsion (Scheme 15).[161] Remarkable color changes for {[**157**][**200**]} from deep red to yellow were observed upon addition of TFA, which was attributed to a dissociation of the guest; moreover, the red color was recovered upon addition of NEt_3 indicating the neutralization of guest **187** and its incorporation into the host.

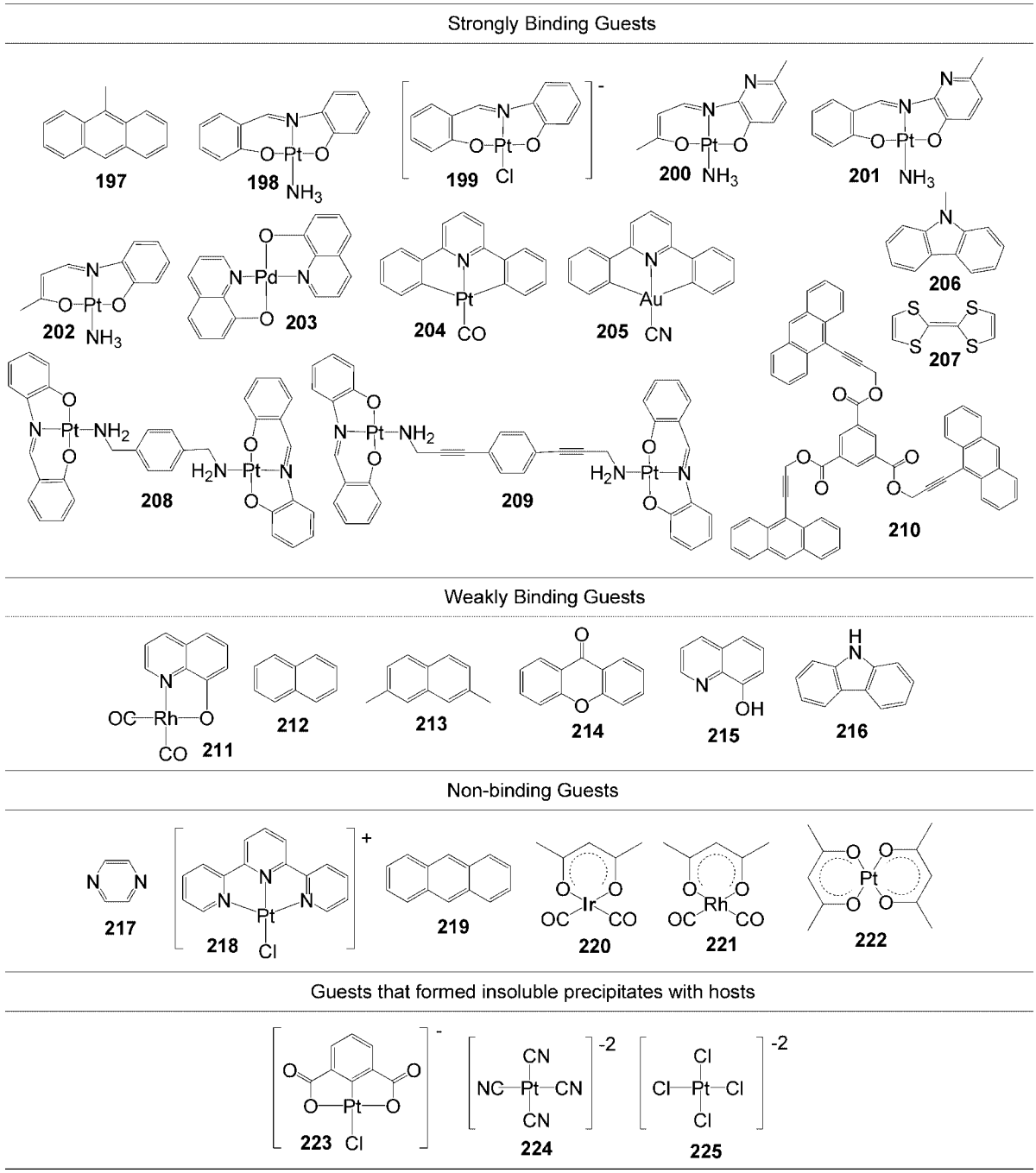

Figure 72. Chemical structures of guest molecules **197**−**225**.[71,154–163]

It is proposed that proton-driven reversible dissociation of the guest **200** from host **157** can be interpreted as a molecular switch, or one stroke of a molecular motor; however, it was concluded that this particular process acts more like a switch than a motor, since molecular motors usually require repetitive cycles.

Table 2. Host−guest Interactions and Their Stoichiometry

guest	host	host:guest stoichiometry	interplaner distances (Å)	ref	guest	host	host:guest stoichiometry	ref
197	**157**	1:2	3.44, 3.48	71, 154, 156	**197**	**190**	1:7	157
	159	1:2	-	156	**202**	**157**	1:1	161
	160	1:2	-	162		**162**	1:1	163
	187	1:5	-	154		**186**	1:2	163
	185	1:4	-	154		**188**	1:2	163
	189	1:6	-	157	**203**	**157**	1:1	71
198	**157**	1:1	-	156, 158, 159		**163**	1:1	71
	160	1:1	3.27, 3.29	159, 162	**205**	**160**	1:2	162
	162	1:1	-	163		**186**	1:4	163
	186	1:2	-	163	**205**	**160**	1:2	162
	188	1:2	-	163	**209**	**157**	1:1	158
199	**157**	1:1	3.21, 3.29	160		**185**	1:1	158
200	**157**	1:1	3.27, 3.29	161	**209**	**157**	2:1	158
201	**157**	1:1	3.24, 3.24	160, 161	**210**	**189**	1:2	157

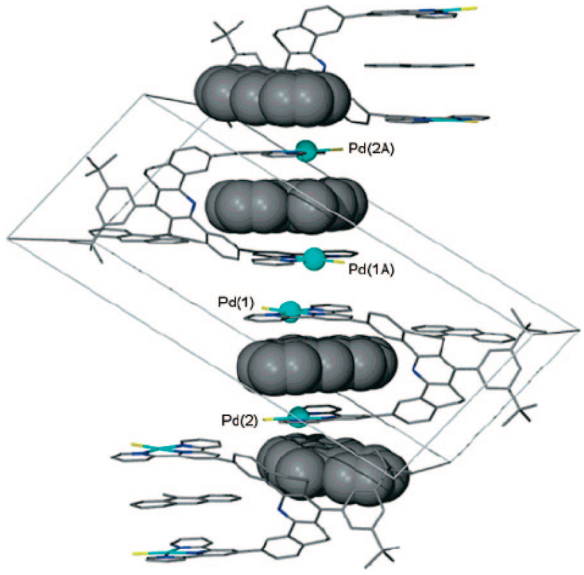

Figure 73. Single crystal packing diagram of [**157**][(**197**)$_2$]. (Reprinted with permission from ref 71. Copyright 2001 American Chemical Society).

4.4. Multimetallic Peptide Scaffolds

Tanaka et al.[170] reported the liquid phase synthesis of 18- and 24-membered cyclic peptides **229**−**232** with a repeating unit of [glycine-L-cysteine] (Scheme 16). Trinuclear **227** and tetranuclear **228** oligopeptides, in which the thiol groups in cysteine were connected to square planar Pt(II) terpyridine complexes, were cyclized to give the desired cyclopeptides **229** and **230**, respectively, which were subsequently converted to their corresponding cyclopeptides **231** and **232**, respectively, by removing the Pt−terpyridine complex.

Williams' group[171,172] reported the preparation of multimetallic artificial oligopeptides **233**−**240** (Figure 78) in which peptide backbone, containing pyridine and bipyridine, was utilized as a scaffold to assemble diverse metal complexes (Figure 78). These particular oligopeptides, which are analogous to peptide nucleic acids (PNAs), were synthesized to mimic DNA and RNA structures in order to improve their binding abilities to biomacromolecules. Pyridine-substituted oligopeptides with an aminoethyl-glycine backbone of varying length were treated with $[Pt(tpy)(Cl)]^+$ to give the desired complexes **233**−**237**, which were characterized by UV−vis and ^{1}H NMR spectroscopy.[168] Molecular modeling studies of **233**−**237** suggested that they probably will form extended chain-like structures upon increasing the quantity of metal centers tethered to the backbone due to electrostatic repulsion between positively charged Pt(tpy) moieties. Electrochemical studies of **233**−**237** revealed that the $[Pt(tpy)(pyr)]^{2+}$ redox centers are electronically isolated and behave independently.

A bipyridine moiety was introduced into the center of a peptide backbone, which was tethered with two Pt(II) terpyridine complexes; then, addition of Fe(II), Cu(II) or Zn(II) to this bipyridine-containing oligopeptides promoted the assembly of hetero-multimetallic supramolecular dendrimer-like structures **238**−**240** analogous to divergent dendrimer synthesis.[172] Complex **238** displayed two distinct absorptions at ca. 340 and 537 nm, which were attributed to Pt-tpy and Fe-tpy MLCT bands. EPR studies of paramagnetic **239** indicated a lack of interactions between metal centers; this was also observed in electrochemical studies. It was proposed that these transition metal-incorporated oligopeptide nanostructures could be utilized as inorganic "bar codes" and promote new applications as biocompatible pharmacological agents.[173]

5. Biological Activities

In the following sections, the intercalative and covalent binding modes of square-planar Pt(II), Pd(II), and Au(III) terpyridine complexes to DNA and other biomacromolecules will be considered. The initial focus will be on the details for the intercalation of these complexes with DNA and their subsequent effects on the physical and chemical properties of DNA. Utilization of these Pt complexes as protein tags, as well as the cytotoxic activities of these complexes as antitumor, antiprotozoal, and radiotherapy agents, will be reviewed.

5.1. DNA Intercalation

Intercalation of small molecules into DNA by stacking between its base pairs was first suggested by Lerman[174] to explain the high affinity of planar dyes to DNA. Aminoacridine dyes,[174,175] antimicrobial agents, such as ethidium bromide,[176,177] (Figure 79) and antinomycin antibiotics[178] were studied as a class of planar intercalators. As a result of intercalation of these dyes into DNA, their UV−vis spectra displayed dramatic shifts and they exhibited induced circular dichroism; moreover, they increased the length of DNA, its viscosity and melting temperature, altered the extent of supercoiling in closed circular duplex DNA, and reduced its sedimentation coefficient.[179,180] With similar goals in mind, Lippard's group[11,12] suggested that structurally similar planar Pt(II) terpyridine complexes to these planar dyes would also intercalate into DNA. Complex **241** was chosen over other Pt(II) terpyridine complexes, as an intercalator, in order to eliminate the possible covalent binding of the complex to DNA due to the inert character of the Pt−S bond in **241** compared to Pt−R bonds in $[Pt(tpy)(R)]^+$ (R = Cl, O, N) complexes.

Various characterization methods and general experimental criteria were required to confirm the intercalation process, since the terpyridine complexes can covalently bind to DNA bases as well as electrostatically insert into the DNA groove. These requirements were summarized by Long and Barton.[179]

5.1.1. UV−Vis Spectroscopic Analysis and Binding Modes

The absorption spectra of **241** with increasing amounts of ct-DNA showed dramatic changes, such as a strong decrease in peak intensity (hypochromocity) and red shift of the bands at ca. 550 nm with well-defined isobestic points (Figure 80).[11] These observed shifts were strongly dependent on the concentration of the intercalator and DNA, the buffer solution, and its ionic strength ($I = [M^+]$: total positive ion concentration). Red shifts of the bands are usually observed for the intercalation binding mode, whereas the strong hypochromocity is attributed to an electronic interaction between bound molecules and the DNA.[179]

A classical Scatchard[181] analysis (r/c vs r, r = Bound-[Pt]/[DNA], c = Free-[Pt]) of these spectrophotometric titration data at 342 nm upon addition of ct-DNA to **241** and **242** in a low ionic strength buffers displayed concave upward curves at large r values (Figure 81).[11,13] This

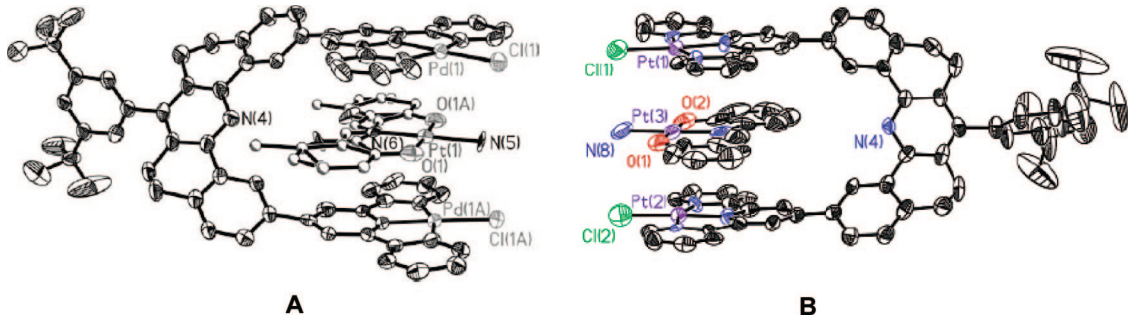

Figure 74. (A) Single crystal X-ray structures of [**157**][**201**], (Reprinted with permission from ref 160. Copyright 2004 Elsevier) and (B) [**160**][**198**]. (Reprinted with permission from ref 159. Copyright 2003 American Chemical Society).

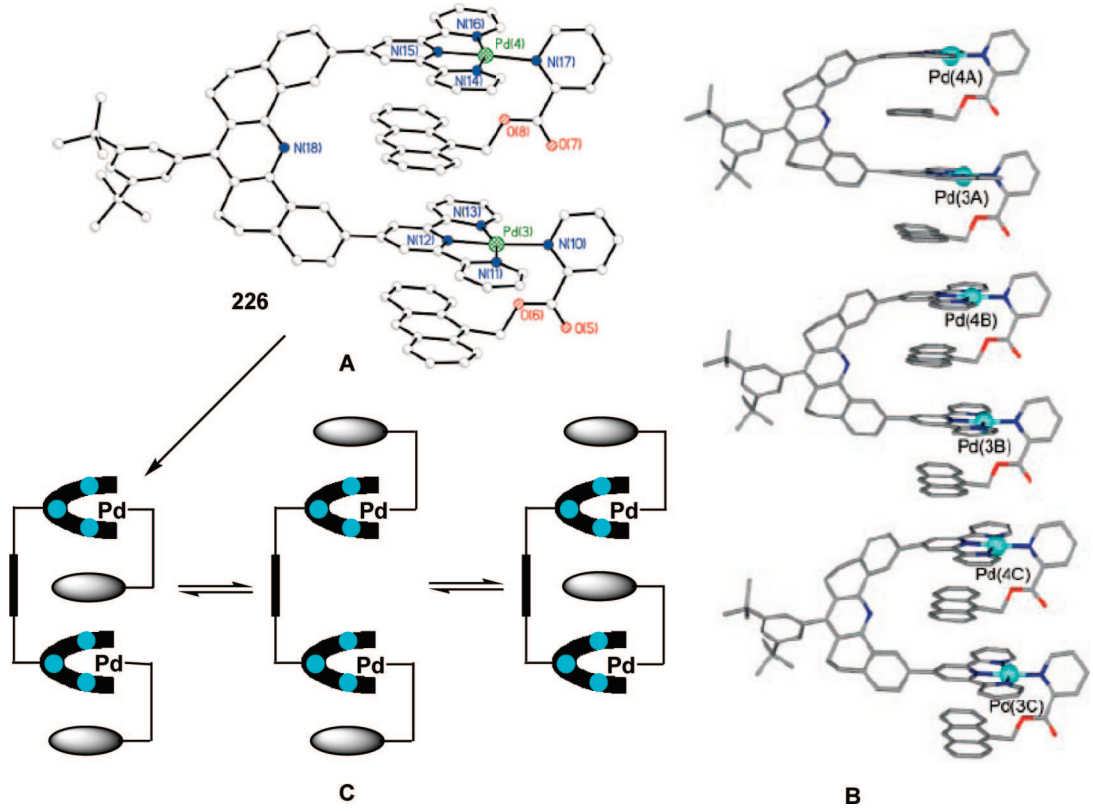

Figure 75. (A) Single crystal X-ray structure and (B) packing diagram of the covalently bound host−guest complex **226** and (C) its fluxional behavior. (Reprinted with permission from ref 156. Copyright 2002 National Academy of Sciences, U.S.A.).

behavior is indicative of two different binding modes: a strong intercalative mode and a weaker nonintercalative secondary interaction.[182] This argument was supported by the analysis of ct-DNA contour length ratio (L/L_0) in the presence (L) and absence (L_0) of **242**, where a linear increase in helix extension was observed up to $r \sim 0.2$, followed by a marked decrease in the helix extension suggesting a nonintercalative binding component.

The binding constants (K_B) of intercalators **241** and **242** into DNA in low ionic strength buffers estimated by extrapolating the data in the Scatchard[181] plot to the ordinate axis,[11,13] since the data did not fit the McGhee-von Hippel[183] equation. However, as the ionic strength of the buffer increased, the secondary nonintercalative interaction of **241** and **242** with ct-DNA was eliminated; eventually, the UV−vis titration data fit the McGhee-von Hippel equation[183] in order to determine K_B, which are summarized in Table 3 for various Pt(II) terpyridine intercalators **241**−**254** (Figure 82).[13,182,184−186] Most of the Pt(II) terpyridine complexes **241**−**250** bound the DNA exclusively *via* intercalation; however, $[Pt(tpy)(Cl)]^+$ (**251**),[184] $[Pd(tpy)(Cl)]^+$ (**254**),[184] and $[Pt(tpy)(OH)]^+$ (**253**)[76] were covalently bound to the DNA as well as intercalatively, since they contain -Cl or -OH, as co-ligands. Various other methods (e.g., CD, competitive fluorescence, and ultradialysis experiments) were also utilized to calculate binding modes and constants.

The linear dependence between the logarithmic scale of the observed binding constant (K_B) of **242** (Figure 83)[13] to DNA and the ionic strength of the medium ($I = [M^+]$) was explained by polyelectrolyte theory[188] in the following equation:

$$\mathrm{Log}(K_B) = -\mathrm{Contant} \times \mathrm{Log}([M^+]) + \mathrm{Log}(K_0)$$

where K_0 is the binding constant of the intercalator to DNA at 1 M positive ion concentration ($I = 1$). This binding constant was considered to be free of ion concentration effects and calculated by extrapolating the plot of $\mathrm{Log}(K_B)$ versus $\mathrm{Log}([M^+])$ to the ordinate axis. Ion free binding constants (K_0) of **241**[189] (3.5×10^3 M^{-1}) and **242**[13] (4.1×10^3 M^{-1}) were ca. 20 times less than that of EthBr[189] (7.4×10^4 M^{-1}).

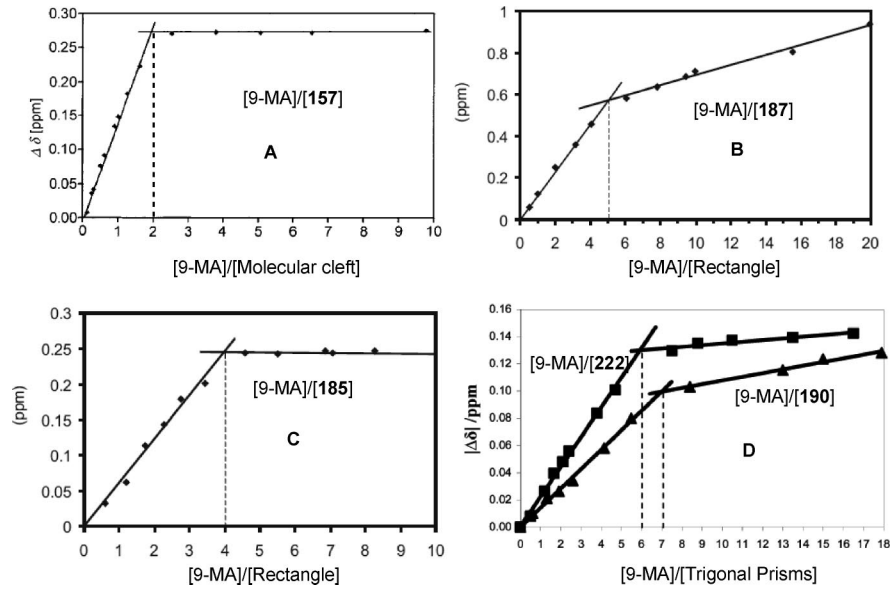

Figure 76. The mole-ratio of guest/host plotted against ^{1}H NMR shifts of host and/or guest protons in order to find the stoichiometry of host−guest complexes. ((A) Reprinted with permission from ref 71. Copyright 2003 American Chemical Society; (B and C) reprinted with permission from ref 154. Copyright 2001 Georg Thieme Verlag Stuttgart · New York; (D) reprinted with permission from ref 157. Copyright 2003 The Royal Society of Chemistry).

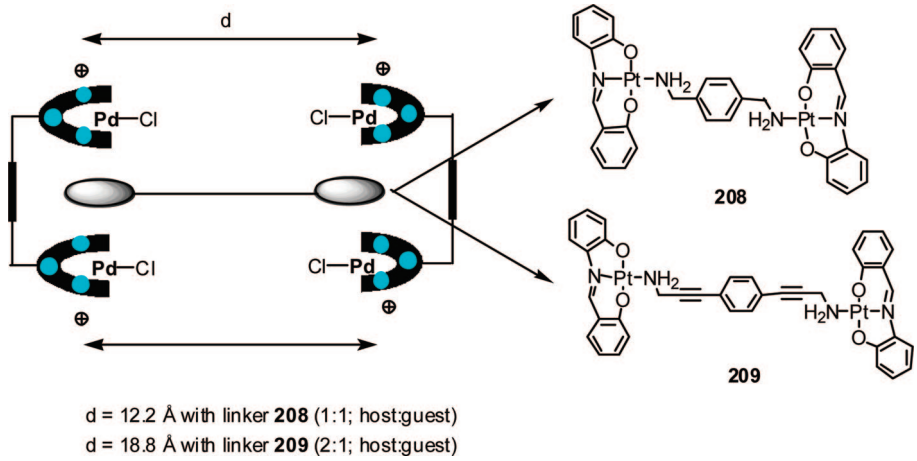

Figure 77. Schematic diagrams of host−guest interactions of **208** and **209** with **157**.[158]

Scheme 15. Host−guest Complex {[157][200]}, as Molecular Switching and/or Motors[161]

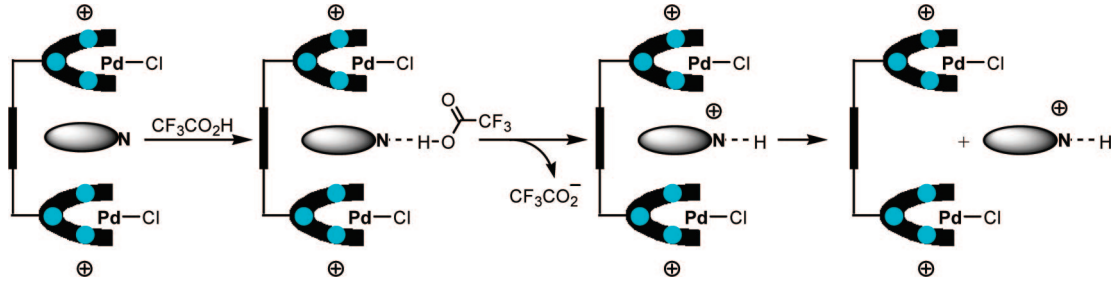

5.1.2. Viscosity and Thermal Denaturation

DNA must partly unwind to accommodate the intercalators. The unwinding of DNA induces an increase in its relative contour length[182] (L/L_0) leading to an eventual stiffening of DNA, which results in an increased viscosity,[190] for example, the specific viscosity (η_{sp}) of a DNA solution increased upon addition of **241** and reached a saturation point at r of 0.23 (Figure 84).[11] The relative counter length of DNA (L/L_0) was estimated from viscosity experiments.[191,192] A similar behavior in viscosity and counter length was observed for structurally similar terpyridine-based intercalators to DNA.[11,13,55,182,186,192] Recently, a Quartz Crystal Resonator (QCR) was invented to determine the binding mode of the molecules to DNA by measuring the increase in its viscosity.[193]

The unwinding of DNA as a result of intercalation also leads to an increase in its melting temperature (T_m), which refers to a transition of the double strand to a single strand DNA by thermally breaking the H-bonds. This thermal denaturation of DNA is easily monitored by changes in UV−vis absorption at 260 nm. In the case of intercalators **246**−**248**, the complete thermal denaturation of DNA was

Scheme 16. Formation of Cyclic Peptides 229−232[170]

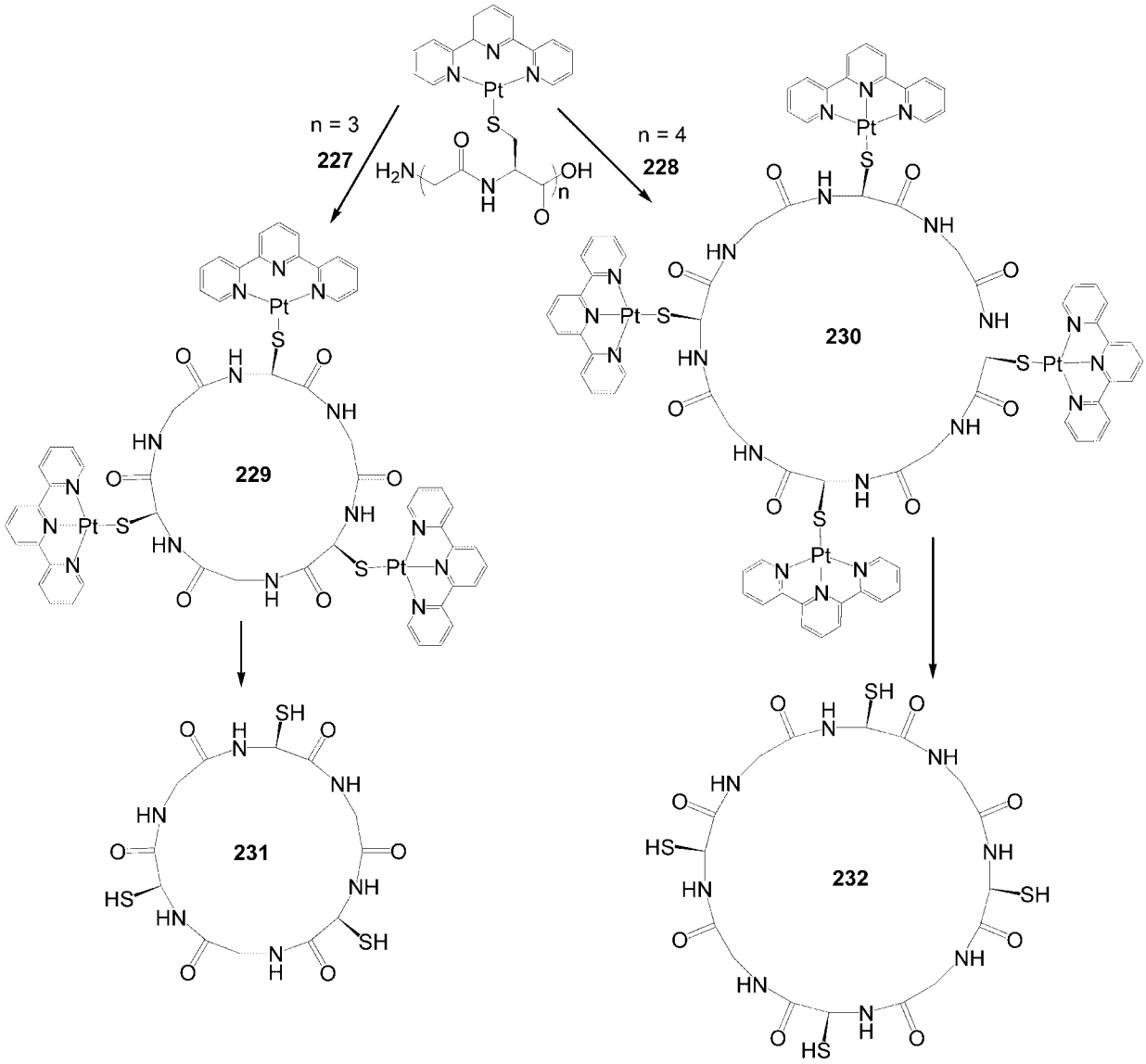

shown to occur in two steps (Figure 85C).[55,186] It was suggested that a part of the DNA, which was not bound to the Pt intercalator, melted in the first transition, then the part containing the intercalator melted at a higher temperature; however, in the case of **241** and **251**, complete denaturation occurred in one-step (Figure 85 E and B, respectively).[11,55,186,192] The differences in melting temperature (ΔT_m) of ct-DNA upon the addition of intercalators are summarized in Table 3.

5.1.3. Induced Circular Dichroism

Other evidence for the intercalation of Pt−terpyridine complexes into DNA is derived from its circular dichroism spectra, which display signals in the range of 300−500 nm caused by an induced circular dichroism (CD).[11,55,77,186] For example, the CD spectrum of **246** and **247** showed positive bands between 300−400 nm in the presence of ct-DNA (Figure 86). Furthermore, McCoubrey et al.[55] used the CD titration spectra of the intercalator to calculate the binding constant of intercalator **248** to DNA. The initial equilibrium binding constant was calculated to be 2×10^7 M^{-1} suggesting a binding site of about the size of four base pairs; as the ratio of the Pt complex to DNA increases, a second binding mode was observed in which K_B was calculated to be 1×10^6 M^{-1} suggesting a binding site of about the size of two base pairs.

5.1.4. Competitive Fluorescence Spectroscopy

The fluorescence Scatchard[181] plot for the binding of EthBr to DNA in the presence of an increasing amount of Pt-terpyridine-based intercalators displayed two different observations.[11,184] The Scatchard plot of EthBr and **241** in the presence of DNA (Figure 87A) revealed only a competitive inhibition between EthBr and **241**, which was characterized by a decrease in the slope caused by the presence of an increasing amount of metal complex with no change in the intercept at the abscissa.[11] However, the Scatchard[181] plot of EthBr and **251** in the presence of DNA revealed two different features resulting from a competitive inhibition between EthBr and **251** (line 1, 2, and 3) as well as a noncompetitive inhibition, which is illustrated with a change in both the slope and the intercept in line 4 and 5 ([DNA]/[**251**] < 2, Figure 87B). The competitive inhibition of EthBr is attributed to intercalation of **241** and **251** and the noncompetitive feature of **251** probably caused by the removal of the labile Cl ion from the intercalator suggesting

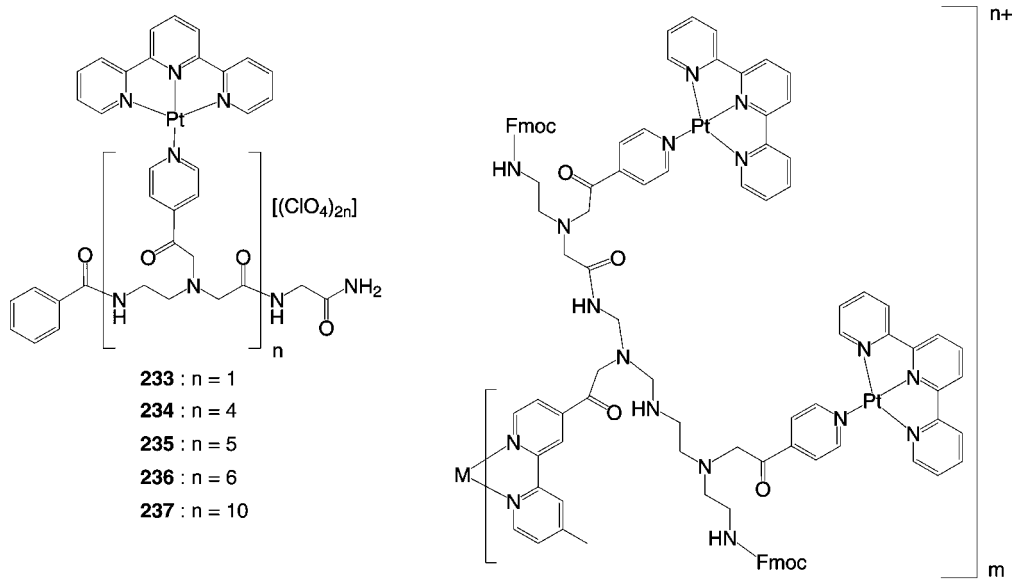

Figure 78. Chemical structures of metal-containing artificial peptides **233**−**240**.[171,172]

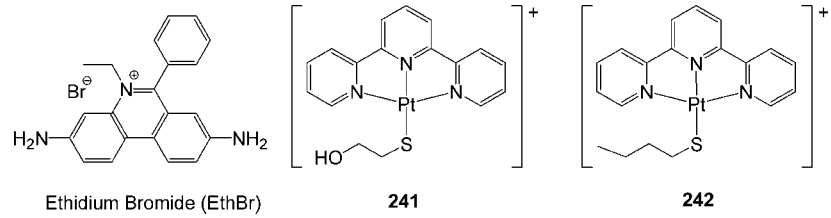

Figure 79. Structures of ethidium bromide (EthBr) and Pt(II) complexes **241** and **242**.

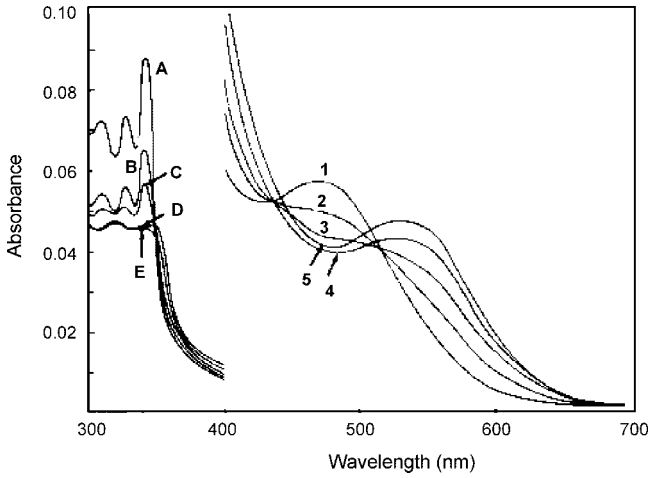

Figure 80. UV−vis spectra of **241** upon addition of various amounts of ct-DNA in a 1 mM sodium phosphate buffer with 3 mM NaCl ($I = 0.003$) at pH 6.8. In curves A−E, concentration of **241** is 6.97 μM and DNA-P concentrations are (A) 0, (B) 17, (C) 34, (D) 146, and (E) 303 μM. In curves 1−5, concentration of **241** is 70.4 μM and DNA concentrations are (1) 0, (2) 97.7, (3) 189, (4) 356, and (5) 700 μM. (Reprinted with permission from ref 11. Copyright 1974 S. J. Lippard).

its covalent binding to the DNA. The binding constants (K_B) of **241** and **251** (in the range of [DNA]/[**251**] > 2) to DNA were calculated via fluorescence competition studies (Table 3).[11] A similar fluorescence competition study revealed that the binding constant of **251** to ct-DNA ($K_B = (4.95 \pm 0.30) \times 10^7\ M^{-1}$) is 250 times larger than the binding constant of **241** to ct-DNA.[55]

5.1.5. Closed Circular DNA

Closed circular DNA was utilized to prove the intercalative binding mode of the Pt-terpyridine-based complexes. Different topologies of circular DNA are depicted in Figure 88. It was mathematically suggested that the total winding of the strands (α) resulting from normal turns (β) and superhelical turns (τ) must remain constant in the absence of backbone chain scission (nicking) according to $\alpha = \beta + \tau$.[194] Unwinding of closed circular DNA (form I or I_0) by the intercalation of **241** was detected by its band sedimentation behavior; however, **241** did not affect the band sedimentation of nicked DNA (form II), which is not subject to the topological constraint;[11,12,184] a similar behavior was observed for EthBr.[195] Helix unwinding angles were calculated by viscosity titration of closed circular DNA to be 17.5°.[182]

5.1.6. Stereochemical Changes in DNA

Although intercalation has been proven and is widely accepted as a binding mode for Pt−terpyridine complexes to DNA, stereochemical details of this process are needed to understand the real effect of intercalation on the backbone DNA geometry, especially with regard to the pucker of the deoxyribose ring. To this extent, Crothers[196] suggested a "neighbor exclusion model," which proposes that every other interbase pair site contains a bound intercalator upon

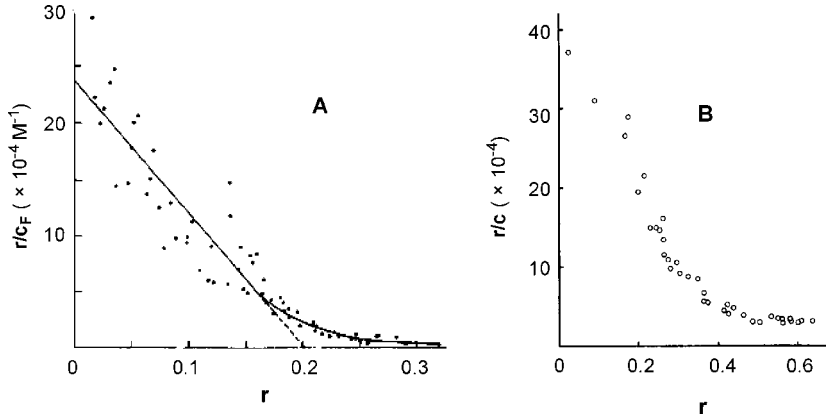

Figure 81. (A) Scatchard[181] plot for **241** in a buffer $I = 0.003$, (Reprinted with permission from ref 11. Copyright 1974 S. J. Lippard), and (B) **242** in a buffer with at $I = 0.01$, binding to calf thymus DNA. (Reprinted with permission from ref 13. Copyright 1987 The Biochemical Society).

Table 3. The DNA Binding Constants (K_B) of Intercalators 241−254 and Their Effect in Melting Temperature (ΔT) of ct-DNA

intercalator	K_B, M^{-1}(binding constants)	$I =$ [M^+]	ΔT, (deg) (ct-DNA)	reference
241	$(1.2 \pm 0.2) \times 10^5$ [a,e]	0.003	5.0[e]	11
	$(5.1 \pm 0.2) \times 10^5$ [c,f]	0.1	3.4[f]	
	$(3.9 \pm 0.3) \times 10^5$ [c,g]	0.2	2.5[g]	
242	$(4.5 \pm 0.3) \times 10^5$ [b,i]	0.1	NA	13
	$(4.3 \pm 0.2) \times 10^4$ [b,i]	0.1		
	$(8.4 \pm 0.5) \times 10^3$ [b,i]	0.1		
243	$(4.3 \pm 0.5) \times 10^5$ [c,g]	0.2	NA	184
244	$(0.5 \pm 0.1) \times 10^5$ [c,g]	0.2	NA	184
245	$(1.0 \pm 0.2) \times 10^5$ [c,g]	0.2	NA	184
246	$(3.5 \pm 0.3) \times 10^4$ [b,h]	0.15	12.2[h]	186
247	$(3.0 \pm 0.3) \times 10^3$ [b,h]	0.15	12.3[h]	186
248	$(5.3 \pm 0.5) \times 10^4$ [b,h]	0.15	6.0[f]	55, 186
	$(1.8 \pm 0.5) \times 10^7$ [d,f]	0.1		
	$(4.9 \pm 0.3) \times 10^7$ [c,f]	0.1		
249	NA	0.003	3.0[e]	77
250	$(9.8 \pm 1.3) \times 10^3$ [b,h]	0.15	NA	187
251	$(1.3 \pm 0.2) \times 10^5$ [c,f]	0.2	5.0[f]	55, 184
252	NA	0.001	7.8[k]	40
253	$(7.0 \pm 0.6) \times 10^4$ [a,j]	NA	NA	76
254	$(1.9 \pm 0.2) \times 10^5$ [c,f]	0.1	NA	184

[a] Calculated by classical Scatchard[181] analysis of UV−vis. [b] Calculated by McGhee-von Hippel[183] analysis of UV−vis. [c] Calculated by Scatchard[181] analysis of florescence study. [d] Calculated by analysis of circular dichroism. [e] One millimolar phosphate buffer with 3 mM NaCl at pH = 6.8. [f] Fifty millimolar Tris·HCl buffer with 0.1 M NaCl at pH = 7.5. [g] Fifty millimolar Tris·HCl buffer with 0.2 M NaCl at pH = 7.5. [h] One millimolar phosphate buffer with 0.15 M $NaNO_3$ at pH = 7. [i] Two millimolar Hepes buffer with 0.1 M KF at pH = 7. [j] Fifty millimolar EPPS buffer at pH = 9. [k] 45 mM Tris buffer with 1 mM Na_2H_2EDTA at pH = 7.5.

saturation (Figure 89). The electron-dense intercalator **241** was utilized as a labeling agent to investigate the X-ray fiber diffraction pattern of calf thymus DNA. Quality X-ray fiber diffraction pictures strongly supported this neighbor exclusion model in which electron-dense Pt atoms are evenly distributed by 10.2 Å throughout the backbone of DNA, in every other interbase pair site.[197]

The single crystal X-ray structure of **241** with two base pair DNA fragments (deoxy-CpG, Figure 90) provided a clear picture of how intercalation occurred by modifying the DNA's backbone conformation.[198] In the crystal lattice, two **241** cations formed a neutral complex with a dimer of deoxy-CpG, which was formed by three H-bonding of paired guanine and cytosine bases, as in the double helical DNA. The complex **241** is intercalated between two base pairs in the DNA fragment, as envisioned down the *a* axis of the lattice (Figure 91). The conformation of deoxyribose at the 3′-end of the DNA fragment possesses a C2′ endo pucker, which is the normal pucker conformation found in B-DNA. However, deoxyribose at the 5′-end of the DNA fragment is a C3′ endo pucker, which is a modified pucker conformation found generally in double helical RNA and not in B-DNA. This conformational modification of the deoxyribose ring was initially suggested by Bond et al. [197] from X-ray fiber diffraction pattern, model building, and Fourier transform studies. Furthermore, the unwinding angle (23°)[198] of a double helical deoxy-CpG dimer with **241** was found to be very similar to the 22.6° angle[197] of ct-DNA with **241**, as determined by its X-ray fiber diffraction pattern.

The difference in the conformation of the deoxyribose ring in 3′- and 5′-end of the double helical fragment can be clearly seen by looking down the *b* axis in Figure 92.[198] The guanine and cytosine bases displayed extensive $\pi-\pi$ interactions with **241**; specifically, the O6 of both guanines is positioned virtually above and below the central Pt(II) metal that was separated by 3.4 Å from each oxygen.

5.1.7. Site-Specific Intercalation

The intercalation of **241** into different DNAs with various guanine-cytosine (G-C) contents was investigated by means of the binding affinity (σ) parameter, which was calculated by the extrapolation of a Scatchard plot to its *r/c* axis.[189] As well, the relative binding affinity (ϵ) was calculated by the ratio of binding affinity of the two different DNAs. Both binding parameters are summarized in Table 4. Linear relationships between different G-C content of DNAs and binding affinities (σ) of **241** (Figure 93) revealed its preference to intercalate between the G-C DNA base pair. One of the reasons for this specific binding is the stabilization of Pt(II) metal that can be sandwiched between two guanine O6 atoms, as observed in its crystal structure (Figure 92).[198] Relative binding affinity (ϵ) of **242** between *Micrococcus lysodeikticus* (72% G-C) and *Clostridium perfringens* DNA (30% G-C) was calculated to be 2.4 displaying the same behavior compared to **241** ($\epsilon = 2.62$).[13,189]

5.1.8. Other Mononuclear Intercalators

A new generation of Pt−terpyridine complexes **255**−**258** that are connected to a ^{10}B-containing carboran[199–202] cage (^{10}B natural abundance is ∼ 20%) through a monothiolate

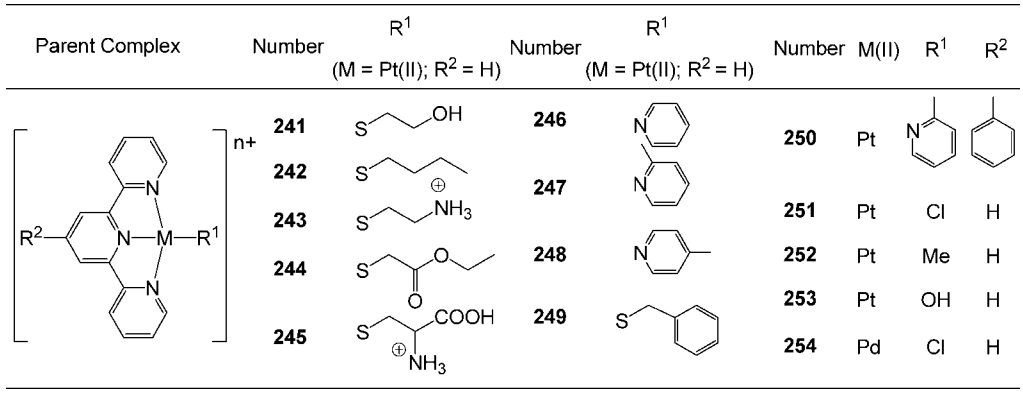

Figure 82. Structures of intercalators **241**−**254** to ct-DNA.[11,13,40,55,182,184–187]

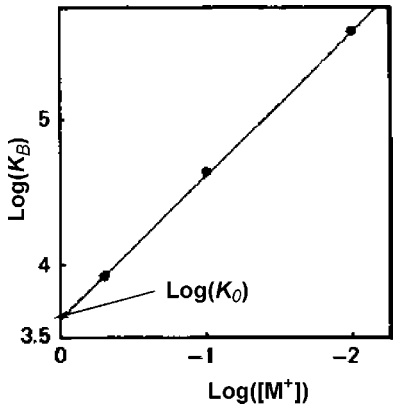

Figure 83. Plot of Log(K_B) vs Log([M^+]) for **242** and ct-DNA. (Reprinted with permission from ref 13. Copyright 1987 The Biochemical Society).

bridge (Figure 94) was synthesized for DNA intercalation opening the possibility to its potential application of boron neutron capture therapy (BNCT)[203] to treat cancer cells. The glycerol group was introduced to the carborane cage in **258** in order to overcome the solubility problems in aqueous media, which can limit its application.[199] The UV−vis titration of these complexes with an increasing amount of DNA displayed bathochromic shifts and hypochromocity indicative of intercalation;[201] however, the titration data did not fit the Scatchard plot to calculate binding constants (K_B), since deviation from Beer's law suggested an aggregation of complexes **255**-**258** at concentrations greater than 13 μM.

Ma et al.[20] reported DNA binding studies of the water-soluble glycosylated acetylide and arylacetylide Pt-tpy complexes **259**−**266** (Figure 95), as possible antitumor drugs and potential luminescent probes *via* binding to glycosylated biomolecules. The binding constants of **264**−**266** to ct-DNA were measured to be 4.8×10^5, 3.7×10^5, and 6.9×10^5 M^{-1}, respectively, by Scatchard plots of absorption spectra. Hypochromic and bathochromic shifts in absorption titration of **264** and **266** with DNA suggested intercalation; moreover, gel mobility shift assay studies for **259** possessing bulky *t*-butyl groups on terpyridine as well as **265** revealed that **259** binds electrostatically to the DNA minor groove, whereas **265** binds electrostatically and intercalatively.

The Au(III)-containing complexes **267**−**271** have been utilized as intercalators to DNA (Figure 96). The binding constant of **267** to DNA was calculated to be 5×10^3 M^{-1}, which is lower than for **241**.[204] Ultradialysis experiments revealed the possible electrostatic binding of the complex **267** to DNA as well as intercalation. Other evidence for intercalation came from an induced circular dichroism of **267** with DNA and an increase for the melting temperature of ct-DNA ($\Delta T_m = 12.4°$) in 10 mM $NaClO_4$ buffer with $I = 0.001$ in the presence of the complex.

Various charged sites and bulky groups were introduced to Au(III)-terpyridine complexes **268**−**271** in order to investigate their effect on binding properties of these complexes to DNA.[205] The intercalation of **268**−**271** into DNA was proven by hypochromic and bathochromic shifts in UV−vis titration, induced circular dichroism, and competitive fluorescence studies with EthBr. The decreased fluorescence intensity of EthBr with DNA follows the order **268** ≥ **270** > **271** > **269**, which revealed that smaller groups on these complexes favored the replacement of EthBr *via* intercalation; however, the intensity decrease in CD spectral shifts in the presence of increasing amounts of complex follows the order of **271** > **268** > **270** > **269**, suggesting that increasing charge favored the binding. The UV and CD of **268**−**271** gave similar results reflecting both steric and electrostatic effects of the chemical groups on binding, whereas competitive fluorescence studies mainly illustrated the effect on intercalation. The *in vitro* DNA binding studies of Au(III) complexes were performed by incubating **268** and **271** with human epichelical kidney cells (293T). After 12 h of incubation, DNA was isolated from the cells and it was determined that the concentration was 207.8 μg mL^{-1}. The ICP-MS analysis revealed that the isolated DNA contained 18.9 and 24.9 ng $mL^{-1}$of **268** and **271**, in which one gold ion is present for each 6400 and 4900 nucleotides, respectively.

5.1.9. Multinuclear Intercalators

Various dinuclear DNA intercalators **272**−**280** were synthesized by linking two Pt-terpyridine moieties through α,ϵ-dithiols of the type HS-$(CH_2)_n$-SH ($n = 4-10$) and a xylyl group (Figure 97).[13,77,182] Intercalative binding of these complexes was demonstrated by UV−vis bathochromic shifts and hypochromocity, induced circular dichroism, and increased viscosity and melting temperatures for ct-DNA.

Helix-extension parameters for **272**−**278** were calculated from the plot of relative contour length (L/L_0) versus drug/nucleotide (D/P) or binding ratio (r).[182] The unwinding angles were determined by viscosity titration measurements with closed circular DNA. Comparison of the helix extension parameters and unwinding angles between monointercalator **242** and bisintercalators **272**−**278** suggested that **273**, **274**, and **277** showed mainly bisintercalation, whereas **276** and **278** displayed a mixture of mono- and bisintercalation (Table 5); however, the data from **272** and **278** did not permit a definitive assignment of the binding mode. Binding constants

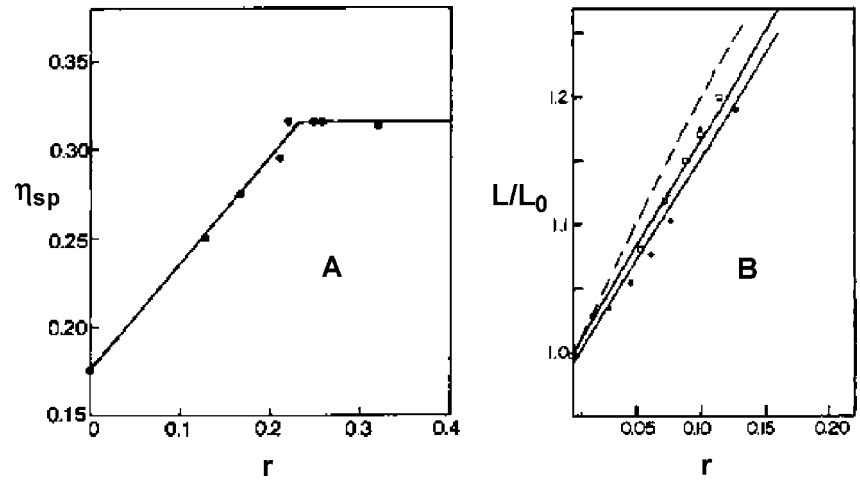

Figure 84. (A) The specific viscosity with intercalator **241** in 1 mM phosphate buffer with $I = 0.003$ at pH 6.8 (Reprinted with permission from ref 11. Copyright 1974 S. J. Lippard), and (B) their relative counter length (L/L_0) in 50 mM Tris·HCl buffer with $I = 0.2$ at pH 7.5 of DNA as a function of r (Bound-[Pt]/[DNA]). (Reprinted with permission from ref 192. Copyright 1979 American Chemical Society).

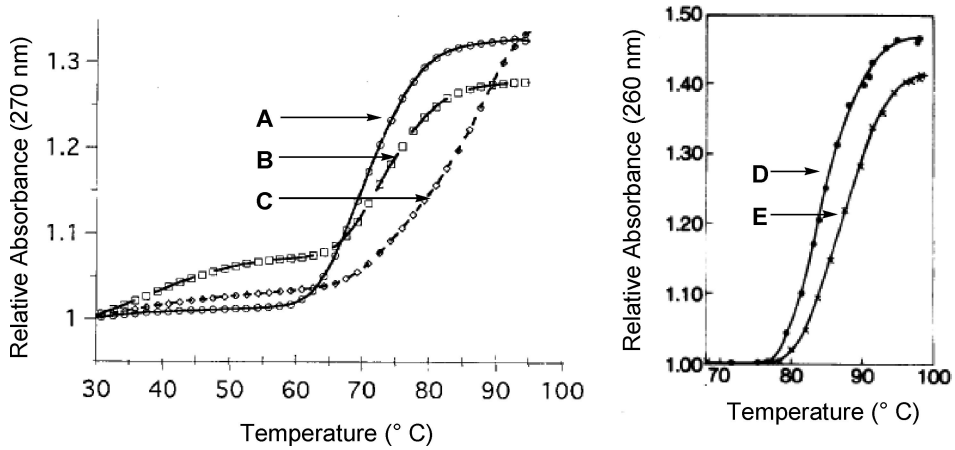

Figure 85. Thermal denaturation curves of 400 μM of ct-DNA (A) alone, with (B) 20 μM of **251**, and (C) **248**; 85 μM of ct-DNA (D) alone and with (E) 3.5 μM of **241** ((A−C) Reprinted with permission from ref 55. Copyright 1996 Elsevier; (D and E) reprinted by permission from ref 11. Copyright 1974 S. J. Lippard).

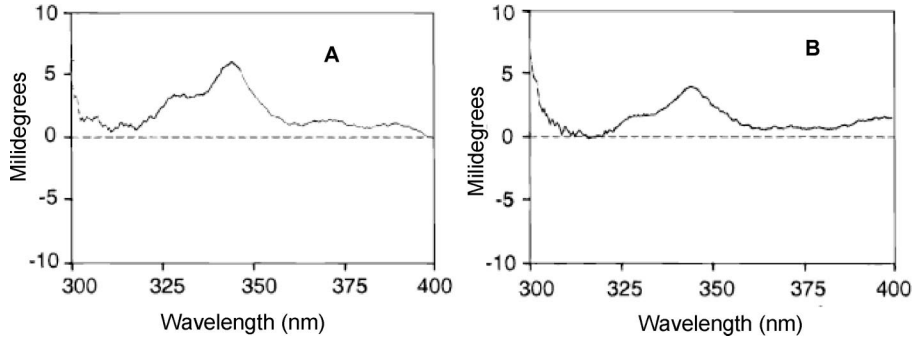

Figure 86. CD spectrum of (A) **247** and (B) **246** (50−80 μM) in the presence of 10-fold excess of DNA at 25 °C (1 mM phosphate buffer with $I = 0.0015$ at pH 7.0). (Reprinted with permission from ref 186. Copyright 1999 American Chemical Society).

were calculated only for **242**, **272**, and **274**.[13] Relative binding affinity (ϵ) for bisintercalators revealed that they prefer to bind G-C base pair of the DNA with a lower affinity than the monointercalator **242**.

The bis-Pt complexes **279** and **280**, connected through the xylyl group from either the 1,3- or 1,4-positions, respectively, were utilized as a bisintercalator.[77] The CD spectra displayed a normal induced circular dichroism for bisintercalator **280** and its mono analogue **249**; however, the CD spectra for **279** displayed a new negative Cotton effect, suggesting that **279** distorted the DNA. The bis-Pt complex **280** was monofunctionally bound to the DNA (Figure 98).

Inspired by the higher affinity of bisintercalators **281**−**284** compared to their monoanalogues, Woodhouse et al.[200] reported a series of bis-Pt-terpyridine complexes connected through the 1,2-, 1,7-, and 1,12-positions of a carborane cage (Figure 99). Their DNA binding studies have not yet been reported but *in vitro* cytotoxicity was investigated against L1210 murine leukemia cell line.

van der Schilden et al.[206] reported the first heteronuclear dimetallic complex **285** containing a pseudo-octahedral $Ru(tpy)_2$ connected to a square-planar Pt(tpy)Cl through flexible diethyleneglycol ether linker, which was crystallized by slow precipitation of the reaction mixture with Et_2O

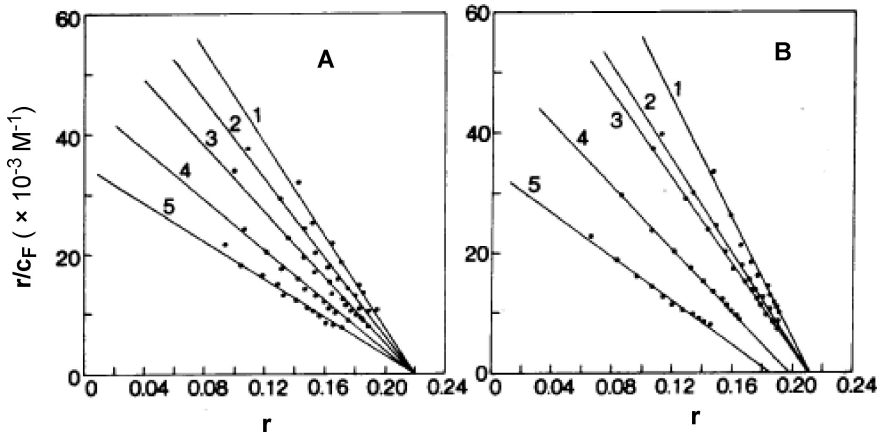

Figure 87. (A) Fluorescence Scatchard plot for binding of EthBr ([EthBr] = 4.9−12 μM) to ct-DNA ([DNA] = 3.5 μM) in a buffer with I = 0.2 at pH 7.5 (line 1) and the presence of an increasing amount of **241**, [DNA]/[**241**] = 4.5 (line 2), 1.8 (line 3), 0.90 (line 4), and 0.45 (line 5). (B) Fluorescence Scatchard plot for binding of EthBr ([EthBr] = 5.2−20 μM) to ct-DNA ([DNA] = 5.8 μM) in a buffer with I = 0.1 at pH 7.5 (line 1) and the presence of an increasing amount of **251**, [DNA]/[**251**] = 5.2 (line 2), 2.6 (line 3), 1.0 (line 4), and 0.52 (line 5). (Reprinted with permission from ref 11. Copyright 1974 S. J. Lippard).

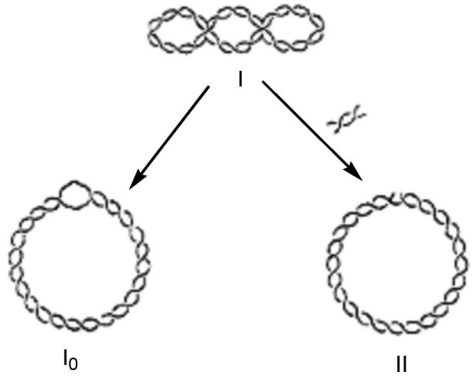

Figure 88. Different topologies of closed circular DNA with several superhelical turns (form I), no superhelical turns (form I_0), and nicked (form II). (Reprinted with permission from ref 12. Copyright 1978 American Chemical Society).

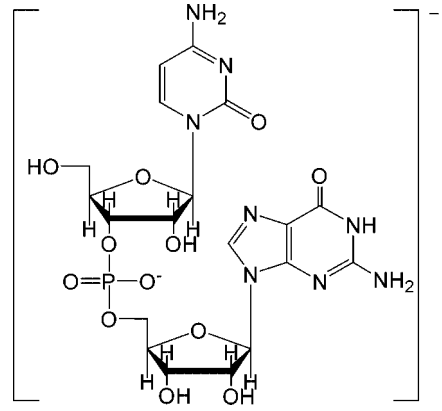

Figure 90. Structure of deoxycytidinyl-(3′,5′)-deoxyguanosine (deoxy-CpG).[198]

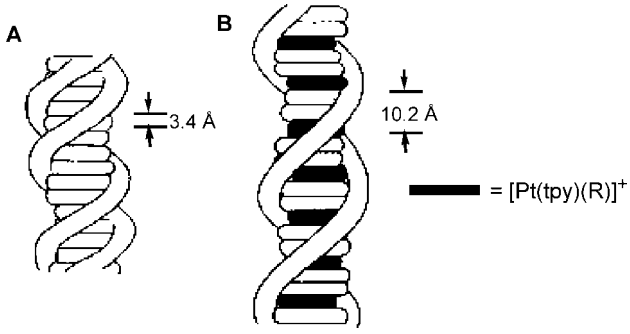

Figure 89. (A) Schematic presentation of double helix B-DNA and (B) neighbor exclusion binding of the intercalator (dark area) to the B-DNA. (Reprinted with permission from ref 197. Copyright 1975 S. J. Lippard).

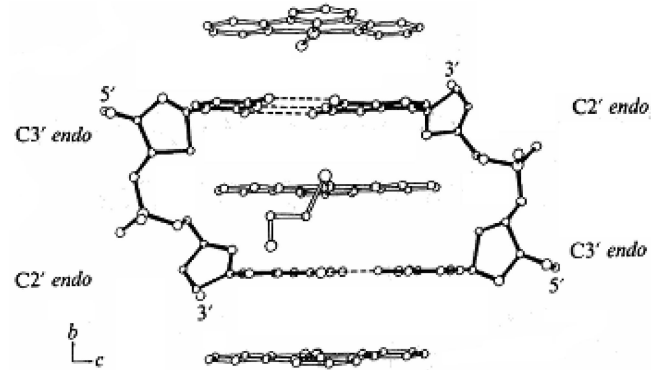

Figure 91. X-ray crystal structure of deoxy-CpG:**241** (2:2) looking down the *a* axis. (Reprinted with permission from Nature (http://www.nature.com, ref 198. Copyright 1978 Nature Publishing Group).

(Figure 100). The single crystal X-ray structure of **285** revealed an intermolecular stacking between the Pt-terpyridine moieties despite the bulky $Ru(tpy)_2$ groups in which Pt metals were infinitely stacked in a head-to-tail fashion with alternating short and long Pt−Pt distances (3.49 and 6.7 Å). Covalent binding of the complex to 9-ethylguanine was reported proving that **285** can intercalate and covalently bind to DNA even when the complex contains a large $Ru(tpy)_2$ that can electrostatically bind to DNA.

Heteronuclear dimetallic complexes **286**−**288** containing a planar Pt(II)-terpyridine moiety connected to another planar Ir(III)-dppz moiety through peptide linkers were synthesized as bisintercalators (Figure 101).[207,208] The UV−vis spectra of **286** with a short peptide linker as well as **287** and **288** possessing longer peptide linkers in the presence of DNA revealed that only monointercalation to DNA occurred from the Ir(III)-dppz end, since hypochromic and bathochromic shifts observed at 382 nm corresponded to dppz moiety not the terpyridine.[207] Binding constants (K_B) of **286** (3.3×10^6 M^{-1}),[208] **287**, and **288** (1.4×10^6 M^{-1})[207] were calculated by UV−vis titration data at 382 nm, which were fit in the

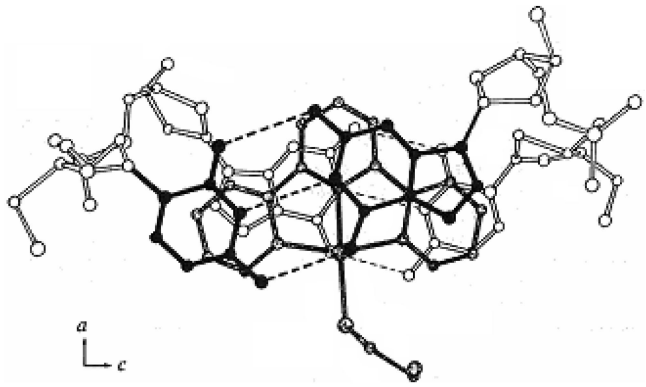

Figure 92. A view of X-ray crystal structure of deoxy-CpG:**241** (2:2) looking down the *b* axis. Top base pairs are drawn in shaded solid black, **241** in the center is stippled, while bottom base pair is unshaded. (Reprinted with permission from Nature (http://www.nature.com, ref 198. Copyright 1978 Nature Publishing Group).

noncooperative nonspecific binding model by Carter et al.[209] and Smith et al.[210]

Recently, ligand **289** containing five oxygens and three nitrogens, self-assembled in a hairpin-like multimetallic structure **290** by wrapping itself around a lanthanide metal (Nd, Eu or La) and connecting to two $[Pt(tpy)Cl]^+$ from its thiol ends (Scheme 17).[211] The Nd−Pt_2 complex **290** showed NIR emissions at 1060 and 1340 nm characteristic for Nd(III) ion with an excited-state lifetime of 670 ns. Intercalation of Nd−Pt_2 complex **290** to ct-DNA and its binding constant was investigated by linear flow dichroism revealing that the complex *bis*-intercalated into DNA with a binding constant (K_B) of 9.5×10^6 M^{-1}.

Peptide nucleic acids (PNA), as an analogue of DNA, were designed and functionalized with pyridines, which were later utilized as scaffolds to connect to Pt-terpyridine moieties, for example, in complexes **233**−**240**.[171,172] It was assumed that the four-tethered Pt-terpyridine complexes on the backbone of the peptide chain, as in **234**, which resemble nucleic acids on the DNA sugar−phosphate backbone, would increase binding affinity of **234**. To this extent, a double-stranded (ds) DNA fragment with 12 base pairs (bp) was chosen as a model for binding studies (Figure 102).[212] The oligomeric sequence of 12 bp ds-DNA with 5′-CGT GAC CAG CTG-3′ containing 75% G-C content was chosen to improve the hybridization efficiency and to circumvent hairpin formation. The binding constants were calculated by isothermal titration microcalorimetry (ITC) revealing that two tetrapeptide **234** bound to each 12 bp ds-DNA has a K_B of 1.7×10^6 M^{-1} and 0.67 Pt atoms per base pair. ITC binding studies of **248** with 12 bp ds-DNA revealed a K_B of 2.5×10^4 M^{-1} and 0.16 Pt atoms per base pair, which showed a dramatic increase in binding affinity of tetranuclear **234** to the DNA compared to mononuclear **248**. Moreover, the CD spectra and thermal denaturation experiments of **234** with DNA confirmed the formation of a 2:1 (**234**:12 bp ds-DNA) adduct by an increase in the T_m of 12 bs ds-DNA from 60 to 85 °C (ΔT_m = 25 °C),[212] which is twice the effect of monointercalators **246**−**248** on T_m of ct-DNA (ΔT_m = 12 °C).[186]

5.2. Covalent Binding to Biomolecules

The intercalation of Pt(II) terpyridine complexes into a DNA offers an aperture route to antitumor drugs, comparable to the well-known cisplatin.[213–215] The Pt drugs administered by injection or infusion could be reacted with other sulfur-containing biomolecules in the blood to form a stable Pt−S bond prior to reaching the targeted DNA intercalate or covalently react with guanine base in order to interrupt its functions.[14,216,217] To shed more light onto the reactivity and mechanism of some of the biomolecules with Pt drugs, many sulfur- and nitrogen-containing amino acids, short peptides, small biomolecules, nucleic acids, ribonucleosides and ribonucleotides were investigated for their covalent binding abilities and kinetics with $[Pt(tpy)(R)]^{n+}$ [R(*n*) = Cl (1), H_2O (2)]. The square-planar Pt(II)-based terpyridine complexes were chosen, as model compounds, because they contain labile leaving groups, such as Cl or H_2O, and have a lower $pK_a \sim 4.5$ ($[Pt(tpy)(H_2O)]^{2+}$) compared to similar $[Pt(NNN)(R)]^{n+}$ complexes.[16–18] Site-specific covalent binding of these Pt(II) terpyridine complexes to biological macromolecules can be utilized as labels to investigate primary, secondary, and tertiary structures in these biomolecules. Furthermore, a few examples of Pd(II) and Au(III) terpyridine complexes that were covalently bound to biomolecules are considered here.

Kostić's group[16–18,152] reported that only three chemical moieties in all of the amino acids were able to react with $[Pt(tpy)(Cl)]^+$; they are the thiol in cysteine, the imidazole in histidine, and the guanidine in arginine. Binding of biomolecules containing these amino acids to $[Pt(tpy)(Cl)]^+$ was characterized by the appearance of new MLCT bands between 300−350 nm in UV−vis, ^1H and ^{195}Pt NMR, and mass spectroscopy. Kinetic studies showed that thiol-containing biomolecules (cysteine, glutathione) reacted 300 times faster than imidazole containing histidine, his-his or gly his-gly under similar conditions.[18] Mixture of glutathione and gly his-gly (1:1) with $[Pt(tpy)(Cl)]^+$ revealed that the Pt(II) terpyridine moiety was bound exclusively to the thiol group in glutathione. It was possible to substitute histidine-bound Pt complex **291** with cysteine leading to complex **292** (Figure 103).[16] The $[Pd(tpy)(Cl)]^+$ complex strongly bound to the thiol in cysteine.[61] Reaction kinetics and their rate constants of $[Pt(tpy)(Cl)]^+$ and $[Pd(tpy)(Cl)]^+$ with cysteine, glutathione, and penicillamine were reported.[63,218] The thiols being smaller nucleophiles and having smaller pK_a values than imidazole were much more reactive toward $[Pt(tpy)(Cl)]^+$ than imidazole. Moreover, Appleton et al.[219] suggested that the Pt(II) terpyridine complex can bind to the N^1 (major) and N^3 (minor) positions of the imidazole moiety in histidine and *N*-acetylhistidine, which termed linkage isomerism.

Guanidine-containing biomolecules (methylguanidine, arginine, *N*-acetylarginine; pK_a = 13.5, 12.5, 12.5, respectively) were reacted with $[Pt(tpy)(Cl)]^+$ under forcing conditions, for example, as high temperatures and mildly basic or both; canavanine (pK_a = 7) is the exception in that it reacted with $[Pt(tpy)(Cl)]^+$under neutral condition.[152] Guanidine-containing biomolecules formed monometallic yellow (**293** and **294**) or dimetallic red (**147** and **148**) complexes with $[Pt(tpy)(Cl)]^+$ (Figure 104). The single crystal X-ray structure of **147** revealed that the interplanar distance between Pt-terpyridyl moieties connected through guanidinyl group is 2.8 Å, suggesting that the d−d orbital interaction between Pt−Pt metal centers and $\pi-\pi$ interaction between terpyridine moieties caused the low energy absorption bands.

The R_2S-containing biomolecules (methionine, L-methionine, *N*-acetyl-methionine, *N*-acetyl-L-methionine, methionine methyl ester, *S*-methyl-L-cysteine, cystine, oxidized glu-

Table 4. Binding Parameters of Intercalator 241 with DNAs of Varying G-C Contents in a 50 mM Tris·HCl Buffer with 0.1 M NaCl at pH = 7.5[189]

DNA	% G-C	$K_B \times 10^{-4}$ (M^{-1})	$\sigma \times 10^{-4}$ (M^{-1})	$K_0 \times 10^{-4}$(M^{-1})	ϵ^a (calculated)	ϵ^b (observed)
C. perfringens	30	5.9 ± 0.6	0.89	2.2 ± 0.2	1.0	1.0
Escherichia coli	42	8.5 ± 0.4	1.24	3.2 ± 0.2	1.40	1.39
Calf thymus	51	10 ± 2	1.55	4.2 ± 0.5	1.70	1.71
Micrococcus luteus	72	10 ± 3	2.34	4.2 ± 0.5	2.40	2.62

[a] G-C mole fraction of DNA_x divided by mole fraction of *C. perfringens* DNA. [b] Binding affinity (σ) of DNA_x divided by binding affinity (σ) of *C. perfringens* DNA.

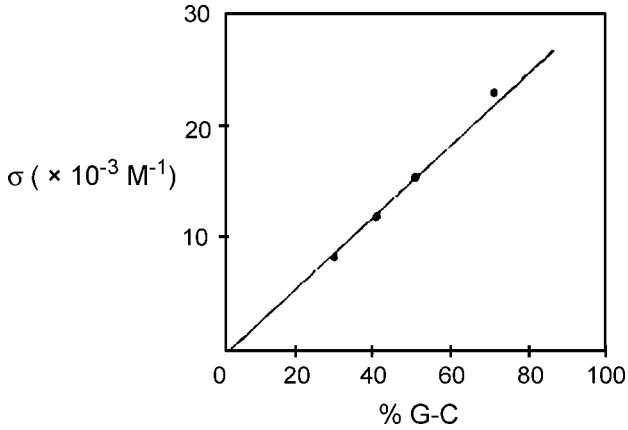

Figure 93. Binding affinity dependence of **241** in DNA possessing various G-C content. (Reprinted with permission from ref 189. Copyright 1979 American Chemical Society).

tathione, and tetrapeptide Trp-Met-Asp-Phe; Figure 105) did not display any reactivity toward $[Pt(tpy)Cl]^+$ or $[Pd(tpy)Cl]^+$ even under forcing conditions, that is, 100 °C, or using a 10-fold excess of the biomolecules.[17,61]

Studies by Bugarcic et al.[14,217,220] confirmed the dominating reactivity of sulfur-containing biomolecules, such as thiourea, DETDC, thiosulfate, Cys, GSH, and penicillamine, over nitrogen-containing nucleosides **295**, **296**, and **298** (Figure 106) toward $[Pt(tpy)(H_2O)]^{2+}$ under neutral conditions. Reaction kinetics and rate constants (k_1) of thiourea, Cys, GSH and PCA were investigated under acidic conditions (pH 1) to keep the nucleophiles fully protonated in order to neglect other rate constants, such as k_2, k_3 and k_4 (Scheme 18).[217] Reactivity order of sulfur-containing nucleophiles toward $[Pt(tpy)(H_2O)]^{2+}$ was found by comparing their pseudofirst order rate constants (k_{obsd}/s^{-1}) as DL-penicillamine < L-Cys < GSH < thiurea.[14,220] The single crystal X-ray structures of thiourea- and cysteine-containing complexes **305** and **306**, respectively, proved the basic distorted square-planar Pt(II) terpyridine structure (Figure 107).[14]

The guanine-containing nucleosides and nucleotides **295**−**298** were covalently bound to $[Pt(tpy)]^{2+}$ *via* N^7 position of the guanine base, which was proven by a single crystal X-ray structure **307** (Figure 107) coupled with their detailed mass spectroscopy analysis.[14,19] However, adenosine **299** and cytidine **300** were each covalently bound to the $[Pt(tpy)]^{2+}$ complex either mono- or difunctionally from N^1,N^6 and N^3,N^4, respectively, which was proven by their ^1H and ^{195}Pt NMR and mass spectroscopy analysis.[19,221] Furthermore, the single crystal structures of mono- and dinuclear *N*-methylcytosine containing Pt(II) and Pd(II) terpyridine complexes **143** and **144** confirmed that the binding sites were N^3,N^4 positions (Figure 57).[69] Since the N^1,N^6 and N^3,N^4 positions of adenosine and cytidine, respectively, were engaged in H-bonding in the double-stranded DNA, the Pt(II) terpyridine complexes can only covalently bind to the guanine base from its N^7 position. Nucleoside-containing Pt(II) terpyridine complexes were easily displaced by thiol-containing biomolecules (thiourea, DEDTC, GSH, Cys, sts), which were stable and could not be replaced by ribonucleotides.[14] Strothkamp and Lippard[15] also introduced a phosphorothioate group to adenosine **302** and uridine **304** observing that these molecules exclusively bind to Pt(II) terpyridine complexes through Pt−S bonding from phosphorothioate moiety rather than from the bases.

Reactivity of coplanar $[Pt(tpy)(R)]^{n+}$ [R (*n*) = Cl (1), H_2O (2)] complexes with biomolecules was attributed to the π-accepting effect and electronic communication between the pyridine rings of the terpyridine.[222,223]

5.3. Labeling Biomolecules

Covalent modification of the amino acid side-chain residues has been an important tool for structural, spectroscopic, and mechanistic studies of proteins.[16–18] Proteins labeled with transition metals have been utilized for their X-ray crystallography, electron microscopy, NMR relaxation, and EPR spectroscopy experiments.[224,225] Toward this goal, selective reactivity of $[Pt(tpy)(Cl)]^+$ toward cysteine, histidine, and arginine among all other amino acids prompted Kostić's group[17,18] to investigate this Pt(II) complex, as a protein labeling agent. Cytochrome *c* proteins from horse and tuna heart, *Candida krusei* and baker's yeast were chosen for labeling studies, since they contain amino acids such as cysteine, histidine and arginine, which can be easily reacted with $[Pt(tpy)(Cl)]^+$ complex. Protein structural studies of cytochrome *c* revealed that the accessible positions of these reactive amino acids were on the outer-sphere of the protein (Table 6).[226–235] Cytochrome *c* protein from Bakers' yeast (*iso*-1 form)[234,235] contains all the reactive amino acids (cysteine, histidine and arginine) exposed to the surface of the protein; however, cytochrome *c* from tuna, horse heart and *C. krusei* only contains histidine and arginine on the surface (Table 6).

Cytochrome *c* proteins were incubated with an equimolar amount of [Pt(tpy)Cl]Cl at 25 °C in 0.1 M acetate buffer at pH = 5.0 for 24 h.[17,18] This procedure allowed only the cysteine and histidine residues to react with $[Pt(tpy)(Cl)]^+$; however, arginine-91 residues in cytochrome *c* proteins reacted upon longer incubation time and additional heating in a buffer at pH 7.0. These reactions were terminated by ultrafiltration and the products were separated by cation-exchange chromatography, and then characterized by UV−vis, ESI-MS, and ^1H and ^{195}Pt NMR spectroscopy. The resulting tagged fractions of the proteins and their yields were summarized in Table 7

Cytochrome *c* protein from horse heart was labeled with $[Pt(tpy)(Cl)]^+$ mainly at His-33 (50%), which was in the hydrophilic region and the protein's outer-sphere;[226] however, only 5% of the protein was labeled at His-26, which was H-bonded in a hydrophobic pocket of the protein.

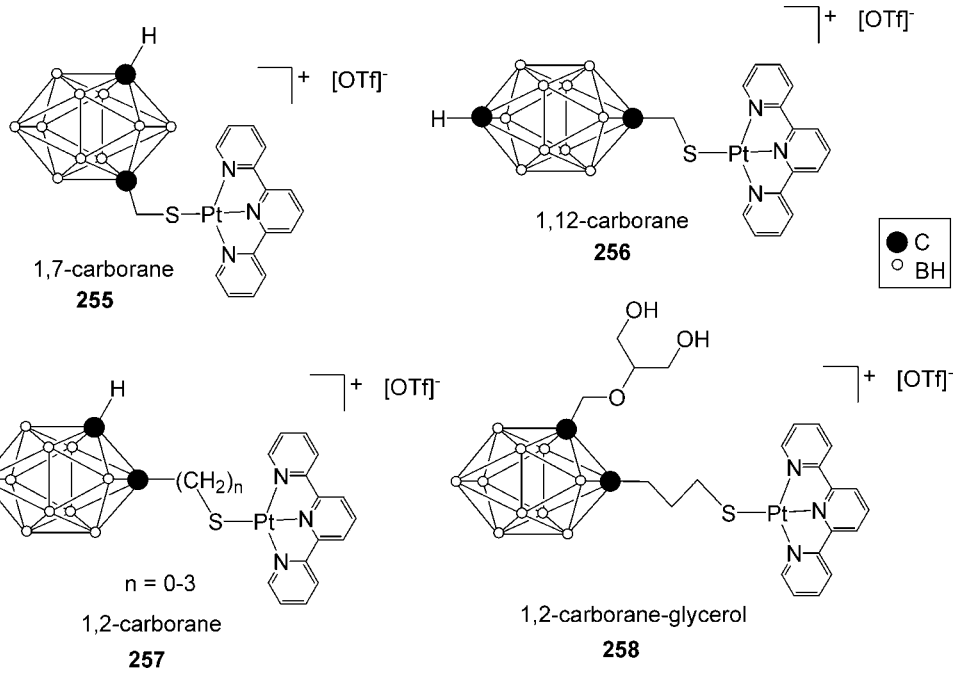

Figure 94. Pt(II) complexes **255**−**258** modified with carborane moieties for use of boron neuron capture theory (BNCT) agents.[199–202]

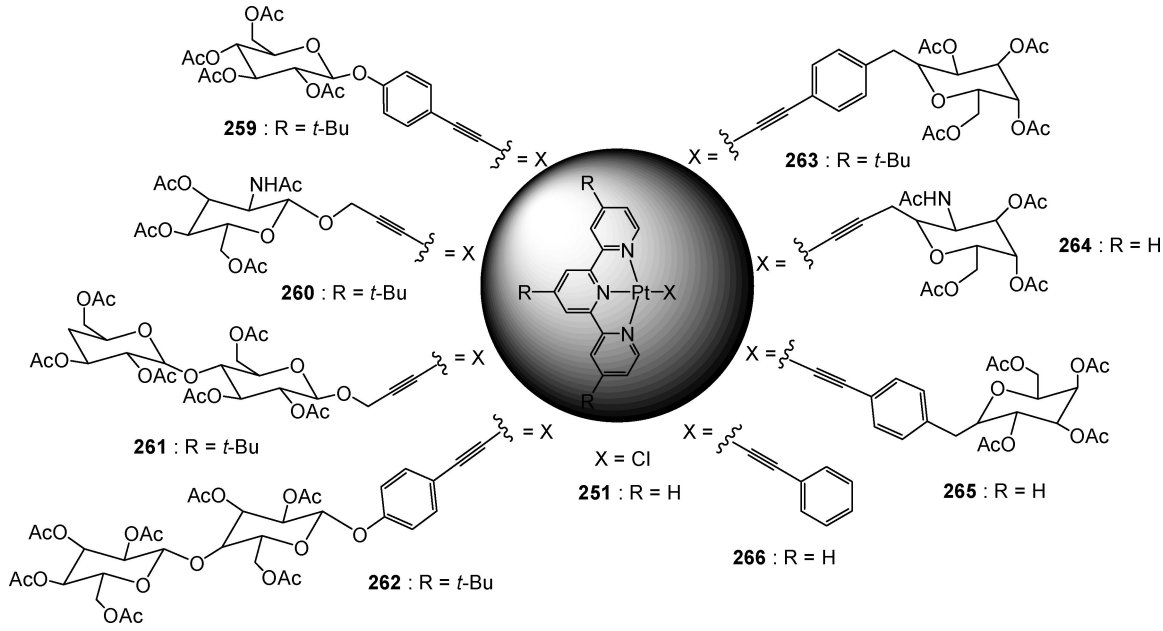

Figure 95. Structures of glycosylated complexes **259**−**266** prepared as potential antitumor agents.[20]

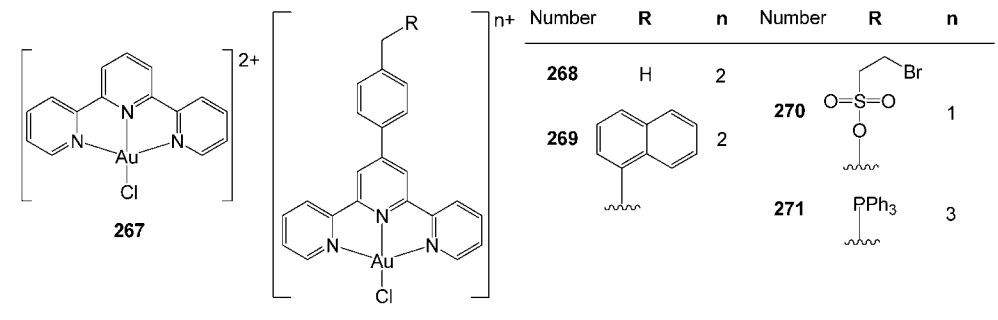

Figure 96. Chemical structures of Au(III)-containing intercalators **267**−**271**.[204,205]

Further, 10% of cytochrome *c* from tuna[227–232] was labeled, since it has only His-26, which is less reactive than His-33 residue.[17,18] The UV−vis spectrum of Pt-tagged cytochrome *c* from horse revealed two unique bands at 328 and 342 nm corresponding to MLCT bands of $[Pt(tpy)(His)]^{2+}$, which displayed different intensity ratios ($\epsilon_{342}/\epsilon_{328}$) depending on

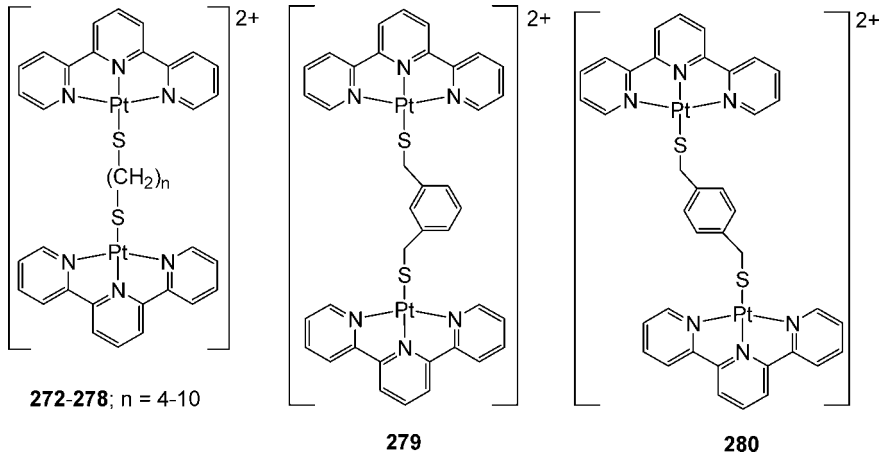

Figure 97. Dinuclear intercalators **272**−**280** prepared by treatment with alkyl and aryl dithiols.[13,77,182]

Table 5. Binding Parameters of Mono- and Bisintercalators to ct-DNA[13,182]

intercalator	helix-extension parameter	increase in counter length (L/L_0, Å)	unwinding angle (deg)	binding constant $K_B \times 10^{-4}$ (M^{-1})[a]	ϵ^b (observed)
242	0.60	2.0	17.5	0.84	2.4
272	0.73	2.5	31.1	3.0	1.1
273	1.12	3.8	31.7	NA	1.4
274	1.13	3.8	36.0	19	1.3
275	1.14	3.9	32.0	NA	1.7
276	0.83	2.8	23.4	NA	1.2
277	1.13	3.8	25.2	NA	1.4
278	0.92	3.1	22.9	NA	1.2

[a] In a 2 mM Hepes/KOH buffer with 0.5 M KF at pH 7.0. [b] The relative binding affinity of complexes between *M. lysodeikticus* (72% G-C) and *C. perfringens* (30% G-C) DNA.

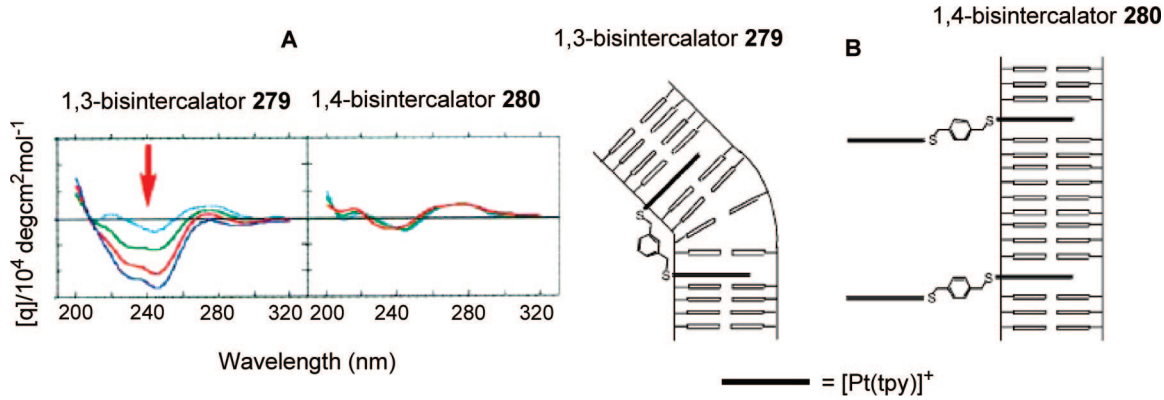

Figure 98. (A) CD spectra and (B) proposed binding modes for bisintercalators **279** and **280** to ct-DNA. (Reprinted with permission from ref 77. Copyright 2003 Elsevier).

the position that the Pt was attached, 1.51 for His-33 and 1.15 for His-26. The absorption of the complex bound to the protein is sensitive to its environment suggesting that the $[Pt(tpy)(Cl)]^+$ tag could be utilized as a protein probe.

Among cytochrome *c* proteins, only the one from Bakers' yeast contains a cysteine residue at the 102 position near the carbonyl terminus.[234,235] The cysteine residue was expected to react with $[Pt(tpy)(Cl)]^+$, since it was proven that the thiol-containing biomolecules are much more reactive than N-containing analogues.[18] However, the yeast protein (*iso*-1 form) was mainly labeled at the His-33 and His-39 residues not at Cys-102 residue, which is buried in the protein's hydrophobic region,[234,235] thus, inaccessible for complexation (Table 7).[18] The *C. krusei* protein,[233] an analogue to the yeast protein lacking the free cysteine, was labeled at His-33 (30%) and His-39 (30%).[18] The arginine-91 residues, which are barely exposed at the surface in either horse or tuna proteins,[226–232] were labeled with 10% yield by $[Pt(tpy)(Cl)]^+$ under forcing conditions.[16] These results have proven that the noninvasive labeling agent, $[Pt(tpy)(Cl)]^+$, is only attached to reactive groups on the protein's surface.[18] Moreover, UV−vis, ^1H NMR, EPR spectroscopy, and cyclic and pulse voltammetry of the tagged proteins did not display any significant perturbation of the protein's morphology.[17] Brothers and Kostic[236] reported a reversible noninvasive modification of serine proteases enzymes, α-chymotrypsin and α-lytic proteases, at their His-57 and His-40 positions in the former and His-57 in the later. Even though labeling the His-57 residue of these enzymes alters their catalytic triad site (Ser-195, His-57, and Asp-102), the platinum-tagged enzymes still possess esterase and amidase activity suggesting that the Pt(II) terpyridine labels for these enzymes are noninvasive.[236]

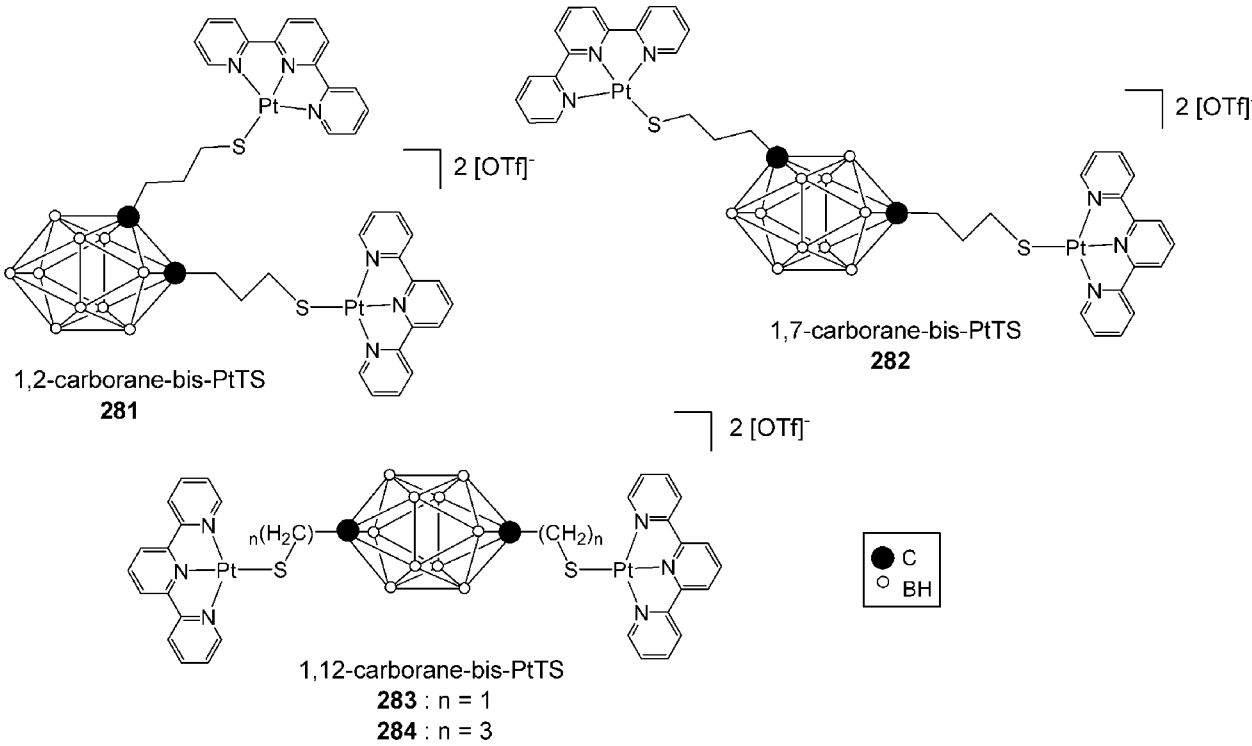

Figure 99. Structure of bis-Pt(tpy) intercalators **281**−**284** containing carborane cages.[200]

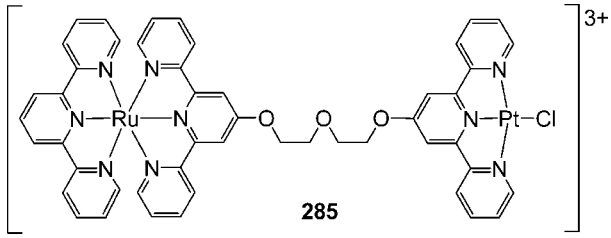

Figure 100. Chemical and crystal structure of Ru(II)−Pt(II) complex **285**. (Reprinted with permission from ref 206. Copyright 2004 Wiley-VCH).

Strothkamp and Lippard[15] reported the exclusive labeling of the alternating copolymer of nucleosides adenine and uracil possessing the phosphorothioate backbone poly($_S$-A-U) with a Pt(II) terpyridine complex, which was connected to the sulfur of a phosphorothioate group; moreover, there was no evidence of degradation or loss of sulfur from poly($_S$-A-U) following Pt binding (Figure 108). It was proposed that the $[Pt(tpy)(R)]^{n+}$ [R(n) = Cl (1), H_2O (2)] complexes could be labeling agents for sequencing the nucleic acids by electron microscopy, since Pt complex reacts exclusively with phosphorothioate groups that are incorporated into the RNA or DNA backbone adjacent to a specific base (Figure 108).

Lowe et al.[237] designed the dinuclear Pt-terpyridine complexes **308**, (Figure 109) which can intercalate into two DNA duplexes in close spacial proximity in order to study the topology of DNA. The azido groups were introduced at 4′-positions of terpyridines to allow the sites-of-intercalation to be photoaffinity labeled and the linker (pyr-R-pyr) is designed to be susceptible to cleavage with thiols and cyanides, a requirement for 2-D electrophoresis to identify the sites of intercalation.

A new generation of luminescent biolabeling agents was designed by introducing reactive isothiocyanate and iodoacetimide groups to the acetylene co-ligand of complexes **18** and **309**, respectively (Figure 110).[83] Specifically, human serum albumin (HSA), which is the most abundant plasma protein with many physiological functions, was successfully labeled with complex **18** and **309** from its amine and thiol functional residues forming thiourea and thioether linkages, as in **310** and **311**, respectively. These Pt(II)-tagged HSAs displayed induced low energy MLCT/LLCT absorption and ^{3}MLCT/^{3}LLCT emission bands at ca. 470 and 630 nm, respectively. Emission bands of the labeled HSAs **310** and **311** were uniquely different than labeling agents **18** and **309**, proving successful labeling. The $[Au(tpy)(Cl)]^{2+}$ complex was also tried as a label for bovine serum albumin (BSA); however, progressive reduction of Au(III) metal center and a complete break down of the complex was observed.[238]

The estrogen-containing Pt(II) terpyridine complex **312** (Figure 111) was elegantly designed to facilitate the cellular delivery of the Pt intercalator to cells with estrogen receptor.[239] The single crystal X-ray structure of **312** revealed an extended chain-like stacking through $\pi-\pi$ and the unusual Pt-π packing without any Pt−Pt interactions (Figure 111). This complex was successfully bound to the estrogen receptors in MCF-7 cell lines, human and bovine serum albumins, which are steroid transporting proteins and were covalently attached to guanine base in DNA and 12-base pair DNA fragment. The binding of **312** to these biomolecules was characterized by competitive radiometric binding assay, CD, FTICR, and ESI mass spectroscopy.

5.4. Cytotoxicity

It is well-known and accepted that Pt(II)-terpyridine complexes can intercalate into the DNA and covalently bind to biomolecules, such as proteins and enzymes. The intercalation and/or covalent binding of small molecules to the DNA or enzymes induces morphology deformations causing a dysfunction of these biomolecules and eventually leads to cell destruction. Planar dyes such as dactinomycin, adria-

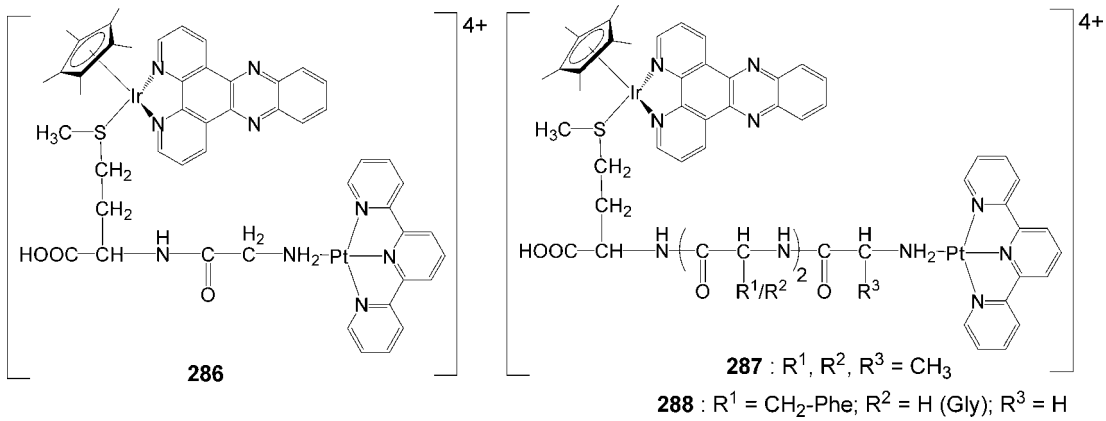

Figure 101. Structures of Ir(III)−Pt(II) complexes **286**−**288** connected through peptide linkers.[207,208]

Scheme 17. Assembly of Hairpin-like Structure Ln-Pt$_2$ 290 from 289[211]

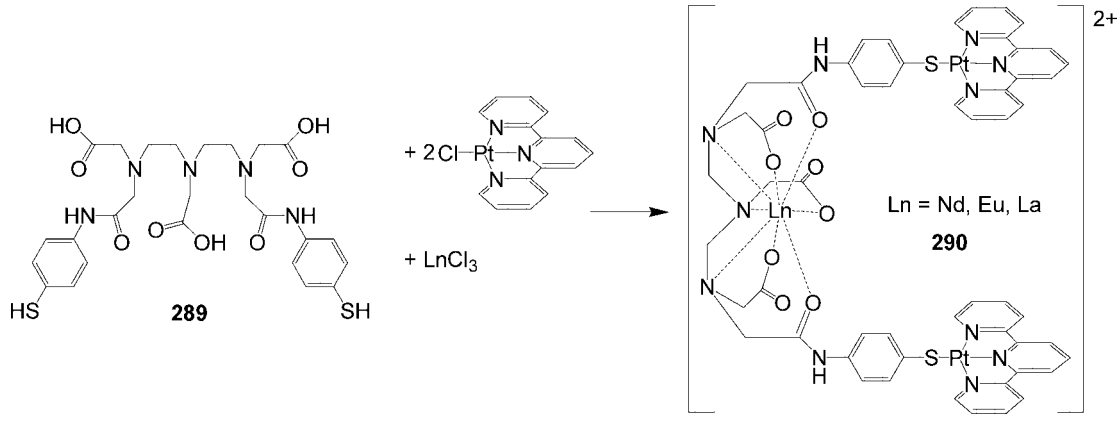

mycin, elipticine, belomycin, and their analogues that can intercalate into DNA were clinically used as antitumor and antiprotozoal drugs.[240] The coplanar Pt(II), Pd(II), and Au(III) terpyridine complexes were investigated *in vitro* and *in vivo* as antitumor and antiprotozoal drugs.

5.4.1. Chemotherapeutic Agents

In 1985, McFadyen et al.[241] reported the first cytotoxicity study of various Pt(II) terpyridine complexes **313**−**323** (Figure 112) and [Pt(tpy)(Cl)]$^+$ against L1210 murine

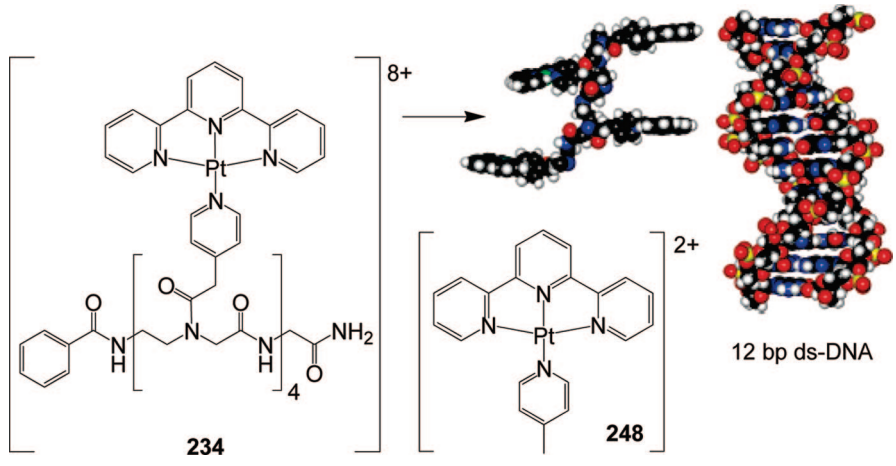

Figure 102. Chemical structure of tetrapeptide complex **234** and comparison of its space filled molecular model with 12 bp ds-DNA. (Reprinted with permission from ref 212. Copyright 2005 American Chemical Society).

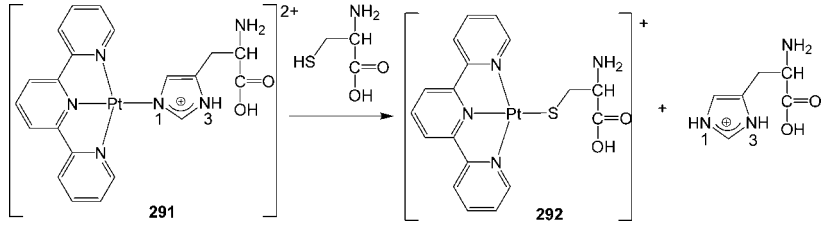

Figure 103. Substitution reaction of **291** with cysteine forming **292**.[16]

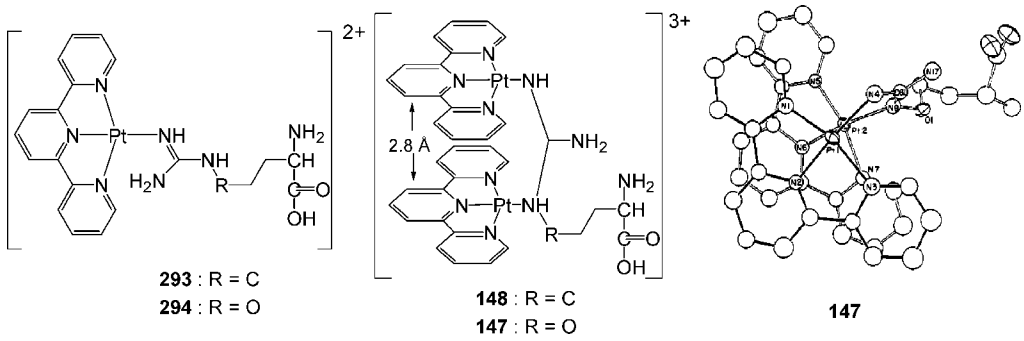

Figure 104. Structures of **147**, **148**, **293**, and **294** and crystal structure of **147**. (Reprinted with permission from ref 152. Copyright 1990 American Chemical Society).

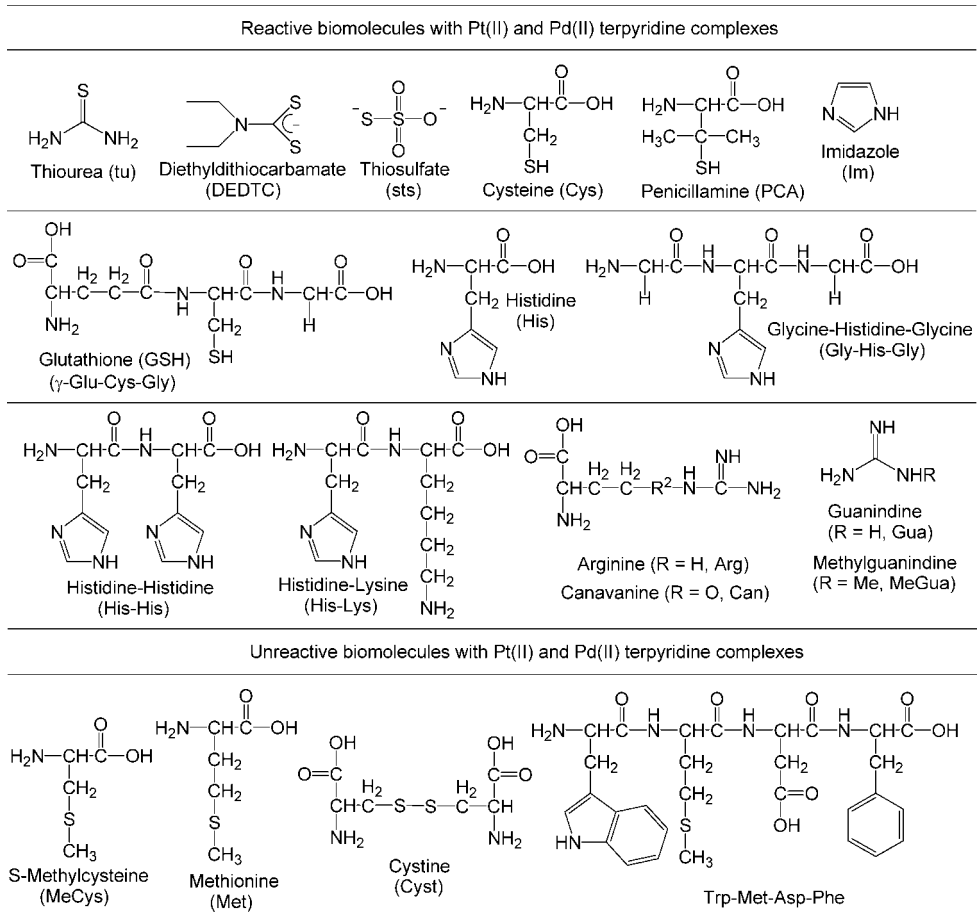

Figure 105. Structures of reactive and unreactive biomolecules towards $[M(tpy)(Cl)]^+$ [M = Pd(II), Pt(II)] complexes.[14,16–18,152,217,220]

leukemia cells in culture and mice. To determine the cytotoxicity of these complexes, L1210 cells were incubated with these complexes for 2 days at 37 °C, and then, cells were counted on a Coulter counter. The IC_{50}value, which is the concentration required to inhibit the growth of cells by 50%, was determined by plotting cell growth as a percentage of control versus drug concentration. The IC_{50} values of **313**−**323** against L1210 lines were in the 4−32 μM range; however, the $[Pt(tpy)(Cl)]^+$ complex had IC_{50} of 450 μM against L1210, suggesting the possible covalent binding of this complex to other biomolecules before reaching the DNA. The $[Pt(tpy)(Cl)]^+$ showed enhanced cytotoxicity against MCF-7 breast cancer epithelial cells (IC_{50} of 25 μM *in vitro*) when compared to L1210, but it was not as good as cisplatin, which has an IC_{50} of 5.6 μM *in vitro* against MCF-7.[242] The antitumor complex **314** (IC_{50} of 4 μM *in vitro*) was investigated *in vivo* against L1210 in mice; however, it did not show any antitumor activity.[241] Furthermore, free terpyridine ligands displayed unexpected cytotoxicity with IC_{50} of 2 μM against L1210 that was even higher than the corresponding Pt complexes, suggesting that a free terpyridine ligand may induce metal-deficient states or form metal complexes in the media that can inhibit cell growth.

Mono- and dinuclear intercalators (**242** and **272**−**278**, respectively) with thioalkyl chains displayed *in vitro* cytotoxicity against L1210 cells with IC_{50} values in the range of 4−14 μM, suggesting that cytotoxicity is independent of the intercalator character.[182] Moreover, these complexes produced extensive cell lysis, proposing that they may be only effective on the cell membrane and might not even reach the cell nucleus to intercalate into DNA.

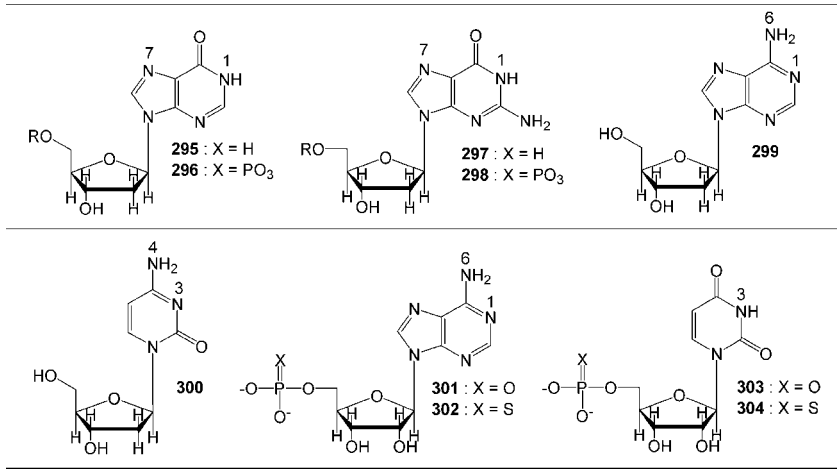

Figure 106. Structures of nucleoside-containing biomolecules **295**−**304**.[14,15,17–19,220,221]

Scheme 18. Acid Dissociation Constants of Cysteine and Its Reactions with $[Pt(tpy)(H_2O)]^{2+}$[217]

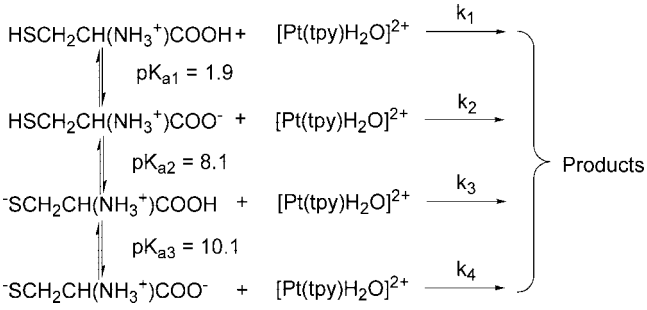

Table 6. Positions of Accessible Amino Acids Which Are Reactive with $[Pt(tpy)(Cl)]^+$ and Exposed on the Surface of Cytochrome *c* Proteins

cytochrome *c* from	amino acid and its position	reference
Horse heart	His-26, His-33, Arg-91	226
Tuna heart	His-26, Arg-91	227–232
C. krusei	His-33, His-39, Arg-91	233
Bakers' yeast (*iso*-1 form)	His-33, His-39, Arg-91, Cys-102	234, 235

Reports for the high intercalative[55] binding affinity and covalent binding[19,221] of the $[Pt(tpy)(pyr)]^{2+}$ complex and its derivatives to DNA prompted Lowe et al. to investigate their cytotoxic properties against parasites[26] and cancer[21] cells. Thus, a variety of mononuclear **324**−**326** (Figure 113) and dinuclear **327** and **328** (Figure 114) complexes were investigated as antiprotozoal and antitumor agents and their results were compared with conventional cisplatin and carboplatin drugs.

Some of the mono- and dinuclear complexes **325**−**328** were investigated for their *in vitro* cytotoxicity against five human ovarian carcinoma cell lines, such as CH1, cisplatin-resistant $CH1cis^R$, deoxorubicin-resistant $CH1dox^R$, A2780, and cisplatin-resistant $A2780cis^R$ cell lines; moreover, the SKOV3 cell line was included since it is one of the most resistant to the Pt drugs.[21] Cells were incubated with Pt drugs for 4 days, and then, the IC_{50} values were calculated (Table 8). The most effective complexes against human ovarian carcinoma cells *in vitro* were proven to be dinuclear Pt complexes with short and rigid linkers, such as **327** (R^1 = H, R^2 = *trans*-CH=CH and butadiene), which are slightly more effective than cisplatin against cisplatin-resistant lines ($CH1cis^R$ and $A2780cis^R$). The dinuclear complexes **328** with flexible linkers showed relatively low cytotoxicity compared to **327** (Table 8).

Several of the mononuclear complexes showed significant cytotoxicity, such as **326** (R^1 = H, R^2 = 4-Br), against human ovarian carcinoma cells; however, complexes with bulky and electron-donating substitutes on terpyridine, such as **326** (R^2 = 4-Me, R^2 = NMe[CH_2CH_2OH]), led to a significant loss in their antitumor activities since bulky substituents prevented the intercalation mode.[21] Further, the $[Pt(tpy)R]^{n+}$ (R[*n*] = Cl [1], H_2O [2], NH_3 [2]) complexes

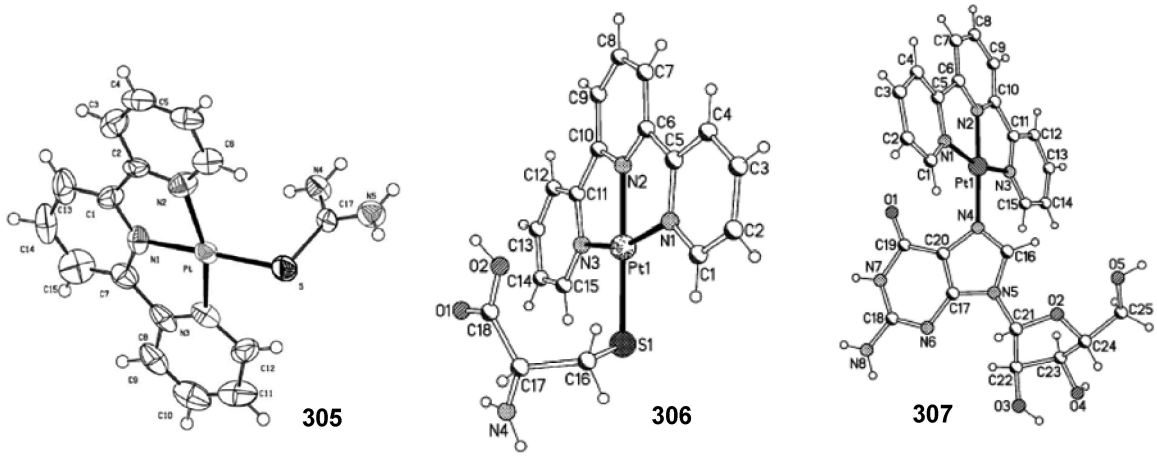

Figure 107. Single crystal X-ray structures of **305**−**307**. (Reprinted with permission from refs 14 and 217. Copyright 2004 and 2002 The Royal Society of Chemistry).

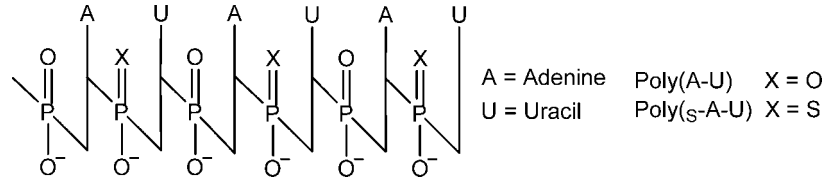

Figure 108. Alternating copolymer of nucleosides adenine and uracil with phosphate and phosphorothioate backbone.[15]

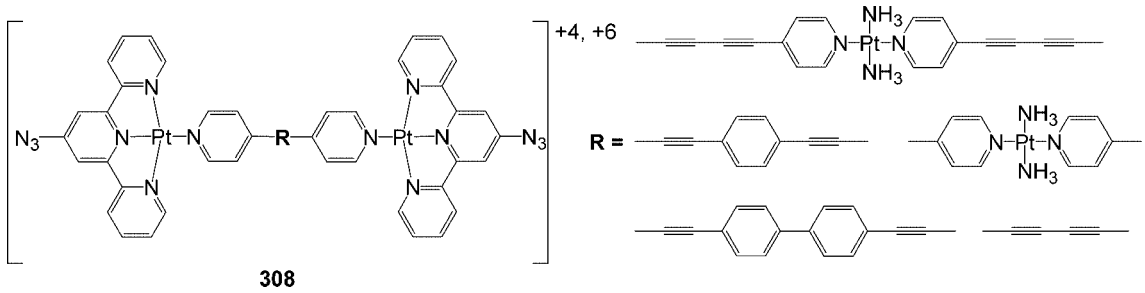

Figure 109. Structures of the bis-[4′-azido-terpyridine Pt(II)] complexes **308**.[237]

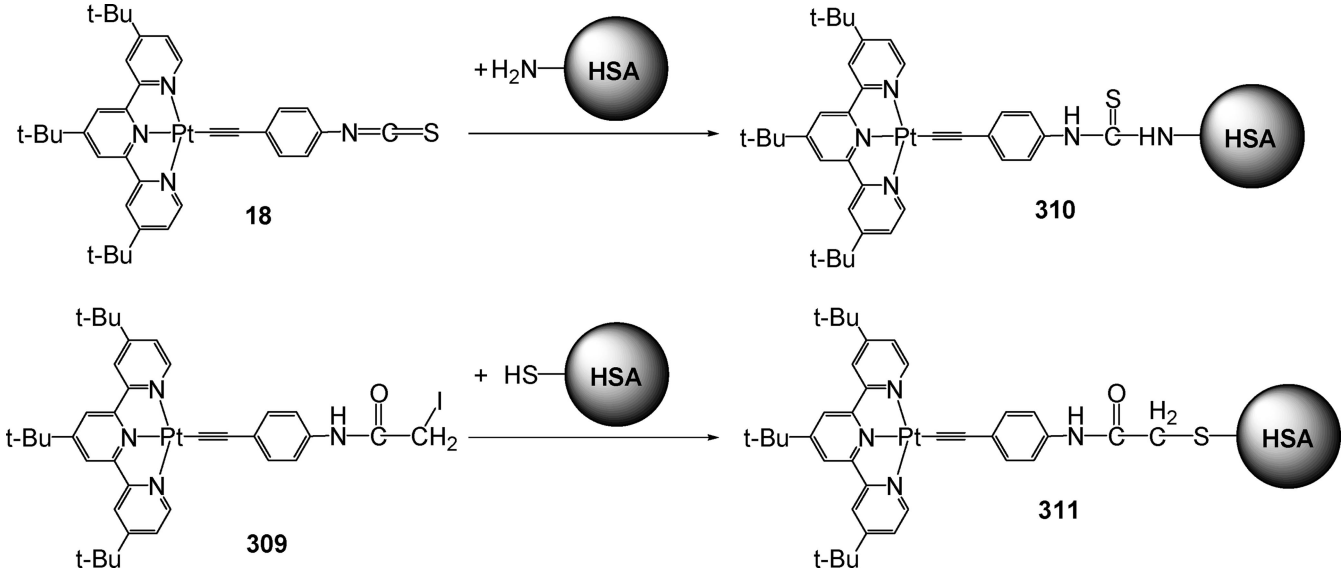

Figure 110. Luminescent labeling of HSA with **18** and **309**.[83]

were less cytotoxic than other mononuclear Pt complexes due to its covalent binding affinity toward other biomolecules.

Carborane cage-containing mononuclear **255**−**258** and dinuclear complexes **281**−**284** were investigated against L1210 murine leukemia cell line, its cisplatin resistant variant

Table 7. Products obtained from reactions between cytochrome *c* proteins and $[Pt(tpy)(Cl)]^+$ in 0.1 M acetate buffer at pH 5.0, separated by cation-exchange chromatography[17,18]

cytochrome *c* from	fractions	binding sites	number of $[Pt(tpy)]^{2+}$ tags	relative yield ± 3%
Tuna heart	1	none	0	90
	2	His-26	1	10
Horse heart	1	none	0	35
	2	His-33	1	50
	3	His-26	1	5
	4	His-33, His-26	2	10
C. krusei	1	none	0	30
	2	His-33	1	30
	3	His-39	1	30
	4	His-33, His-39	2	10
Bakers' yeast (*iso*-1 form)	1	none	0	40
	2	Cys-102	1	10
	3	His-33	1	15
	4	His-39	1	20
	5	Cys-102, His-39	2	5
	6	Cys-102, His-33	2	5
	7	His-33, His-39	2	5

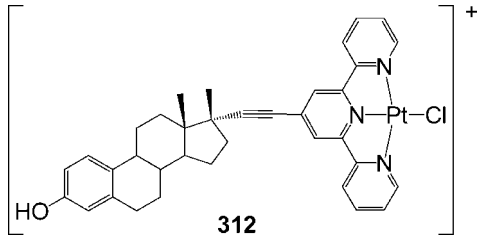

Figure 111. Chemical structure of estrogen Pt(II) complex **312**.[239]

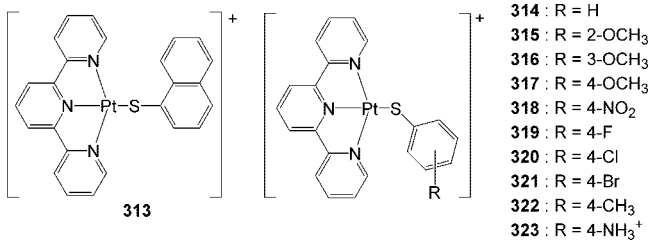

Figure 112. Structure of potential Pt-terpyridine antitumor agents **313**−**323**.[241]

L1210cis^R, 2008 human ovarian cell line, and its cisplatin resistant variant C13cis^R.[200,202] The mononuclear **257** (n = 1) displayed significant *in vitro* cytotoxicity against these cell lines when compared to cisplatin (Table 9). Moreover, **281** (n = 3) displayed remarkable cytotoxicity *in vitro* against L1210 and L1210cis^R (Table 9).[200] Low cytotoxicity of other dinuclear complexes and **256** (n = 1) was attributed to their poor solubility in physiological conditions.[200,202]

The antiprotozoal activity of mono- and dinuclear complexes **325**−**328** was investigated against *Leishmania donovani*, *Typanosoma cruzi* and *Typanosoma brucei*, which are the causes for leishmaniasis, Chaga's disease and sleeping sickness, respectively, since many planar dyes are active against *Typanosoma* and *Leishmania* parasites, such as ethidium bromide, acriflavine, ellipticine, and belomycin. Inhibition percentages of selected complexes against *L. donovani*, *T. cruzi*, and *T. brucei* parasites *in vitro* were summarized in Table 10.[26]

The first generation Pt-terpyridine drugs for parasites revealed that complexes **325** (R = H, L = H_2O, NH_3) were effective against *L. donovani* and *T. cruzi*, whereas complexes **325** (R^1 = H, R^2 = 4-Me and 4-Br) and **324** (R = H, L = NH_3) worked better against *T. brucei*.[26] The second generation Pt-terpyridine drugs were more effective than the first generation drugs against these parasites. The complexes **324** (R^1 = 4-Me-Ph and 4-Br-Ph, R^2 = 4-Me) against *L. donovani*, **324** (R^1 = 4-Me-Ph and Cl, R^2 = 4-Me) against *T. cruzi* and **324** (R^1 = 4-Me-Ph, Cl and Br, R^2 = 4-Me) against *T. brucei* were most effective. The third generation Pt-terpyridine drugs were designed by considering former results and gave the best inhibition percentages *in vitro* against these parasites; for example, **325** (R = Cl and 4-Br-

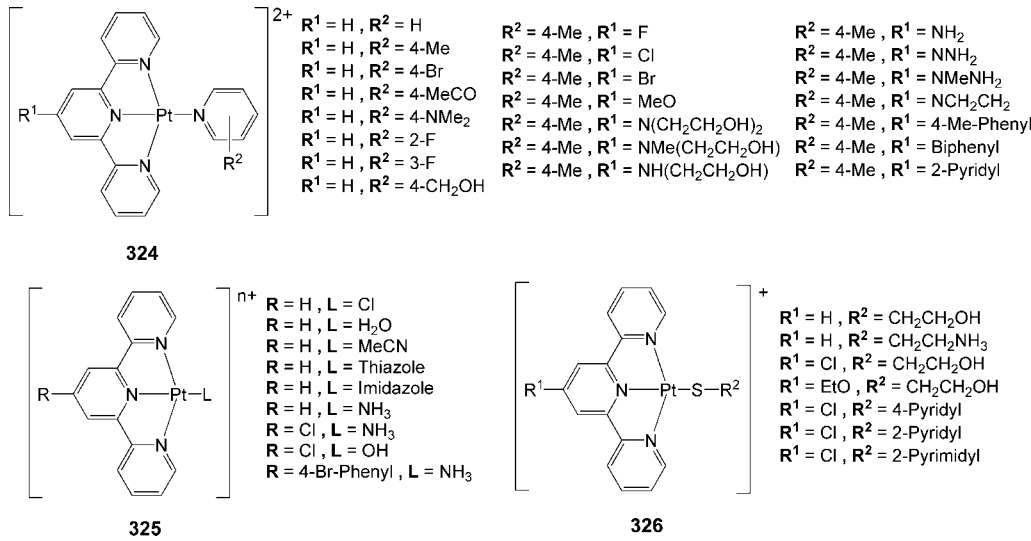

Figure 113. Structure of mononuclear antitumor complexes **324**−**326**.[21,26,27]

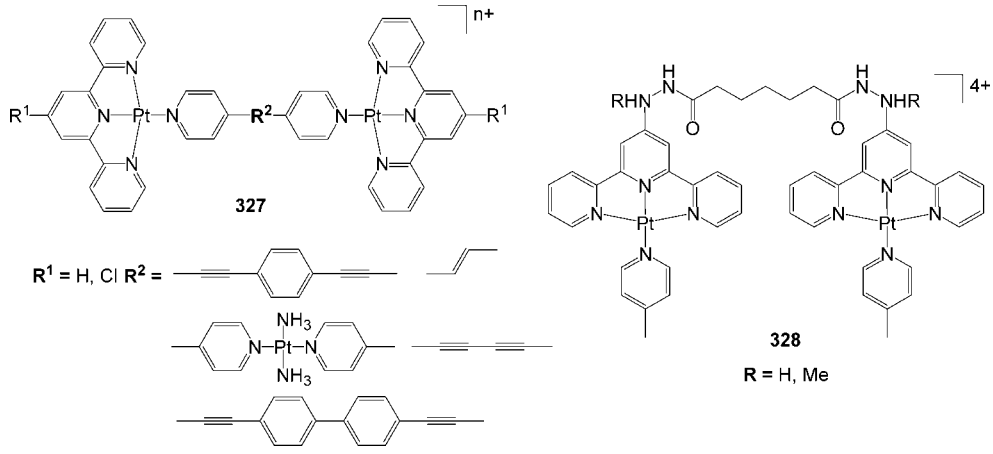

Figure 114. Structure of dinuclear Pt-terpyridine complexes **327** and **328**.[21]

Table 8. IC_{50} Values (μM, 4-days) for the *in vitro* Growth Inhibition of Human Ovarian Cell Lines by Mono- and Dinuclear Pt-terpyridine Complexes[21]

complex	CH1	CH1cis^R	RF[a]	CH1dox^R	RF[a]	A2780	A2780cis^R	RF[a]	SKOV3
Cisplatin	0.4	1.2	3.0	0.5	1.2	0.53	8.8	16.6	2.25
Carboplatin	6.2	14	2.3	6.0	1.0	35	>100		>100
327 (R^1 = H, R^2 = *trans*-CH=CH)	1.35	0.63	0.46	5.1	3.8	1.6	2.4	1.5	1.3
327 (R^1 = H, R^2 = butadiyne)	0.73	0.73	1	0.44	0.6	2	1.8	0.9	1.7
327 (R^1 = Cl, R^2 = Phenyl-Pt$(NH_3)_2$-Phenyl)	0.55	0.81	1.5	0.42	0.8	13.5	20.5	1.5	1.7
324 (R^1 = H, R^2 = 4-Br)	2.1	2.1	1	0.85	0.41	5.8	6.7	1.16	9.2
325 (R = H, L = Cl)	6.6	6.4	1	3.75	0.6	49	41	0.8	19.5
324 (R^1 = NMe(CH_2CH_2OH), R^2 = 4-Me)	>100	>100		17.5		40	>100		>100
328 (R = H)	48	42	0.9	40	0.8	19	40	2.1	9.8

[a] RF is the resistance factor: IC_{50} resistant line/ IC_{50} parent line.

Table 9. IC_{50} values (μM) of carborane containing mono- and dinuclear Pt complexes 255-258 and 281-284 against selected cancer cell lines[200,202]

complex	L1210	L1210cis^R	2008	C13cis^R
257 (n = 1)	1.6	0.9	1.7	2.1
257 (n = 3)	NA	NA	5.3	4.1
255 (n = 1)	NA	NA	4.6	5.1
256 (n = 1)	NA	NA	26	21
281 (n = 3)	0.9	0.8	NA	NA
282 (n = 3)	7.4	10	NA	NA
283 (n = 1)	24.5	5.3	NA	NA
284 (n = 3)	26.5	7.0	NA	NA
cisplatin	0.5	6.9	0.6	10

Ph, L = NH_3) displayed outstanding antiprotozoal activities (Table 10). For *L. donovani*, these complexes were more effective than first and second generation ones; for *T. cruzi*, they displayed comparable toxicity, and for *T. brucei*, they caused complete inhibition at concentrations >0.003 μM.

Kinetic and spectroscopic studies revealed that complexes **324** and **325** irreversibly bound to Cys-52 residue of trypanothione reductase (TR) enzyme from *T. cruzi* and eventually inhibited its function, which contributed significantly to their antiprotozoal activities besides the intercalation into DNA.[27] In contrast to the parasite enzyme, most Pt-terpyridine complexes reversibly interacted with human glutathione reductase (GR), similar to that of TR. Moreover, an irreversible inhibitor, in which the $[Pt(tpy)(SCH_2CH_2OH)]^+$complex was linked to 9-aminoacridine dye through alkyl chain, displayed the same inhibition behavior as in the case of **324** and **325** against *T. cruzi* TR and human GR.[243]

The human thioredoxin system containing the 12-kDa protein thioredoxin (hTrx) and the selenoenzyme thioredoxin reductase (hTrxR) was involved in thiol-mediated antioxidant defense and redox regulatory processes including transcriptional control, DNA synthesis, and apoptosis, thus, supporting cell proliferation. Many tumor cells are known to have increased Trx and TrxR and they can release the TrxR enzyme to stimulate autocrine cell growth. Inhibition of TrxR could selectively induce death of fast growing cancer cells. Becker et al.[22] reported an effective inhibition of hTrxR enzyme with complexes **149**, **329**, and **330** (Figure 115) by the reversible competitive or irreversible tight-binding of these complexes to the enzyme. These complexes displayed effective cytotoxicity *in vitro* against glioblastoma cell lines C6, NCH37, NCH82, NCH89, HNO97, and HNO199 with remarkable IC_{50} values (Table 11).[22,244]

The effects of the potent hTrxR inhibitors **329** and **330** on glioblastoma in rat models were reported.[244] Triple intravenous application of 25−35 mg/kg of these Pt-terpyridine drugs induced a significant decrease in tumor growth, as determined by MRI (Figure 116). The 22% reduction in tumor growth with low dose therapy (15 mg/kg of **329** and 25 mg/kg of **330**) as well as 36 and 40%

Table 10. Percent inhibition of selected complexes *in vitro* against parasites[26 a]

	L. donovani				*T. cruzi*				*T. brucei*			
complex	30 μM	10 μM	3 μM	1 μM	30 μM	10 μM	3 μM	1 μM	30 μM	10 μM	3 μM	1 μM
325 (R = H, L = Cl) 1st Gen.	99.1	94.9	22.0	0	99.3	99.0	76.0	52.0	100	100	100	100
325(R = H, L = H_2O) 1st Gen.	T/100	T/100	96.5	2.0	23.8	0	0	0	100	100	100	100
325 (R = H, L = NH_3) 1st Gen.	96.1	91.7	27.5	5.0	100	100	72.3	0.5	100	100	100	100
324 (R^1 = H, R^2 = H) 1st Gen.	99.5	92.2	0	0	27.2	0	0	0	100	100	100	100
324 (R^1 = Cl, R^2 = 4-Me) 2nd Gen.	93.3	89.5	47.9	2.5	100	97.0	73.5	59.7	100	100	100	100
324 (R^1 = Br, R^2 = 4-Me) 2nd Gen.	100	92.8	5.4	0	T/+	T/+	T/+	T/0	100	100	100	100
325 (R = Cl, L = NH_3) 3rd Gen.	T/100	T/100	99	99	T/100	T/100	T/100	50.8	100	100	100	100
325 (R = 4-Br-Phenyl, L = NH_3) 3rd Gen.	T/100	T/100	T/100	100	T/100	T/100	T/100	64.5	100	100	100	100

[a] T/100 means the compound was toxic to macrophages, 100% inhibition. T/+ means the compound was toxic to macrophages but parasites still present.

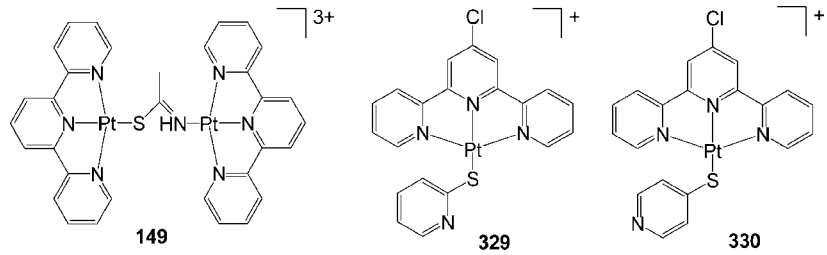

Figure 115. Structures of **149**, **329**, and **330**.[22]

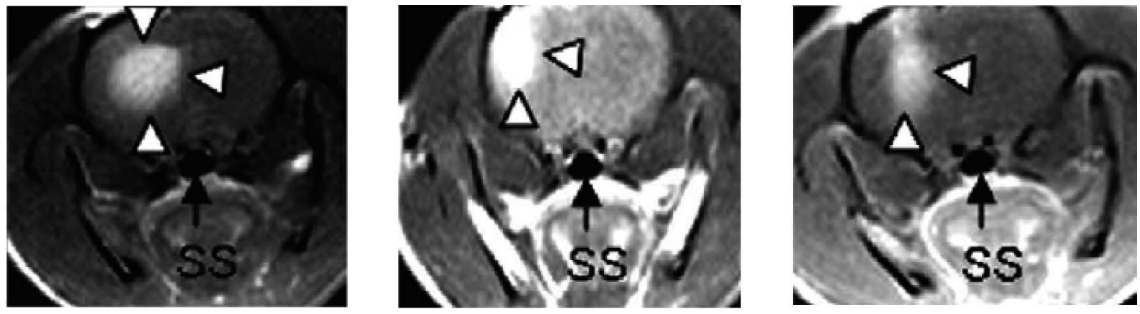

Figure 116. Volumetric MRI scans on day 15 presenting tumor growth in (A) untreated animals, (B) early therapy with 15 mg/kg of **329** and (B) late therapy with 35 mg/kg of **330**. Early therapy, treatment at days 4, 8, and 12 after tumor inoculation; late therapy, treatment at days 9, 11, and 13 after tumor inoculation. The dark arrow indicates the sphenodial sinus (SS) and the arrow heads delineate the tumor region. (Reprinted with permission from ref 244. Copyright 2007 Elsevier).

Table 11. IC_{50} (μM) Values of 330 and 149 against Glioblastoma Cell Lines[22]

	tumor cell line					
	NCH37	NCH87	NCH89	HNO97	HNO199	C6[244]
IC_{50} for **330**	10.5	7.4	2.5	5.5	9.2	3.5
IC_{50} for **149**	5.7	3.9	2.5	4.8	6.2	NA

Table 12. IC_{50} (μM) Values of 259, 261−263, 265, 266 and Cisplatin against Various Human Carcinoma Cells and Normal 293 Cells[20]

complex	HeLa	HepG2	SF−268	NCI-H460	MCF-7	Cell-293
259	0.1	0.1	0.06	0.1	0.08	0.5
261	2.0	1.7	1.3	2.8	1.9	10.5
262	0.09	0.1	0.08	0.1	0.1	0.3
263	0.2	0.1	0.1	0.2	0.2	0.9
265	0.2	0.2	0.1	0.2	0.1	0.5
266	2.7	3.0	2.1	2.5	3.4	4.6
cisplatin	11.6	20.6	15.6	25.1	19.1	>100

reduction with high dose therapy (25 mg/kg of **329** and 35 mg/kg of **330**, respectively) was observed.

Ma et al.[20] reported a new generation of the water-soluble glycosylated acetylide and arylacetylide complexes **259**−**266** and their cytotoxicity against five human carcinoma cells (HeLa, HepG2, SF-268, NCI-H460, MCF-7) and normal kidney cells (293), as a model. The IC_{50} values of **259**−**266** and cisplatin are summarized in Table 12. Complexes **259**, **261**−**263**, **265**, and **266** showed significant cytotoxicity against these human carcinoma cells and **259** displayed remarkable cytotoxicity that is ~100 more effective than clinically proven cisplatin drugs. Moreover, **259** and **263** have higher cytotoxicity against cancer cells than normal 293 human kidney cells.

Gold(III) complexes **267**−**271** displayed cytotoxicity *in vitro* against A2780, cisplatin-resistant A2780cis^R, A-549, SGC-7901, HeLa, HCT-116, BEL-7402, HL-60, and P-388 human cancer cells.[29,205] The IC_{50} values of $[Au(tpy)(Cl)]^{2+}$ *in vitro* against A2780 and A2780cis^R were calculated to be 0.2 and 0.37μM, respectively, which were more effective than cisplatin (1.22, 14.16 μM).[29] The complex **271** showed the highest cytotoxicity by inhibiting 80% of the cell growth in A-549, HeLa, and HCT-116 due to its high solubility in physiological conditions; some of the free terpyridine ligands displayed strong cytotoxicity and sometimes even higher than their corresponding Au(III) complexes.[29,205]

5.4.2. Radiotherapeutic Agents

Biomolecules can be damaged by the photoabsorption of X-rays, which were specifically designed to ionize the molecules by forming Auger electrons.[245] The Auger process, which generates electrons and a charged-center from electron-emitting radionuclides, such as ^{125}I, ^{131}I, and ^{32}P, can induce cleavage of chemical bonds in their neighborhood by direct ionization or charge recombination.[24] This process, which can cause cell death *in vivo*, single-strand breaks (SSBs) and double-strand breaks (DSBs) of DNA *in vitro*, was applied as radiotherapy to kill leukemia and thyroid tumors.

Le Sech et al.[23] introduced heavy Pt(II) atoms to circular plasmid DNA by intercalation and/or covalent binding of the $[Pt(tpy)(Cl)]^+$ to allow their use of energetic X-rays (soft γ-rays, 11 KeV) on DNA. It was suggested that the absorption of photons from soft γ-rays (11 KeV) in L_{III} inner shell of Pt atom, which was bound to circular plasmid DNA (dry sample), induced SSBs and DSBs of the DNA. This process was detected by fluorescence spectroscopy after submitting the sample to agarose gel electrophoresis. Later, SSBs and DSBs of the DNA, which contained $[Pt(tpy)(Cl)]^+$, were spectroscopically enhanced by tuning the experimental procedures.[245] The Pt-bound circular DNA that irradiated by X-ray in aqueous solution increased SSBs and DSBs due to formation of free radicals from water, which could be a possible application to hadrontherapy.[24] Moreover, fast He^{2+} ion irradiation of circular plasmid DNA, which contained $[Pt(tpy)(Cl)]^+$, caused the SSBs and DSBs of the DNA. This experiment displayed similar results to that of X-ray irradiation.[25]

6. Conclusion

The reversible metal d−d orbital interactions and terpyridine $\pi-\pi$ interactions continue to generate new avenues to self-assemble supramolecular structures that can be utilized as molecular switches and sensors *via* either their host−guest interactions or photo- and electrochemical responses. Since square-planar Pt(II), Pd(II), and Au(III) terpyridine complexes show promise as medical probes, their potential as antitumor and antiprotozoal agents, and protein probes, will continue to esculate. Thus, as an active and growing area of interest, terpyridine-based chemistry is destined to garner continued enthusiasm, with respect to its physical, biological, medical, and supramolecular properties, as well as yet to be envisioned areas.

7. Acknowledgments

The authors gratefully acknowledge the National Science Foundation [DMR-0401780 and 0705015], the Air Force Office of Scientific Research [F496200−02-1-0428,03], and the Ohio Board of Reagents for financial support.

8. References

(1) Schubert, U. S.; Hofmeier, H.; Newkome, G. R. *Modern Terpyridine Chemistry*; Wiley-VCH: Weinheim, Germany, 2006.
(2) McMillin, D. R.; Moore, J. J. *Coord. Chem. Rev.* **2002**, *229*, 113.
(3) Yam, V. W. W.; Tang, R. P. L.; Wong, K. M. C.; Cheung, K. K. *Organometallics* **2001**, *20*, 4476.
(4) Kunugi, Y.; Mann, K. R.; Miller, L. L.; Exstrom, C. L. *J. Am. Chem. Soc.* **1998**, *120*, 589.
(5) Wadas, T. J.; Wang, Q. M.; Kim, Y. J.; Flaschenreim, C.; Blanton, T. N.; Eisenberg, R. *J. Am. Chem. Soc.* **2004**, *126*, 16841.
(6) Exstrom, C. L.; Sowa, J. R.; Daws, C. A.; Janzen, D.; Mann, K. R.; Moore, G. A.; Stewart, F. F. *Chem. Mater.* **1995**, *7*, 15.
(7) Daws, C. A.; Exstrom, C. L.; Sowa, J. R.; Mann, K. R. *Chem. Mater.* **1997**, *9*, 363.
(8) Tang, W. S.; Lu, X. X.; Wong, K. M. C.; Yam, V. W. W. *J. Mater. Chem.* **2005**, *15*, 2714.
(9) Du, P. W.; Schneider, J.; Jarosz, P.; Eisenberg, R. *J. Am. Chem. Soc.* **2006**, *128*, 7726.
(10) Cortes, M.; Carney, J. T.; Oppenheimer, J. D.; Downey, K. E.; Cummings, S. D. *Inorg. Chim. Acta* **2002**, *333*, 148.
(11) Jennette, K. W.; Lippard, S. J.; Vassiliades, G. A.; Bauer, W. R. *Proc. Natl. Acad. Sci. U.S.A.* **1974**, *71*, 3839.
(12) Lippard, S. J. *Acc. Chem. Res.* **1978**, 211.
(13) McFadyen, W. D.; Wakelin, L. P. G.; Roos, I. A. G.; Hillcoat, B. L. *Biochem. J.* **1987**, *242*, 177.
(14) Bugarcic, Z. D.; Heinemann, F. W.; van Eldik, R. *Dalton Trans.* **2004**, 279.
(15) Strothkamp, K. G.; Lippard, S. J. *Proc. Natl. Acad. Sci. U.S.A.* **1976**, *73*, 2536.
(16) Ratilla, E. M. A.; Kostić, N. M. *J. Am. Chem. Soc.* **1988**, *110*, 4427.
(17) Ratilla, E. M. A.; Brothers, H. M.; Kostić, N. M. *J. Am. Chem. Soc.* **1987**, *109*, 4592.
(18) Brothers, H. M.; Kostić, N. M. *Inorg. Chem.* **1988**, *27*, 1761.
(19) Lowe, G.; Vilaivan, T. *J. Chem. Soc., Perkin Trans. 1* **1996**, 1499.
(20) Ma, D. L.; Shum, T. Y. T.; Zhang, F. Y.; Che, C. M.; Yang, M. S. *Chem. Commun.* **2005**, 4675.
(21) Lowe, G.; Droz, A. S.; Vilaivan, T.; Weaver, G. W.; Park, J. J.; Pratt, J. M.; Tweedale, L.; Kelland, L. R. *J. Med. Chem.* **1999**, *42*, 3167.
(22) Becker, K.; Herold-Mende, C.; Park, J. J.; Lowe, G.; Schirmer, R. H. *J. Med. Chem.* **2001**, *44*, 2784.
(23) Le Sech, C.; Takakura, K.; Saint-Marc, C.; Frohlich, H.; Charlier, M.; Usami, N.; Kobayashi, K. *Radiat. Res.* **2000**, *153*, 454.
(24) Kobayashi, K.; Frohlich, H.; Usami, N.; Takakura, K.; Le Sech, C. *Radiat. Res.* **2002**, *157*, 32.
(25) Usami, N.; Furusawa, Y.; Kobayashi, K.; Frohlich, H.; Lacombe, S.; Le Sech, C. *Int. J. Radiat. Biol.* **2005**, *81*, 515.
(26) Lowe, G.; Droz, A. S.; Vilaivan, T.; Weaver, G. W.; Tweedale, L.; Pratt, J. M.; Rock, P.; Yardley, V.; Croft, S. L. *J. Med. Chem.* **1999**, *42*, 999.
(27) Bonse, S.; Richards, J. M.; Ross, S. A.; Lowe, G.; Krauth-Siegel, R. L. *J. Med. Chem.* **2000**, *43*, 4812.
(28) Crowley, J. D.; Bosnich, B. *Eur. J. Inorg. Chem.* **2005**, 2015.
(29) Messori, L.; Abbate, F.; Marcon, G.; Orioli, P.; Fontani, M.; Mini, E.; Mazzei, T.; Carotti, S.; O'Connell, T.; Zanello, P. *J. Med. Chem.* **2000**, *43*, 3541.
(30) Hofmeier, H.; Schubert, U. S. *Chem. Soc. Rev.* **2004**, *33*, 373.
(31) Morgan, G. T.; Burstall, F. H. *J. Chem. Soc.* **1934**, 1498.
(32) Intille, G. M. Ph.D. Dissertation, Syracuse University, Syracuse NY, 1967.
(33) Howe-Grant, M.; Lippard, S. J. *Inorg. Synth.* **1980**, *20*, 101.
(34) Bailey, J. A.; Hill, M. G.; Marsh, R. E.; Miskowski, V. M.; Schaefer, W. P.; Gray, H. B. *Inorg. Chem.* **1995**, *34*, 4591.
(35) Yip, H. K.; Cheng, L. K.; Cheung, K. K.; Che, C. M. *J. Chem. Soc., Dalton Trans.* **1993**, 2933.
(36) Lai, S.-W.; Chan, M. C. W.; Cheung, K.-K.; Che, C.-M. *Inorg. Chem.* **1999**, *38*, 4262.
(37) Arena, G.; Calogero, G.; Campagna, S.; Scolaro, L. M.; Ricevuto, V.; Romeo, R. *Inorg. Chem.* **1998**, *37*, 2763.
(38) Chakraborty, S.; Wadas, T. J.; Hester, H.; Flaschenreim, C.; Schmehl, R.; Eisenberg, R. *Inorg. Chem.* **2005**, *44*, 6284.
(39) Chakraborty, S.; Wadas, T. J.; Hester, H.; Schmehl, R.; Eisenberg, R. *Inorg. Chem.* **2005**, *44*, 6865.
(40) Arena, G.; Scolaro, L. M.; Pasternack, R. F.; Romeo, R. *Inorg. Chem.* **1995**, *34*, 2994.
(41) Cini, R.; Donati, A.; Giannettoni, R. *Inorg. Chim. Acta* **2001**, *315*, 73.
(42) Annibale, G.; Brandolisio, M.; Pitteri, B. *Polyhedron* **1995**, *14*, 451.
(43) Buchner, R.; Field, J. S.; Haines, R. J.; Cunningham, C. T.; McMillin, D. R. *Inorg. Chem.* **1997**, *36*, 3952.
(44) Buchner, R.; Cunningham, C. T.; Field, J. S.; Haines, R. J.; McMillin, D. R.; Summerton, G. C. *J. Chem. Soc., Dalton Trans.* **1999**, 711.
(45) Field, J. S.; Haines, R. J.; McMillin, D. R.; Summerton, G. C. *J. Chem. Soc., Dalton Trans.* **2002**, 1369.
(46) Field, J. S.; Gertenbach, J. A.; Haines, R. J.; Ledwaba, L. P.; Mashapa, N. T.; McMillin, D. R.; Munro, O. Q.; Summerton, G. C. *Dalton Trans.* **2003**, 1176.
(47) Field, J. S.; Haines, R. J.; McMillin, D. R.; Munro, O. Q.; Summerton, G. C. *Inorg. Chim. Acta* **2005**, *358*, 4567.
(48) McDermott, J. X.; White, J. F.; Whitesides, G. M. *J. Am. Chem. Soc.* **1976**, 6521.
(49) Crites, D. K.; Cunningham, C. T.; McMillin, D. R. *Inorg. Chim. Acta* **1998**, *273*, 346.
(50) Hobert, S. E.; Carney, J. T.; Cummings, S. D. *Inorg. Chim. Acta* **2001**, *318*, 89.
(51) Michalec, J. F.; Bejune, S. A.; Cuttell, D. G.; Summerton, G. C.; Gertenbach, J. A.; Field, J. S.; Haines, R. J.; McMillin, D. R. *Inorg. Chem.* **2001**, *40*, 2193.
(52) Monnereau, C.; Gomez, J.; Blart, E.; Odobel, F.; Wallin, S.; Fallberg, A.; Hammarström, L. *Inorg. Chem.* **2005**, *44*, 4806.
(53) Jennette, K. W.; Gill, J. T.; Sadownick, J. A.; Lippard, S. J. *J. Am. Chem. Soc.* **1976**, 6160.
(54) Aldridge, T. K.; Stacy, E. M.; McMillin, D. R. *Inorg. Chem.* **1994**, *33*, 722.
(55) McCoubrey, A.; Latham, H. C.; Cook, P. R.; Rodger, A.; Lowe, G. *FEBS Lett.* **1996**, *380*, 73.
(56) Yang, Q. Z.; Wu, L. Z.; Wu, Z. X.; Zhang, L. P.; Tung, C. H. *Inorg. Chem.* **2002**, *41*, 5653.
(57) Hollis, L. S.; Lippard, S. J. *J. Am. Chem. Soc.* **1983**, *105*, 4293.
(58) Sampath, U.; Putnam, W. C.; Osiek, T. A.; Touami, S.; Xie, J.; Cohen, D.; Cagnolini, A.; Droege, P.; Klug, D.; Barnes, C. L.; Modak, A.; Bashkin, J. K.; Jurisson, S. S. *J. Chem. Soc., Dalton Trans.* **1999**, 2049.
(59) Pitteri, B.; Marangoni, G.; Visentin, F.; Bobbo, T.; Bertolasi, V.; Gilli, P. *J. Chem. Soc., Dalton Trans.* **1999**, 677.
(60) Liu, X. M.; Mcinnes, E. J. L.; Kilner, C. A.; Thornton-Pett, M.; Halcrow, M. A. *Polyhedron* **2001**, *20*, 2889.
(61) Karkalic, R.; Bugarcic, Z. D. *Monatsh. Chem.* **2000**, *131*, 819.
(62) MacLean, E. J.; Robinson, R. I.; Teat, S. J.; Wilson, C.; Woodward, S. *J. Chem. Soc., Dalton Trans.* **2002**, 3518.
(63) Bugarcic, Z. D.; Liehr, G.; van Eldik, R. *J. Chem. Soc., Dalton Trans.* **2002**, 951.
(64) Castan, P.; Dahan, F.; Wimmer, S.; Wimmer, F. L. *J. Chem. Soc., Dalton Trans.* **1990**, 2679.
(65) Bugarcic, Z. D.; Petrovic, B.; Zangrando, E. *Inorg. Chim. Acta* **2004**, *357*, 2650.
(66) Annibale, G.; Marangoni, G.; Pitteri, B.; Visentin, F.; Bobbo, T. *Transition Met. Chem.* **2000**, *25*, 485.
(67) Liu, X. M.; Renard, S. L.; Kilner, C. A.; Halcrow, M. A. *Inorg. Chem. Commun.* **2003**, *6*, 598.
(68) Zhang, W. G.; Bensimon, C.; Crutchley, R. J. *Inorg. Chem.* **1993**, *32*, 5808.
(69) Cosar, S.; Janik, M. B. L.; Flock, M.; Freisinger, E.; Farkas, E.; Lippert, B. *J. Chem. Soc., Dalton Trans.* **1999**, 2329.
(70) Hamann, C.; Kern, J. M.; Sauvage, J. P. *Dalton Trans.* **2003**, 3770.
(71) Sommer, R. D.; Rheingold, A. L.; Goshe, A. J.; Bosnich, B. *J. Am. Chem. Soc.* **2001**, *123*, 3940.
(72) azlurrahman, A. K.; Verkade, J. G. *Inorg. Chem.* **1992**, *31*, 2064.
(73) Romeo, R.; Scolaro, L. M.; Plutino, M. R.; Albinati, A. *J. Organomet. Chem.* **2000**, *594*, 403.
(74) Lai, S. W.; Chan, M. C. W.; Cheung, K. K.; Che, C. M. *Inorg. Chem.* **1999**, *38*, 4262.
(75) Akiba, M.; Sasaki, Y. *Inorg. Chem. Commun.* **1998**, *1*, 61.
(76) Peyratout, C. S.; Aldridge, T. K.; Crites, D. K.; McMillin, D. R. *Inorg. Chem.* **1995**, *34*, 4484.
(77) Kurosaki, H.; Yamakawa, N.; Sumimoto, M.; Kimura, K.; Goto, M. *Bioorg. Med. Chem. Lett.* **2003**, *13*, 825.
(78) Wilson, M. H.; Ledwaba, L. P.; Field, J. S.; McMillin, D. R. *Dalton Trans.* **2005**, 2754.
(79) Field, J. S.; Haines, R. J.; Ledwaba, L. P.; McGuire, R.; Munro, O. Q.; Low, M. R.; McMillin, D. R. *Dalton Trans.* **2007**, 192.
(80) Tears, D. K. C.; McMillin, D. R. *Coord. Chem. Rev.* **2001**, *211*, 195.
(81) Michalec, J. F.; Bejune, S. A.; McMillin, D. R. *Inorg. Chem.* **2000**, *39*, 2708.

(82) Sakuda, E.; Funahashi, A.; Kitamura, N. *Inorg. Chem.* **2006**, *45*, 10670.
(83) Wong, K. M. C.; Tang, W.-S.; Chu, B. W. K.; Zhu, N.; Yam, V. W. W. *Organometallics* **2004**, *23*, 3459.
(84) Hill, M. G.; Bailey, J. A.; Miskowski, V. M.; Gray, H. B. *Inorg. Chem.* **1996**, *35*, 4585.
(85) Tannai, H.; Tsuge, K.; Sasaki, Y. *Bull. Chem. Soc. Jpn.* **2006**, *79*, 1223.
(86) Abel, E. W.; Orrell, K. G.; Osborne, A. G.; Pain, H. M.; Sik, V.; Hursthouse, M. B.; Malik, K. M. A. *J. Chem. Soc., Dalton Trans.* **1994**, 3441.
(87) Abel, E. W.; Orrell, K. G.; Osborne, A. G.; Pain, H. M.; Sik, V. *J. Chem. Soc., Dalton Trans.* **1994**, 111.
(88) Abel, E. W.; Dimitrov, V. S.; Long, N. J.; Orrell, K. G.; Osborne, A. G.; Pain, H. M.; Sik, V.; Hursthouse, M. B.; Mazid, M. A. *J. Chem. Soc., Dalton Trans.* **1993**, 597.
(89) Abel, E. W.; Dimitrov, V. S.; Long, N. J.; Orrell, K. G.; Osborne, A. G.; Sik, V.; Hursthouse, M. B.; Mazid, M. A. *J. Chem. Soc., Dalton Trans.* **1993**, 291.
(90) Gelling, A.; Orrell, K. G.; Osborne, A. G.; Sik, V. *J. Chem. Soc., Dalton Trans.* **1998**, 937.
(91) Gelling, A.; Olsen, M. D.; Orrell, K. G.; Osborne, A. G.; Sik, V. *J. Chem. Soc., Dalton Trans.* **1998**, 3479.
(92) Barloy, L.; Gauvin, R. M.; Osborn, J. A.; Sizun, C.; Graff, R.; Kyritsakas, N. *Eur. J. Inorg. Chem.* **2001**, 1699.
(93) Ramdeehul, S.; Barloy, L.; Osborn, J. A.; DeCian, A.; Fischer, J. *Organometallics* **1996**, *15*, 5442.
(94) Barloy, L.; Ramdeehul, S.; Osborn, J. A.; Carlotti, C.; Taulelle, F.; De Cian, A.; Fischer, J. *Eur. J. Inorg. Chem.* **2000**, 2523.
(95) Guo, F. Q.; Sun, W. F.; Liu, Y.; Schanze, K. *Inorg. Chem.* **2005**, *44*, 4055.
(96) Zhou, X.; Zhang, H. X.; Pan, Q. J.; Xia, B. H.; Tang, A. C. *J. Phys. Chem. A* **2005**, *109*, 8809.
(97) Moore, J. J.; Nash, J. J.; Fanwick, P. E.; McMillin, D. R. *Inorg. Chem.* **2002**, *41*, 6387.
(98) Sielemann, D.; Winter, A.; Florke, U.; Risch, N. *Org. Biomol. Chem.* **2004**, *2*, 863.
(99) Baik, C.; Han, W.-S.; Kang, Y.; Kang, S. O.; Ko, J. K. *J. Organomet. Chem.* **2006**, 5900.
(100) Chan, C. W.; Che, C. M.; Cheng, M. C.; Wang, Y. *Inorg. Chem.* **1992**, *31*, 4874.
(101) Tannai, H.; Tsuge, K.; Sasaki, Y.; Hatozaki, O.; Oyama, N. *Dalton Trans.* **2003**, 2353.
(102) Oyama, N.; Tatsuma, T.; Sato, T.; Sotomura, T. *Nature* **1995**, *373*, 598.
(103) Tzeng, B. C.; Lee, G. H.; Peng, S. M. *Inorg. Chem. Commun.* **2003**, *6*, 1341.
(104) Okamura, R.; Wada, T.; Aikawa, K.; Nagata, T.; Tanaka, K. *Inorg. Chem.* **2004**, *43*, 7210.
(105) Hayoun, R.; Zhong, D. K.; Rheingold, A. L.; Doerrer, L. H. *Inorg. Chem.* **2006**, *45*, 6120.
(106) Yu, C.; Wong, K. M. C.; Chan, K. H. Y.; Yam, V. W. W. *Angew. Chem., Int. Ed.* **2005**, *44*, 791.
(107) Yu, C.; Chan, K. H. Y.; Wong, K. M. C.; Yam, V. W. W. *Proc. Natl. Acad. Sci. U.S.A.* **2006**, *103*, 19652.
(108) Scolaro, L. M.; Romeo, A.; Terracina, A. *Chem. Commun.* **1997**, 1451.
(109) Yam, V. W. W.; Wong, K. M. C.; Zhu, N. Y. *J. Am. Chem. Soc.* **2002**, *124*, 6506.
(110) Gillard, R. D.; Sengul, A.; Oldroyd, A. *Transition Met. Chem.* **2001**, *26*, 339.
(111) Wong, K. M. C.; Tang, W. S.; Lu, X. X.; Zhu, N. Y.; Yam, V. W. W. *Inorg. Chem.* **2005**, *44*, 1492.
(112) Yang, Q. Z.; Tong, Q. X.; Wu, L. Z.; Wu, Z. X.; Zhang, L. P.; Tung, C. H. *Eur. J. Inorg. Chem.* **2004**, 1948.
(113) Han, X.; Wu, L. Z.; Si, G.; Pan, J.; Yang, Q. Z.; Zhang, L. P.; Tung, C. H. *Chem. Eur. J.* **2007**, *13*, 1231.
(114) Yam, V. W. W.; Tang, R. P. L.; Wong, K. M. C.; Ko, C. C.; Cheung, K. K. *Inorg. Chem.* **2001**, *40*, 571.
(115) Yam, V. W. W.; Tang, R. P. L.; Wong, K. M. C.; Lu, X. X.; Cheung, K. K.; Zhu, N. Y. *Chem. Eur. J.* **2002**, *8*, 4066.
(116) Yutaka, T.; Mori, I.; Kurihara, M.; Mizutani, J.; Tamai, N.; Kawai, T.; Irie, M.; Nishihara, H. *Inorg. Chem.* **2002**, *41*, 7143.
(117) Zhang, D.; Wu, L. Z.; Yang, Q. Z.; Li, X. H.; Zhang, L. P.; Tung, C. H. *Org. Lett.* **2003**, *5*, 3221.
(118) Lee, P. C.; Meisel, D. *J. Am. Chem. Soc.* **1980**, *102*, 5477.
(119) Lee, P. C.; Meisel, D. *Photochem. Photobiol.* **1985**, *41*, 21.
(120) Tung, C. H.; Guan, J. Q. *J. Am. Chem. Soc.* **1998**, *120*, 11874.
(121) Maldotti, A.; Molinari, A.; Andreotti, L.; Fogagnolo, M.; Amadelli, R. *Chem. Commun.* **1998**, 507.
(122) Ogumi, Z.; Kuroe, T.; Takehara, Z. *J. Electrochem. Soc.* **1985**, *132*, 2601.
(123) Yang, Y.; Zhang, D.; Wu, L. Z.; Chen, B.; Zhang, L. P.; Tung, C. H. *J. Org. Chem.* **2004**, *69*, 4788.
(124) Li, X. H.; Wu, L. Z.; Zhang, L. P.; Tung, C. H.; Che, C. M. *Chem. Commun.* **2001**, 2280.
(125) Abe, T.; Hirano, K.; Shiraishi, Y.; Toshima, N.; Kaneko, M. *Eur. Polym. J.* **2001**, *37*, 753.
(126) Zhang, D.; Wu, L. Z.; Zhou, L.; Han, X.; Yang, Q. Z.; Zhang, L. P.; Tung, C. H. *J. Am. Chem. Soc.* **2004**, *126*, 3440.
(127) Narayana-Prabhu, R.; Schmehl, R. H. *Inorg. Chem.* **2006**, *45*, 4319.
(128) Sun, W. F.; Wu, Z. X.; Yang, Q. Z.; Wu, L. Z.; Tung, C. H. *Appl. Phys. Lett.* **2003**, *82*, 850.
(129) Guo, F. Q.; Sun, W. F. *J. Phys. Chem. B* **2006**, *110*, 15029.
(130) Mckay, T. J.; Bolger, J. A.; Staromlynska, J.; Davy, J. R. *J. Chem. Phys.* **1998**, *108*, 5537.
(131) Staromlynska, J.; Mckay, T. J.; Wilson, P. *J. Appl. Phys.* **2000**, *88*, 1726.
(132) Mckay, T. J.; Staromlynska, J.; Davy, T. R.; Bolger, J. A. *J. Opt. Soc. Am. B* **2001**, *18*, 358.
(133) Jude, H.; Bauer, J. A. K.; Connick, W. B. *J. Am. Chem. Soc.* **2003**, *125*, 3446.
(134) Chen, W. H.; Reinheimer, E. W.; Dunbar, K. R.; Omary, M. A. *Inorg. Chem.* **2006**, *45*, 2770.
(135) Ziessel, R.; Diring, S. *Tetrahedron Lett.* **2006**, *47*, 4687.
(136) Ziessel, R.; Diring, S.; Retailleau, P. *Dalton Trans.* **2006**, 3285.
(137) Yam, V. W. W.; Wong, K. M. C.; Zhu, N. *Angew. Chem., Int. Ed.* **2003**, *42*, 1400.
(138) Yam, V. W. W.; Hui, C.-K.; Yu, S.-Y.; Zhu, N. *Inorg. Chem.* **2004**, *43*, 812.
(139) Tao, C. H.; Wong, K. M. C.; Zhu, N. Y.; Yam, V. W. W. *New J. Chem.* **2003**, *27*, 150.
(140) Lo, H. S.; Yip, S. K.; Wong, K. M. C.; Zhu, N. Y.; Yam, V. W. W. *Organometallics* **2006**, *25*, 3537.
(141) Derosa, M. C.; Al-mutlaq, F.; Crutchley, R. J. *Inorg. Chem.* **2001**, *40*, 1406.
(142) Aumuller, A.; Erk, P.; Klebe, G.; Hunig, S.; Vonschutz, J. U.; Werner, H. P. *Angew. Chem., Int. Ed.* **1986**, *25*, 740.
(143) Kato, R.; Kobayashi, H.; Kobayashi, A. *J. Am. Chem. Soc.* **1989**, *111*, 5224.
(144) Wudl, F.; Bryce, M. R. *J. Chem. Educ.* **1990**, *67*, 717.
(145) Yam, V. W. W.; Chan, K. H. Y.; Wong, K. M. C.; Chu, B. W. K. *Angew. Chem., Int. Ed.* **2006**, *45*, 6169.
(146) Bailey, J. A.; Miskowski, V. M.; Gray, H. B. *Inorg. Chem.* **1993**, *32*, 369.
(147) Bailey, J. A.; Miskowski, V. M.; Gray, H. B. *Acta Crystallogr., Sect. C: Cryst. Struct. Commun.* **1993**, *49*, 793.
(148) Yip, H. K.; Che, C. M.; Zhou, Z. Y.; Mak, T. C. W. *J. Chem. Soc., Chem. Commun.* **1992**, 1369.
(149) Lowe, G.; Ross, S. A.; Probert, M.; Cowley, A. *Chem. Commun.* **2001**, 1288.
(150) Ziolkowski, E. J.; Turner, P.; Rendina, L. M. *Inorg. Chem. Commun.* **2006**, *9*, 53.
(151) Wong, K. M. C.; Zhu, N. Y.; Yam, V. W. W. *Chem. Commun.* **2006**, 3441.
(152) Ratilla, E. M. A.; Scott, B. K.; Moxness, M. S.; Kostić, N. M. *Inorg. Chem.* **1990**, *29*, 918.
(153) Dewan, J. C.; Lippard, S. J.; Bauer, W. R. *J. Am. Chem. Soc.* **1980**, *102*, 858.
(154) Goshe, A. J.; Bosnich, B. *Synlett* **2001**, 941.
(155) Goshe, A. J.; Crowley, J. D.; Bosnich, B. *Helv. Chim. Acta* **2001**, *84*, 2971.
(156) Goshe, A. J.; Steele, I. M.; Ceccarelli, C.; Rheingold, A. L.; Bosnich, B. *Proc. Natl. Acad. Sci. U.S.A.* **2002**, *99*, 4823.
(157) Crowley, J. D.; Goshe, A. J.; Bosnich, B. *Chem. Commun.* **2003**, 2824.
(158) Crowley, J. D.; Goshe, A. J.; Bosnich, B. *Chem. Commun.* **2003**, 392.
(159) Goshe, A. J.; Steele, I. M.; Bosnich, B. *J. Am. Chem. Soc.* **2003**, *125*, 444.
(160) Goshe, A. J.; Steele, I. M.; Bosnich, B. *Inorg. Chim. Acta* **2004**, *357*, 4544.
(161) Crowley, J. D.; Goshe, A. J.; Steele, I. M.; Bosnich, B. *Chem.—Eur. J.* **2004**, *10*, 1944.
(162) Crowley, J. D.; Steele, I. M.; Bosnich, B. *Inorg. Chem.* **2005**, *44*, 2989.
(163) Crowley, J. D.; Steele, I. M.; Bosnich, B. *Eur. J. Inorg. Chem.* **2005**, 3907.
(164) Okamura, R.; Wada, T.; Tanaka, K. *Bull. Chem. Soc. Jpn.* **2006**, *79*, 1535.
(165) Wada, T.; Tsuge, K.; Tanaka, K. *Angew. Chem., Int. Ed.* **2000**, *39*, 1479.
(166) Wada, T.; Tsuge, K.; Tanaka, K. *Inorg. Chem.* **2001**, *40*, 329.
(167) Monnereau, C.; Gomez, J.; Blart, E.; Odobel, F. *Inorg. Chem.* **2005**, *44*, 4806.

(168) Lam, S. C. F.; Yam, V. W. W.; Wong, K. M. C.; Cheng, E. C. C.; Zhu, N. Y. *Organometallics* **2005**, *24*, 4298.
(169) Hui, C. K.; Chu, B. W. K.; Zhu, N. Y.; Yam, V. W. W. *Inorg. Chem.* **2002**, *41*, 6178.
(170) Tanaka, K.; Shigemori, K.; Shionoya, M. *Chem. Commun.* **1999**, 2475.
(171) Ohr, K.; Gilmartin, B. P.; Williams, M. E. *Inorg. Chem.* **2005**, *44*, 7876.
(172) Gilmartin, B. P.; McLaughlin, R. L.; Williams, M. E. *Chem. Mater.* **2005**, *17*, 5446.
(173) Gilmartin, B. P.; Ohr, K.; McLaughlin, R. L.; Koerner, R.; Williams, M. E. *J. Am. Chem. Soc.* **2005**, *127*, 9546.
(174) Lerman, L. S. *J. Mol. Biol.* **1961**, 18.
(175) Lerman, L. S. *Proc. Natl. Acad. Sci. U.S.A.* **1963**, 94.
(176) Waring, M. J. *Biochim. Biophys. Acta* **1964**, 358.
(177) Bauer, W.; Vinograd, J. *J. Mol. Biol.* **1970**, 419.
(178) Hollstein, V. *Chem. Rev.* **1974**, *74*, 625.
(179) Long, E. C.; Barton, J. K. *Acc. Chem. Res.* **1990**, *23*, 271.
(180) Hahn, F. E. *Progress in Molecular and Sub-Cellular Biology*; Springer-Verlag: Berlin, 1971.
(181) Scatchard, G. *Ann. N.Y. Acad. Sci.* **1949**, 660.
(182) McFadyen, W. D.; Wakelin, L. P. G.; Roos, I. A. G.; Hillcoat, B. L. *Biochem. J.* **1986**, *238*, 757.
(183) McGhee, J. D.; von Hippel, P. H. *J. Mol. Biol.* **1974**, *86*, 469.
(184) Howe-Grant, M.; WU, K. C.; Bauer, W. R.; Lippard, S. J. *Biochemistry* **1976**, *15*, 4339.
(185) Wakelin, L. P. G.; McFadyen, W. D.; Walpole, A.; Roos, I. A. G. *Biochem. J.* **1984**, *222*, 203.
(186) Cusumano, M.; Di Pietro, M. L.; Giannetto, A. *Inorg. Chem.* **1999**, *38*, 1754.
(187) Cusumano, M.; Di Pietro, M. L.; Giannetto, A.; Romano, F. *Inorg. Chem.* **2000**, *39*, 50.
(188) Record, M. T.; Anderson, C. F.; Lohman, T. M. *Q. Rev. Biophys.* **1978**, *11*, 103.
(189) Howe-Grant, M.; Lippard, S. J. *Biochemistry* **1979**, *18*, 5762.
(190) Cohen, G.; Eisenberg, H. *Biopolymers* **1966**, *4*, 429.
(191) Schmechel, D. E.; Crothers, D. M. *Biopolymers* **1971**, *10*, 465.
(192) Barton, J. K.; Lippard, S. J. *Biochemistry* **1979**, *18*, 2661.
(193) Yau, H. C. M.; Chan, H. L.; Yang, M. S. *Sens. Actuators, B* **2002**, *81*, 283.
(194) Vinograd, J.; Lebowitz, J. *J. Gen. Physiol.* **1966**, *49*, 103.
(195) Gray, H. B.; Upholt, W. B.; Vinograd, J. *J. Mol. Biol.* **1971**, *62*, 1.
(196) Crothers, D. M. *Biopolymers* **1968**, 575.
(197) Bond, P. J.; Langridge, R.; Jennette, K. W.; Lippard, S. J. *Proc. Natl. Acad. Sci. U.S.A.* **1975**, *72*, 4825.
(198) Wang, A. H.; Nathans, J.; van der, M. G.; van Boom, J. H.; Rich, A. *Nature* **1978**, *276*, 471.
(199) Crossley, E. L.; Caiazza, D.; Rendina, L. M. *Dalton Trans.* **2005**, 2825.
(200) Woodhouse, S. L.; Ziolkowski, E. J.; Rendina, L. M. *Dalton Trans.* **2005**, 2827.
(201) Todd, J. A.; Rendina, L. M. *Inorg. Chem.* **2002**, *41*, 3331.
(202) Todd, J. A.; Turner, P.; Ziolkowski, E. J.; Rendina, L. M. *Inorg. Chem.* **2005**, *44*, 6401.
(203) Soloway, A. H.; Tjarks, W.; Barnum, B. A.; Rong, F. G.; Barth, R. F.; Codogni, I. M.; Wilson, J. G. *Chem. Rev.* **1998**, *98*, 1515.
(204) Messori, L.; Orioli, P.; Tempi, C.; Marcon, G. *Biochem. Biophys. Res. Commun.* **2001**, *281*, 352.
(205) Shi, P. F.; Jiang, Q.; Zhao, Y. M.; Zhang, Y. M.; Lin, J.; Lin, L. P.; Ding, J.; Guo, Z. J. *J. Biol. Inorg. Chem.* **2006**, *11*, 745.
(206) van der Schilden, K.; Garcia, F.; Kooijman, H.; Spek, A. L.; Haasnoot, J. G.; Reedijk, J. *Angew. Chem., Int. Ed.* **2004**, *43*, 5668.
(207) Gencaslan, S.; Sheldrick, W. S. *Eur. J. Inorg. Chem.* **2005**, 3840.
(208) Stodt, R.; Gencaslan, S.; Frodl, A.; Schmidt, C.; Sheldrick, W. S. *Inorg. Chim. Acta* **2003**, *355*, 242.
(209) Carter, M. T.; Rodriguez, M.; Bard, A. J. *J. Am. Chem. Soc.* **1989**, *111*, 8901.
(210) Smith, S. R.; Neyhart, G. A.; Kalsbeck, W. A.; Thorp, H. H. *New J. Chem.* **1994**, *18*, 397.
(211) Glover, P. B.; Ashton, P. R.; Childs, L. J.; Rodger, A.; Kercher, M.; Williams, R. M.; De Cola, L.; Pikramenou, Z. *J. Am. Chem. Soc.* **2003**, *125*, 9918.
(212) Levine, L. A.; Morgan, C. M.; Ohr, K.; Williams, M. E. *J. Am. Chem. Soc.* **2005**, *127*, 16764.
(213) Wong, E.; Giandomenico, C. M. *Chem. Rev.* **1999**, *99*, 2451.
(214) Reedijk, J. *Chem. Rev.* **1999**, *99*, 2499.
(215) Kozelka, J.; Legendre, F.; Reeder, F.; Chottard, J. C. *Coord. Chem. Rev.* **1999**, *192*, 61.
(216) Jaganyi, D.; Hofmann, A.; van Eldik, R. *Angew. Chem., Int. Ed.* **2001**, *40*, 1680.
(217) Bugarcic, Z. D.; Liehr, G.; van Eldik, R. *J. Chem. Soc., Dalton Trans.* **2002**, 2825.
(218) Jaganyi, D.; Tiba, F. *Transition Met. Chem.* **2003**, *28*, 803.
(219) Appleton, T. G.; Pesch, F. J.; Wienken, M.; Menzer, S.; Lippert, B. *Inorg. Chem.* **1992**, *31*, 4410.
(220) Bugarcic, Z. D.; Soldatovic, T.; Jelic, R.; Alguero, B.; Grandas, A. *Dalton Trans.* **2004**, 3869.
(221) Lowe, G.; McCloskey, J. A.; Ni, J. S.; Vilaivan, T. *Bioorg. Med. Chem.* **1996**, *4*, 1007.
(222) Weber, C. F.; van Eldik, R. *Eur. J. Inorg. Chem.* **2005**, 4755.
(223) Hofmann, A.; Jaganyi, D.; Munro, O. Q.; Liehr, G.; van Eldik, R. *Inorg. Chem.* **2003**, *42*, 1688.
(224) Lundblad, R. L.; Noyes, C. M. *Chemical Reagents for Protein Modifications*; CRC Press: Boca Raton, FL, 1984.
(225) Means, G. E.; Feeney, R. E. *Chemical Modification of Proteins* ; Holden-Day: San Francisco, CA, 1971.
(226) Dickerson, R. E.; Takano, T.; Eisenberg, D.; Kallai, O. B.; Samson, L.; Cooper, A.; Margoliash, E. *J. Biol. Chem.* **1971**, *246*, 1511.
(227) Takano, T.; Kallai, O. B.; Swanson, R.; Dickerson, R. E. *J. Biol. Chem.* **1973**, *248*, 5234.
(228) Swanson, R.; Trus, B. L.; Mandel, N.; Mandel, G.; Kallai, O. B.; Dickerson, R. E. *J. Biol. Chem.* **1977**, *252*, 759.
(229) Takano, T.; Trus, B. L.; Mandel, N.; Mandel, G.; Kallai, O. B.; Swanson, R.; Dickerson, R. E. *J. Biol. Chem.* **1977**, *252*, 776.
(230) Mandel, N.; Mandel, G.; Trus, B. L.; Rosenberg, J.; Carlson, G.; Dickerson, R. E. *J. Biol. Chem.* **1977**, *252*, 4619.
(231) Takano, T.; Dickerson, R. E. *J. Mol. Biol.* **1981**, *153*, 95.
(232) Takano, T.; Dickerson, R. E. *J. Mol. Biol.* **1981**, *153*, 79.
(233) Narita, K.; Chitani, K. *J. Biochem.* **1968**, *63*, 226.
(234) Sherwood, C.; Brayer, G. D. *J. Mol. Biol.* **1985**, *185*, 209.
(235) Zuniga, E. H.; Nall, B. T. *Biochemistry* **1983**, *22*, 1430.
(236) Brothers, H. M.; Kostic, N. M. *Biochemistry* **1990**, *29*, 7468.
(237) Lowe, G.; Droz, A. S.; Park, J. J.; Weaver, G. W. *Bioorg. Chem.* **1999**, *27*, 477.
(238) Marcon, G.; Messori, L.; Orioli, P.; Cinellu, M. A.; Minghetti, G. *Eur. J. Biochem.* **2003**, *270*, 4655.
(239) Hannon, M. J.; Green, P. S.; Fisher, D. M.; Derrick, P. J.; Beck, J. L.; Watt, S. J.; Ralph, S. F.; Sheil, M. M.; Barker, P. R.; Alcock, N. W.; Price, R. J.; Sanders, K. J.; Pither, R.; Davis, J.; Rodger, A. *Chem.—Eur. J.* **2006**, *12*, 8000.
(240) Pratt, W. B.; Ruddon, R. W. *The Anticancer Drugs*; Oxford University Press: London, 1979.
(241) McFadyen, W. D.; Wakelin, L. P. G.; Roos, I. A. G.; Leopold, V. A. *J. Med. Chem.* **1985**, *28*, 1113.
(242) Bligh, S. W. A.; Bashall, A.; Garrud, C.; McPartlin, M.; Wardle, N.; White, K.; Padhye, S.; Barve, V.; Kundu, G. *Dalton Trans.* **2003**, 184.
(243) Inhoff, O.; Richards, J. M.; Briet, J. W.; Lowe, G.; Krauth-Siegel, R. L. *J. Med. Chem.* **2002**, *45*, 4524.
(244) Ahmadi, R.; Urig, S.; Hartmann, M.; Helmke, B. M.; Koncarevic, S.; Allenberger, B.; Kienhoefer, C.; Neher, M.; Steiner, H. H.; Unterberg, A.; Herold-Mende, C.; Becker, K. *Free Radical Biol. Med.* **2006**, *40*, 763.
(245) Le Sech, C.; Takakura, K.; Saint-Marc, C.; Frohlich, H.; Charlier, M.; Usami, N.; Kobayashi, K. *Can. J. Physiol. Pharmacol.* **2001**, *79*, 196.

CR0781059